

**PHOTOCHROMIC COATINGS CONTAINING COPPER BROMIDE
NANOCRYSTALS AND Zn^{2+}/Cd^{2+} AS CO-ACTIVATORS**

Dissertation

zur Erlangung des akademischen Grades doctor rerum naturalium
(Dr. rer. nat.)

vorgelegt dem Rat der Chemisch-Geowissenschaftlichen Fakultät der
Friedrich-Schiller-Universität Jena

von Dipl. Material Ing. **Juliana Resende Meirelles**

geboren am 24.02.1977 in Goiânia – Brasilien

Dekan:

Prof. Dr. Peter Sedlacek

Gutachter:

Prof. Dr. Christian Ruessel

PD Dr. rer. nat. Habil. Antje Kritz

Prof. Dr. Doris Erht

Tag der öffentlichen Verteidigung: 09/06/2006

To my parents

Acknowledgements

I would like to thank Prof. Dr. C. Rüssel who gave me the opportunity to work in his group at the Otto Schott Institut für Glaschemie and for the interesting research topic he provided me. I thank him for all scientific support and for the friendly and open relationship. I acknowledge him for running with enormous success a centre of excellence in glass research; it is an honour to be part of the group.

In the same way, I thank Dr. M. Müller, my supervisor, for his attention and availability; he was always there when I needed. He helped me a lot specially at the end when he managed to work with me in a long distance relation (Jena/London) thanks to modern communication; emails and telephone calls. He trusted me throughout my working process and always honoured his word regarding a deadline.

I acknowledge Dr. R. Keding who took the initiative for the exchange program between the Universidade Federal de Sao Carlos in Brazil, where I graduated, and the Friederich Schiller Universität in Jena, Germany. He made a difference for dozens of Brazilian students like me, who had a chance to experience living in Europe and learn the German language. I wish this project will go on in the future.

I also thank the financial support provided by DAAD through the IQN project and the „Thüringer Forschungsschwerpunkt Grenzflächentechnologien“.

I acknowledge all technical assistants, especially Frau Hartmann from Otto Schott Institut für Glaschemie who were responsible for important measurements and made my work easier.

From my heart thanks to my friends Dr. Darja Benne, Dr. Ruzha Harizanova, Dr. Ana C. A. Prado, Dr. Frank Schramm, Jens Almer, Eric Tucker, Liam Murdoch, Nisha Parihar, Adriaan du Toit, Tony Rutter, Thomas Matthiasen, Noah Raford, Marcelo Cordeiro da Silva, Dr. Sandra Hornschuh, Dr. Anja Hunger and Michaela Huter who took the time to help me through contents, English and German language and grammar corrections and revisions.

I also want to thank the friends I made through out those years that made the work easier and who created a positive atmosphere and filled the grey winter days with happiness and joy. They will always be present to me when I speak about those years in Jena in my future life.

A very special thank to my fiancé Erico Rocha who encouraged me to be a powerful woman. He was a very strong stand for me to finish this project. He saves no efforts to make me happy. He played other very important rolls, as my personal coach and financial support in the last year. Without his coach I would still be lost in my own thoughts.

Last but not least I acknowledge the love of my parents Eduardo Meirelles and Neusa Meirelles: they were the first to instigate my taste for discovering unexpected situations. When I was 17 years old they sent me to school in a foreign country. I did not know the language, the culture and anybody in that country. Everything I have achieved today is a result of their excellence in education in all aspects of life. I acknowledge you, mom and dad, for giving us, my sisters and me, all the opportunities we had. I also thank my sisters, Marcela Meirelles and Renata Meirelles, for their unconditional love, they are the most precious treasure I have. They accept me as I am and I can just be myself when they are around. I acknowledge them for taking care of our family while I'm away, for giving our parents and grandmothers the love I would give them if I were present, and for listening to me when I needed someone to speak to. I miss you both so much.

Enjoy the reading.

Juliana Meirelles

CONTENTS

1	ABSTRACT	8
2	KURZFASSUNG	10
3	INTRODUCTION	12
3.1	A VIEW OF THE MARKET	13
3.2	THE SOL-GEL PROCESS	16
3.3	PHOTOCHROMISM	21
4	THE STATE OF THE ART	26
4.1	THE FIRST PHOTOCROMIC GLASSES AND THE SILVER HALIDE SYSTEM	27
4.2	THE SEARCH FOR ALTERNATIVES TO SILVER HALIDE GLASSES	27
4.3	COPPER HALIDE SYSTEMS	28
4.4	INTRODUCTION OF Cd^{2+} AS CO-ACTIVATOR IN COPPER HALIDE SYSTEMS	29
4.5	SOL-GEL PROCESS AS A NEW METHOD OF PRODUCING BULK GLASS AND GLASS COATINGS	30
4.6	PHOTOCROMIC COATING WITH COMPLETE REVERSIBILITY AT ROOM TEMPERATURE AND NORMAL ATMOSPHERE	31
4.7	THE AIM OF THIS WORK	32
5	EXPERIMENTAL PROCEDURE	34
5.1	SOL-GEL PREPARATION	37
5.2	COATING PROCESS	40
5.3	DRYING STAGE	43
5.4	HEAT-TREATMENT	44
6	METHODS	48
6.1	X-RAY POWDER DIFFRACTION	48
6.2	ULTRA VIOLET (UV) AND VISIBLE (VIS) REGION ABSORPTION SPECTROSCOPY 50	
6.3	SCANNING ELECTRON MICROSCOPY	52
6.4	ATOMIC FORCE MICROSCOPY	55
6.5	ELLIPSOMETRY	56
7	RESULTS	59
7.1	X-RAY POWDER DIFFRACTION	59
7.2	POLARIZING MICROSCOPY	69
7.3	ATOMIC FORCE MICROSCOPY	70
7.4	SCANNING ELECTRON MICROSCOPY	77
7.5	ELLIPSOMETRY	81
7.6	UV-VIS SPECTROSCOPY	82
8	DISCUSSION	103
8.1	CRYSTALLINE STRUCTURE OF $CuBr$; $CdBr_2$ AND $ZnBr_2$	103
8.2	ALL STUDIED COMPOSITIONS AND THE EFFECT OF ITS VARIATIONS	106
8.3	CO-ACTIVATORS	113
8.4	THE DARKENING MECHANISM	124
9	SUMMARY	130
10	APPENDIX	132

10.1	ILLUSTRATION OF THE ULTRA VIOLET AND VISIBLE RANGE OF ELECTROMAGNETIC RADIATION.	132
10.2	LIST OF ALL STUDIED COMPOSITIONS.....	133
10.3	INDEX OF FIGURES	135
10.4	INDEX OF TABLES	140
11	BIBLIOGRAPHY.....	143
12	SELBSTSTÄNDIGKEITSERKLÄRUNG.....	151
13	LEBENS LAUF	152

1 ABSTRACT

This dissertation will present the research undertaken in order to produce an inorganic photochromic coating. This means the coating is a glass matrix containing photochromic microcrystals. The coating should be applied to commercial flat glasses, i.e. large surfaces (not suitable for optical glasses) to be used in order to control the luminosity inside buildings.

The coatings are made from sol-gel and applied on glass substrate by dip-coating method. The sol-gel method is an organic route and a glass formation process at low temperatures. The precursors are tetramethoxysilane and 3-glycidoxypropyltrimethoxysilane alkoxides rather than oxides used in the traditional high temperature melting process. The addition of water and solvent (ethanol) will initiate the hydrolysis and condensation, which forms a sol-gel. This sol is used to coat the substrate, and after coated it is called wet gel. After drying at 100 °C, the dried gel undergoes a heat-treatment at temperatures between 150 °C and 500 °C, which produces a xerogel. The xerogel has the same tri-dimensional silicate (Si-O) bonds as in a glass, but to be considered a glass this sample has to undergo a heat-treatment of at least 900 °C to provide the closure of pores present at the structure. That means a xerogel is a “porous glass”.

The photochromic property depends on the presence of photoactive microcrystals embedded in the silica glassy matrix. That means the microcrystals has the characteristic of changing its initial transmission characteristics (by absorbing visible light) depending on actinic irradiation. To be considered photochromic this change in optical characteristic has to be reversible. If the microcrystals darken when activated by incident light, after taking off the actinic irradiation, the microcrystals should return to their original condition.

The aim of this work was to continue the group's research using the results obtained up to now, where the studied system was the copper halide and, more specifically, the copper bromide Cd^{2+} co-activated system.

One important rule is that the crystal growth should not happen during the sol-gel preparation or coating process. That means the Cu^+ should be part of complex-molecules while existing in the sol-gel process. Later on, during the heat-treatment, the CuBr crystal growth is activated.

The introduction of Cd^{2+} , as co-activator, plays an important role in the photochromic effect. The Cd^{2+} causes lattice disorder in the CuBr structure. A bivalent Cd^{2+} ion occupies an octahedral position in the CuBr lattice, while Cu^+ ions are monovalent and occupy tetrahedral positions. This charge imbalance causes adjacent Cu^+ ions to move throughout the crystal to areas called sensitizer regions. Due to irradiation and release of electron-hole pairs those mobile Cu^+ ions at the sensitizer zone will react to form Cu atoms. The atoms agglomerate themselves causing the darkening of the sample while under irradiation. In this work, we tried to increase the induced defects in CuBr lattices by adding Zn^{2+} to the composition. The intention was to substitute the Cd^{2+} content for a non-toxic compound.

The introduction of Zn^{2+} was successful in terms of maintaining a satisfactory photochromism, but the complete substitution of Cd^{2+} was not possible because the sample loses the photochromic property.

The key in introducing defects in the CuBr lattice is based on the balance between two commitments. Those commitments are: the crystal size that provides satisfactory darkening intensity and the optimisation of the Cu^{2+} diffusion to provide a fast-fading process when the irradiation stops. The crystal size has an upper limit (300 nm), and above this level the samples are opaque. This happens because the crystals have the same size of visible light wavelength and they scatter the light instead of transmitting it. The level of disorder in the CuBr lattice will be the tool to optimise the photochromic property by adding the so-called co-activators.

2 KURZFASSUNG

In der vorliegenden Arbeit werden Untersuchungen zu anorganischen fotochromen Schichten vorgestellt. Das bedeutet: die Schicht ist eine Glasmatrix, in der fotochrome Mikrokristalle eingebettet sind. Solche Schichten können beispielsweise auf kommerziellen Flachgläsern angebracht werden (für optische Gläser sind sie weniger geeignet), um die Helligkeit in Gebäuden zu regeln.

Die Schichten werden über ein Sol-Gel-Verfahren hergestellt und mittels dip-coating aufgebracht. Diese Methode bedient sich organischer Ausgangsmaterialien, die Glasbildung findet bei vergleichsweise niedrigen Temperaturen statt. Anstelle von Oxide werden Tetramethoxysilan (TMOS) und 3-Glycidoxypropyltrimethoxysilan (GPTS), also Alkoxide, in Ethanol gelöst verwendet. Durch die Zugabe von Wasser wird die Hydrolyse und die Kondensation initiiert, was dann zur Bildung des Sols und schließlich des Gels führt. Das Gel wird benutzt, um ein Substrat zu beschichten. Nach der Beschichtung ist es ein so genanntes ‚nasses Gel‘. Nach einer Trocknung bei 100 °C wird das nun ‚trockene Gel‘ bei Temperaturen zwischen 150 °C und 500 °C Wärme behandelt, und man erhält ein Xerogel. Das Xerogel weist eine dreidimensionale Verknüpfung der Si-O-Bindungen auf wie in einem ‚normalen‘ Glas, aber im Unterschied zu diesem sind Xerogele sehr porös, sodass sie einer Wärmebehandlung von mindestens 900 °C unterworfen werden müssten, um die Poren zu schließen.

Das fotochrome Verhalten ist an das Vorhandensein von fotoaktiven Mikrokristallen in der Glasmatrix gebunden. Diese Mikrokristalle besitzen die Eigenschaft, nach Anregung mit UV- oder kurzwelliges sichtbares Licht ihren Absorptionszustand zu verändern, wobei diese Änderung nach Beendigung der Bestrahlung reversibel sein muss.

Ein Ziel dieser Arbeit war die Fortsetzung bereits vorliegender Untersuchungen, in denen Kupfer (I) halogenide, insbesondere Kupfer(I)-bromid, die mit Cd^{2+} -Ionen koaktiviert sind.

Wichtig für die Herstellung derartiger fotochromer Schichten ist es zu vermeiden, dass die Bildung und das Wachstum der Kristalle bereits während

der Herstellung der Sole und/oder Gele oder während des Beschichtungsprozesses stattfinden. Das bedeutet, dass Cu^+ komplex maskiert werden sollte, so lange bis durch die Wärmenachbehandlung das Wachstum der CuBr-Kristalle aktiviert wird.

Der Einbau von Cd^{2+} -Ionen in die Kristallstruktur von CuBr spielt eine entscheidende Rolle für den fotochromen Effekt. Die Cd^{2+} -Ionen rufen eine chemische Fehlordnung hervor: die zweiwertigen Cd^{2+} -Ionen besetzen Oktaederlücken im Halogenid-Teilgitter, während Cu^+ -Ionen Tetraederlücken besetzen. Zusätzlich erzeugen die Cd^{2+} -Ionen auch noch eine Kationenlücke. Dadurch wird offenbar die Beweglichkeit der Cu^+ -Ionen durch den Kristall hin zu den so genannten Empfindlichkeitszentren gefördert, wo sie mit den im ersten Schritt der Bestrahlung gebildeten Elektronen zu Cu^0 (Kupferatomen) reagieren können. Diese bilden in der Folge Kolloide und bewirken auf diese Weise eine Eindunkelung. In der vorliegenden Arbeit wird versucht die entsprechenden Defekte durch Zugabe von Zn^{2+} -Ionen zu verstärken. Damit könnte Cd^{2+} zumindest zum Teil durch ungiftige Komponenten ersetzt werden. Es ist gelungen durch Zn^{2+} einen Teil der Cd^{2+} zu ersetzen und die fotochromen Eigenschaften zu erhalten. Ein kompletter Ersatz war nicht möglich, weil dabei die fotochromen Eigenschaften verloren gingen.

Der Schlüssel für die gezielte Einführung von Defekten in die Kristallstruktur der fotoaktiven CuBr-Mikrokristalle besteht in der Beachtung von zwei Voraussetzungen: erstens ist für eine hinreichende Eindunkelung eine gewisse Kristallitgröße erforderlich, zweitens aber dürfen die Kristallite nicht zu groß sein, damit die Diffusion der Cu^{2+} -Ionen (Cu^+ und eingefangenes Defektelektron) durch den Kristallit zum Cu^0 -Kolloid schnell genug erfolgt für die Aufhellung. Wenn die Kristallite zu groß sind, dann werden die Schichten opak. Das passiert, wenn die Kristallitgröße in die Größenordnung der Wellenlänge des sichtbaren Lichtes kommt. Letztlich sind die Art und der Grad der chemischen Fehlordnung durch die so genannten Koaktivatoren in den CuBr-Kristalliten die effektivsten Mittel zur Steuerung der fotochromen Eigenschaften.

3 INTRODUCTION

Follows a short overview of some important concepts relative to the subject: “copper halide-based photochromic glass coatings”.

The first topic is about the demand for photochromic-coated flat glass in the world market; the position of the glass industry today and an idea about the demand for flat glass worldwide; the most recent technological developments on modified glass surfaces; the increasing environmental responsibility regarding energy consumption / efficiency; the options available in glass-modified surface technology to supply the energy efficiency demand. The routes for fulfilling the needs of the world market for photochromic coatings can be resumed in three different types of coatings: low-emission coatings (low-e coatings); smart electrochromic coatings and photochromic coatings. The advantage of the photochromic glass coating is that it is a single layer coating and contains less expensive active components compared to electrochromic coatings and low-e coatings.

In the second section, the sol-gel process is explained briefly. A description of the sol-gel technique precursors is given. The reactions that occur in the precursor solution are hydrolysis and condensation. These reactions allow the formation of a three-dimensional network Si-O-Si that is similar to the silica network contained in glass structure. The advantage of the sol-gel method is that it includes the organic route at room temperature and low-temperature heat-treatments, compared with the melting of inorganic components in order to obtain bulk glasses. The sol-gel process enables the production of very thin glass films, which can be obtained by diverse techniques such as dip-coating, and spin-coating among others.

The third subject is a brief introduction to the photochromic mechanism. The basic conditions of a photochromic material are presented. As well as an overview of the darkening and fading reactions based on silver halide glasses. The formation of silver colloids and electron holes, and the diffusion of these specimens through the crystal, are described in order to understand how the photochromic-effect works. The crystal size and the inclusion of crystal defects

are a very important tool to control the photochromic mechanism. This improves the level of darkening and the velocity of the fading reaction.

3.1 A view of the market

The new trend in architecture in the last few years has fuelled a great demand for flat glass production. The search for maximising natural light inside buildings increased efforts on researching and designing new flat glass properties, which could provide solar luminosity control and reduce solar heat gain.

According to an investment report from Pilkington [1], the global demand for flat glass is growing 3.5% annually. This growth is fuelled by the demand for building glass and automotive glass, which in turn is driven by economic growth. Glass is an integral building material for most construction projects today. Just take as example the all-glass façade buildings of modernization construction projects in cities like Berlin in the nineties and Warsaw now. Innovative projects as the Sony Center in Berlin and Złote Tarasy in Warsaw have a glazed façade and roof. Not only new building projects but also refurbishment of existing buildings call for large quantities of glass products. Building refurbishment accounts for around 40% of glass consumption worldwide, according to the Pilkington report. In mature markets, windows in residential buildings are replaced every ten to 20 years.

Besides the scenario of large glass consumption worldwide, another factor is also relevant, energy efficiency.

The Kyoto Protocol [2] set to reduce the emissions of greenhouse gases by the years 2008 – 2012 to the same emission levels back in 1990. Over 80% of the total greenhouse gas emission is due to CO₂. The household sector [3] is responsible for 12% of the CO₂ emissions and is one of the 5 target sectors for reduction.

Germany has already reduced 17% of the total CO₂ emission since 1987. The target for Germany [4] is to reduce 25% of the greenhouse gas emissions set by the Eco 92 in Rio de Janeiro compared to the levels in 1990.

According to the Royal Commission for Environmental Pollution, the UK must reduce its carbon dioxide emissions by 60% from its current levels by 2050. The building sector is one of the keys for emission reduction because it is responsible for 40% of the total carbon dioxide emission due to heating devices (boilers). The use of primary energy [5] grew from 2.5% per year from 1971 to 1990 and the building sector is responsible for two-fifths of the total global primary energy use.

Thus, energy efficiency has encouraged tougher building regulation legislation, making insulated glazing units mandatory in most of Europe [6]. Many countries also have regulations requiring energy efficient coated glasses.

Heat loss through windows is the largest energy efficiency problem of window performance. Windows with standard double-glazing have thermal resistance between R2 and R4, while gas filled and low emittance (low-e) glazing (multiple layers) reach up to R10. An R10 window will have a lower annual heat loss than a highly insulated wall. The R-value can be calculated from the thickness of the material “d” and the thermal conductivity “k” as follows:

$$R=d/k \text{ Km}^2/W$$

Equation 3-1

Unfortunately, to obtain those R10 windows (gas filled and low-e windows) at their best performance, many improvements are needed. These improvements are relative to reduction of costs, increase of durability and optical properties optimisation [7].

The low-e coatings can be applied directly to glass surfaces, they are highly reflective to long wavelength infrared radiation, and can be used to reduce the heat-loss and optimise the solar-heat gain. Low-e coatings applied on the inner window glazing allow infrared radiation to pass through the window from the outside and prevent the heat transfer in the other direction (inside towards outside). Thus, the building can take advantage of passive solar heating. This is recommended for buildings in regions of long and severe winter, where the low-e coating will avoid the heating from heating devices and gained solar heating to escape through the window.

On the other hand, low-e coating can be applied on the outside window glazing to reflect the infrared radiation outwards, preventing excessive heating inside the building due to solar heating gain. The use of cooling air conditioners can be reduced once the building inside is not overheated [8]. This is recommended for buildings in tropical climate regions where the year-average temperature is approximately 28 °C, and the winter days are a mere 3 or 4 weeks' a year.

Two kinds of coating can be used for solar gain control: passive and dynamic high performance coatings. The passive high performance coatings combine low-e and high transmittance coating in a multi-layer system. The dynamic high performance coatings are often called smart windows. They are chromogenic systems that change the colour (transparent/dark) according to electric or photo activation. The coatings activated electronically are called electrochromic. The coatings activated by light (photo) are called photochromic coatings. Specially the passive high performance coatings have to be protected against abrasion and corrosion and from impurities like metallic particles. The solution is to apply the coatings in one of the inner sides of a double glazed window to protect the metallic multi-layer coating from metallic particles. Another possibility to single panel window is the hard coating. It is a coating fused to the glass' surface to form a very abrasion and corrosion-resistant coating.

In general glass coatings are recommended for the inner side of a double glazed window. This allows solving mechanical wear problems since the coating will be protected against environment (see Fig. 3-1).

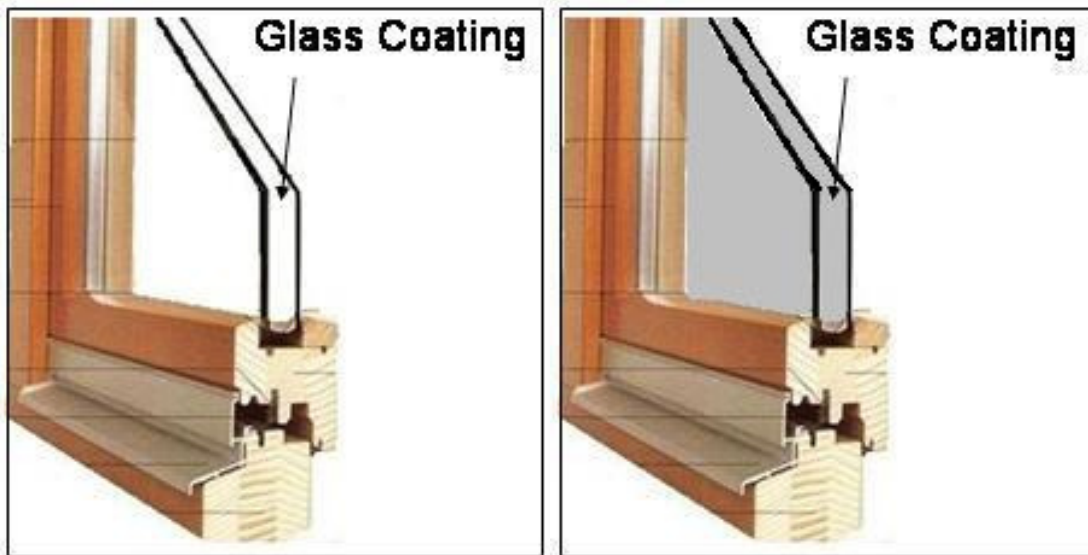


Figure taken from reference [82]

Figure 3-1: Schematic representation of the photochromic glass coating inside a double glazed window in the bleached state and darkened state.

The advantage of electrochromic coatings is that they can be switched on and off. The disadvantage of this system is costly manufacturing.

Photochromic coatings are dynamic systems that react to the presence or absence of solar light. This creates the possibility of having windows that protect the interior from solar light during the daytime and provide transparency at nighttime.

3.2 The sol-gel process

The sol-gel process is used to obtain solid products (bulk materials or coatings) from a precursor solution or suspension due to removal of its solvents, as an alternative method to melting and sintering processes, which need high temperature treatments [9].

The process starts basically with an alkoxide precursor, which is an organic-inorganic monomer molecule containing silicon as an inorganic core and an organic alkoxide-group. The tetra-functional silicon alkoxide behaves as a networking agent.

Through addition of water and alcohol, two reactions take place: hydrolysis which consists of substitution of OR-groups linked to silicon by OH-groups in order to form Si-OH; these silanol groups may react with each other in a condensation reaction, which lead to Si-O-Si bonds and subsequently to silica 3D-network formation. The condensation reaction is simultaneous and concurrent to hydrolysis.

The condensation can take place with partially hydrolysed species i.e. $\text{Si}(\text{OR})_x(\text{OH})_y$ where $(x + y = 4)$ resulting in various species $\text{SiO}_x(\text{OH})_y(\text{OR})_z$ where $(x + y + z = 4)$. During the condensation reaction, water is formed as a product and may contribute to new hydrolysis reactions. Therefore, it is difficult to split up both reactions and fix where each reaction starts and ends.

3.2.1 Thin films

Dip-coating is one of the methods available to produce thin layers on glass substrates. Comparing to other coating processes, the dip-coating process is the most simple due to its low equipment costs.

The dip-coating process in its most simple form is constituted of:

- Recipient with a precursor solution where the substrate is dipped in.
- A wire connected with a motor to withdraw the substrate from the recipient at a constant rate.

Fig. 3-2 shows the process described above.

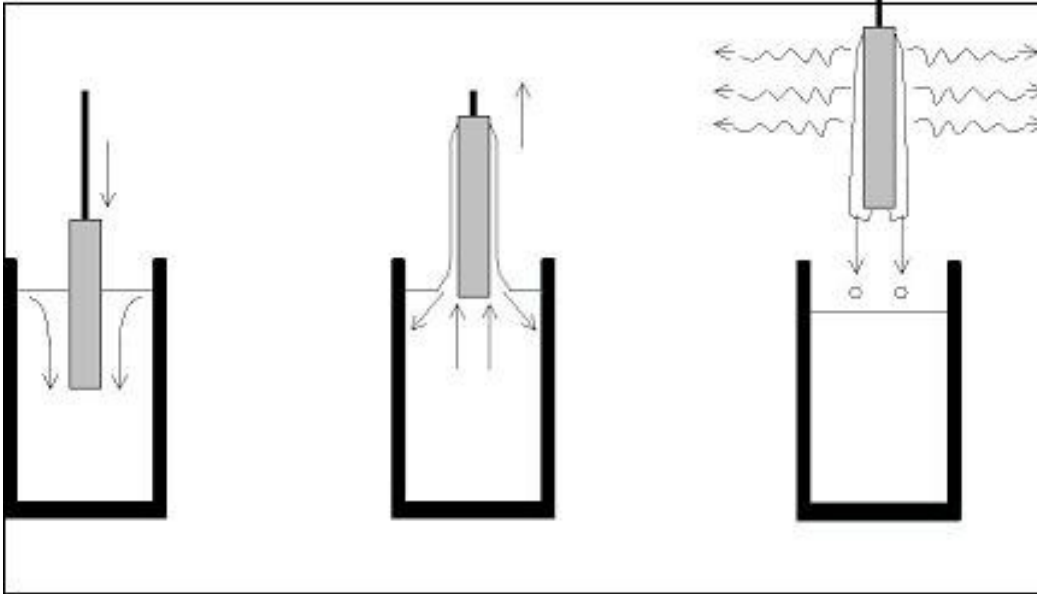


Figure taken from reference [10]

Figure 3-2: Dip-coating scheme: dipping the sample; withdraw at a constant velocity; evaporation of solvents.

The surface of the coating liquid must be undisturbed during withdrawal, otherwise it will result in coatings with horizontal bands. A vibration-damping unit can provide insulation to recipient and motor, which should have a smooth movement, to improve the coating quality. The substrate will be coated on both sides.

Before using any method of coating, it is necessary to clean the substrate surface that must be wetted uniformly and completely by the coating liquid. Anything on the surface that interrupts the liquid film will cause a coating flaw.

There are many other methods of producing thin films on substrates.

Spin-coating is a very rapid process, good for multi-layer applications and only a small quantity of coating liquid is required even for larger substrates. However, this technique is advantageous only for substrates with a rotational symmetry, such as optical lenses or eyeglass lenses. The substrate is attached to a turntable driven by a motor and spins around an axis, which is perpendicular to the area to be coated. The liquid is applied from a dropper to the substrate's centre. Once the substrate is flooded with the coating liquid, the rotation starts. The liquid film moves radially from the centre by centrifugal force and the excess is thrown off. The coated surface solidifies through

solvent evaporation. The coating thickness varies between several hundreds of nanometers up to 10 micrometers. This method requires a very extensive control of the viscosity of the precursor solution, which has to be in the Newtonian regime [10]. Only one side of the substrate will be coated (see Fig. 3-3).

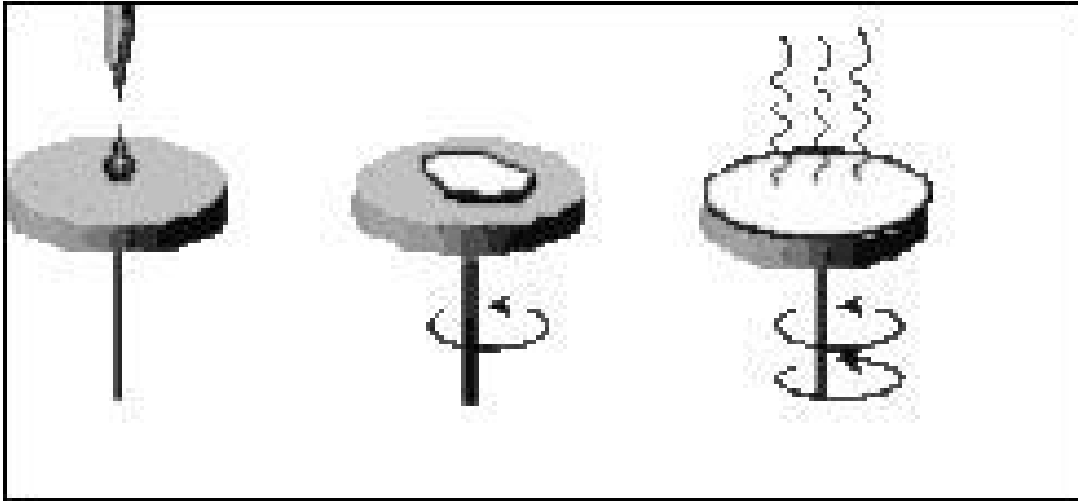


Figure taken from reference [10]

Figure 3-3: Spin-coating schematic representation: deposition of the sol; spin up; spin of and evaporation of solvents.

The capillary coating is an alternative process to enhance the optical quality of the coating and to reduce waste of coating material. A container with the solution to be coated holds a porous cylinder, which rotates while the substrate's surface moves over the cylinder without physical contact. A coating is created by the spontaneous meniscus generated between the cylinder's top and the substrate's surface, which moves horizontally (see Fig. 3-4). Coatings up to 15 μm thickness are obtained.

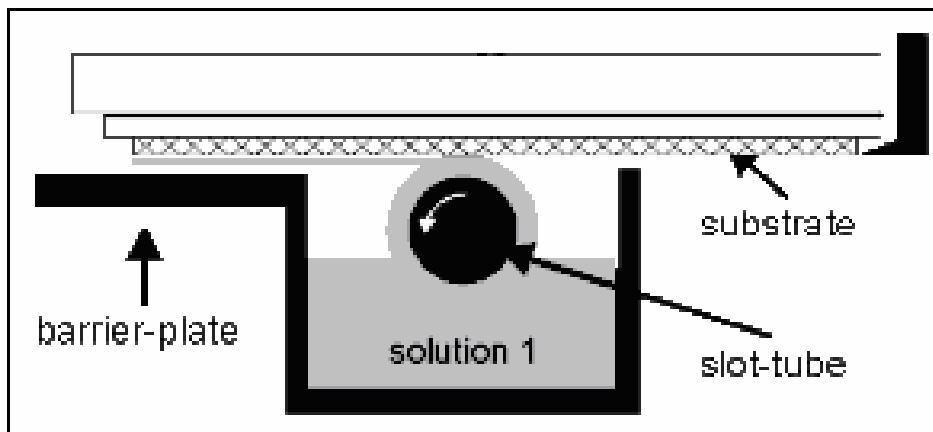


Figure taken from reference [10]

Figure 3-4: Schematic representation of capillary coating.

The flow method produces similar optical results as the dip-coating technique. The substrate is inclined on a specific angle and the coating solution is applied over the substrate (see Fig. 3-5). The thickness depends on the inclination of the substrate as well as coating solution viscosity and solvent evaporation rate. The advantage of this process is the possibility of coating non-planar large areas without excessive coating material waste.

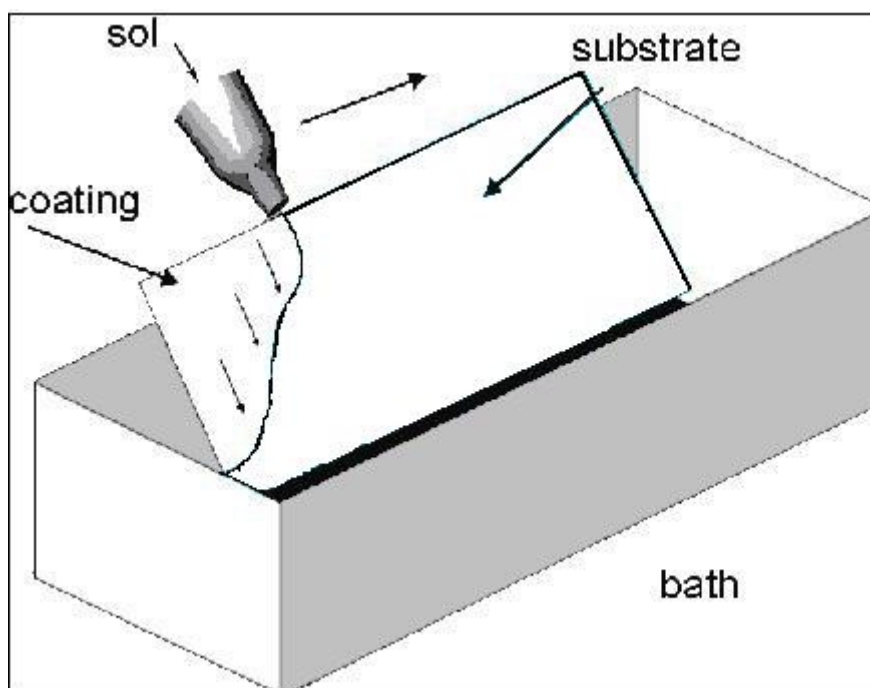


Figure taken from reference [10]

Figure 3-5: Flow-coating technique schema.

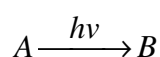
Despite all varieties of wet coating methods, the dip-coating is the preferred option as it can be easily developed by any laboratory.

3.3 Photochromism

The term photochromism has been used to describe the phenomenon of reversible, light-induced colour changes exhibited by many organic and inorganic compounds [11].

Many theories try to explain the mechanism of photochromism. In this brief introduction, the oldest system will be presented, the silver halide system. In the following chapters the copper bromide system will be explained.

Photochromism is a change in colour of a solid or liquid from state A to B when induced by light irradiation. This change is reversible; from B to A when the irradiation stops [12].



Equation 3-2

In a short-term change, photochromic glasses turn completely dark after a short and intense irradiation, they can be used to protect the eye during welding, or from lasers or nuclear explosions.

The first photochromic systems on glass made of organic compounds were reported already in the 50's [12].

The disadvantage of these organic systems is that the reversible effect is lost after a number of cycles depending of the intensity of irradiation, because many competing side-reactions take place using coloured organic molecules.

This problem can be solved using inorganic compounds to achieve the photochromic property.

Later developments on the 60's reported the first inorganic photochromic glasses. Today, they can be used as display, image converts, sunglasses, and glare protection.

According to Veit [13], the photochromic mechanism of silver halides (AgX) starts with the formation of a positive-hole (p^+) due to a missing electron (e^-).

The absorption of a photon may result in the excitation of an electron at a lower band to an upper band. This corresponds to an electron transition from the valence band to the conduction band [22].

The energy necessary to produce excited electronic states, in which electron-hole pairs are bound together (excitons), is smaller than the energy required to produce free-electron and positive-holes for silver halides.



To avoid the re-combination of the released pair electron (e^-) /positive-hole (p^+), Cu^+ is introduced in the crystal. The positive-hole is captured by a Cu^+ . The Cu^+ acts as a hole-trap centre. The Cu^+ ions are called sensitizers.



Allowing ionic motion in the crystal will result trapped-hole centres (Cu^{2+}) and aggregates of silver (Ag^0). The aggregates of atomic silver are responsible for the darkening [14].

The silver cations occupy the centre of an octahedron surrounded by 6 anions one at each corner in the lattice site, whereas a Cu^+ ion occupies a tetrahedral hole [15]. A Cu^{2+} ion, due to its coordination proportion, strives for a silver lattice site. The silver ions are displaced to a space between the lattice sites and start to migrate to the crystal boundaries in order to minimize their energy. The electrons released in the first step combine with these silver ions and form silver atoms, which agglomerate in colloidal particles. This results in darkening.

The bleaching mechanism depends on thermal migration of Cu^{2+} through the crystal. The positive-hole trapped by Cu^+ in the first step of the darkening process, removes one electron of a silver atom when they get close to each

other. The colloidal agglomerate of silver atoms will be disaggregated and the bleaching process is concluded.

The bleaching can also be reached using light of special wavelengths. The light activation will disturb the colloidal agglomerate of silver atoms by exciting electrons. The electrons will be released and be available to combine with Cu^{2+} and revert the process [16].

Later in Chapter 8.4, photochromic mechanism of copper halide systems will be discussed.

3.3.1 Accordance between crystal size and photochromic properties

According to Müller et al. [17] the size of crystal phases influences the photochromic effect. It was observed that the photochromic effect increases with increasing crystal phase size until a maximum (90 nm) then the photochromic effect starts decreasing. Photochromic effect refers to intensity of darkening and velocity of bleaching reactions.

Crystal phases up to 90 nm in diameter size will darken very intensely but the bleaching process will be slower than the bleaching for smaller crystal phases. On the other hand, crystal phases have a minimum size to start having measurable photochromic effects. This phenomenon is explained by Veit [18] for silver containing photochromic glasses and can be used for silver-free glasses as well. The copper halide crystals formed after heat-treatment, are the active component, and the defect lattices of copper halides crystals are the photochromic effect carriers.

Veit [13] affirms that positive-hole traps are volume centres. Cu^+ ions (sensitizers) trap a positive-hole ($\text{Cu}^+ \text{p}^+$) and become Cu^{2+} ions, which are more stable than Cu^+ . Sensitivity centres are boundary centres. In the sensitivity centres the Ag^+ will trap the released e^- and form Ag^0 . Both centres are concurrent with each other until a nucleus of metal colloid is formed. Greater agglomerates of metal colloid cause the darkening effect. The fading occurs when a Cu^{2+} is in the vicinity of a Ag^0 . The reaction opposite to the ones described above will occur and decompose the colloids. Diffusion reactions are

stronger over the crystallite boundaries. This explains why the fading reaction is faster than the darkening reaction [19, 20]. As well as the reasons why small crystallites show a low darkening level and a high fading rate, compared to larger crystallites with the same volume concentration.

Free electrons and positive-holes are released by absorption of light and they move through the crystal randomly. They are scattered by lattice thermal vibration and may become trapped by dislocations in the crystal lattice [21]. The traps can be shallow or deep resulting in temporarily or permanent trapping. Cu^+ is a good hole trap for use in silver halide crystals [22].

In the case of copper halide crystals, the Cu^+ is the active component and the photochromic effect carriers are Frenkel and Schottky defect lattices. Because the formation of those defects is strongly dependent of temperature and ions conductivity laws, the addition of bivalent ions (such as Cd^{2+}) will act as a source of lattice defects. It will reduce the interstitial defects and increase the number of vacancy defects which are more effective for ion conduction than interstitial defects. In this instance, the influence of temperature on ionic conductivity decreases, and consequently the photochromic effect is optimised [25].

The idea of working with defects lattices of CuCd - halides crystals is to create enough defects on the crystallites lattice to improve the diffusion of specimens responsible for the photochromic mechanism. This will allow deeper darkening even on small crystals and a fast bleaching.

3.3.2 Photochromic properties

The following table 3.1 gives an overview of the photochromic characteristics that will be discussed further on this work.

Table 3-1: Description of the measurable photochromic characteristics

Property	Definition
Initial Transmission	Transmitted light before irradiation, which corresponds to the sample's transparency level.
Final Transmission	Transmitted light after 5 minutes under irradiation
Transmission Decrease	Difference between initial transmission and final transmission
Half-Darkening Time	Time necessary to darken 50% of the total transmission change
Half-Fading Time	Time necessary to fade 50% of the total transmission change

4 THE STATE OF THE ART

A brief introduction on development of photochromic glasses and coatings will be shown in this chapter. It describes the first photochromic systems to be discovered in the early sixties and how the need to study new systems appeared through the years.

The photochromic glasses research starts with the very first silver halide based photochromic glass developed by Corning in the sixties. However, the use of melting process at high temperatures are not suitable for silver halides as they have low melting temperature (melting point of silver chloride is approximately 455 °C) what leads to excessive evaporation and loss of material at temperatures as high as 1554 °C. Instead of using silver halides to melt photochromic glasses, silver nitrates and sodium chlorides or bromides are used. Thus, the silver and halogen ions are better protected against evaporation and oxidation (halogen ions). Those ions are dissolved in the cooled glass gain mobility during extra heat-treatment and will precipitate as silver halide crystals. The heat-treatment happens above the glass transition temperature (T_g) approximately 600 °C and above the silver halide melting temperature. In this instance, the silver halide microphases are liquid and have a spherical shape (droplets). When the glass is cooled down to room temperature, the liquid silver halide phases crystallise and keep the spherical shape as it happens below T_g [23].

A new branch of photochromic glass systems was developed in order to substitute the silver halide system. These systems include cadmium oxides, alkaline-earth-tungstates and copper halides among many others. The disadvantages of these systems are, among others, the need of melting in atmosphere and poisonous.

The need to avoid the precipitation of photochromic microcrystals during the melting to control the crystal growth and the final size of the photochromic crystal leads to new developments of alternative processes such as sol-gel method.

Another advantage of the new process is the possibility of obtaining very thin films and work with low temperatures which represent economy of raw material due to lower evaporation rates and energy efficiency in the production plant. Now the photochromic coating can be applied to any glass surface, independent of its substrate composition.

Diverse photochromic coating systems were studied around the world alternating the active photochromic component, the solution preparation and the coating application process [15,16,17,18].

Various authors extensively studied the copper halide system. Being an inexpensive raw material, and due to an intense absorption of visible light, copper halide crystals, as a photochromic material is very attractive. The dip-coating process is the simplest coating technique. Both, the copper halide system and the dip-coating technique are this work's subject of study. The aim of this work is introduced briefly in the end of this chapter.

4.1 The first photochromic glasses and the silver halide system

The photochromic effect of glasses doped with silver chloride was first observed in the early sixties by Armistead and Stookey [24]. Silver and halides (Cl^- , Br^- , $\text{I}^- = \text{X}$) are added to the batch in order to melt alumoborosilicate glasses. Heat-treatment is done between the glass annealing and softening temperatures. This promotes nucleation and growth of molten silver halide microdroplets that crystallize in very small silver halide crystallites (AgX), when the glass cools below the halide melting point. Copper ions are used as sensitizer. They obtained a transparent glass that darkened under exposure to light (sun) and would return to its original transparent state after eliminating the light source. Some obtained glasses were opaque, due to the size of the silver halide crystallites, which scattered the light.

4.2 The search for alternatives to silver halide glasses

Since the end of the sixties there was a demand for photochromic glasses not based on silver halides because in the glass industry, working with silver

compounds was undesirable due to high material costs and process costs at first. Besides, silver halides containing glasses are in some cases too sensitive to incident irradiation light and temperature. New alternatives are created in order to solve these problems.

Garfinkel [25] affirms that glasses melted without any silver salt present in the batch can be made photochromic. Using a proper heat-treatment in a silver salt bath of an initially ion exchanged sample. This allows the use of higher temperature melts, since no high volatile silver salts are present at the batch, and larger amount of silver halide can be introduced to the glass without affecting the transparency.

In 1970 Georg Gliemerth [26] obtains phototropic properties of a glass using the system $\text{SiO}_2 - \text{B}_2\text{O}_3 - \text{CdO}$.

In 1971 Sumio Sakka [27] obtained a phototropic glass ceramic containing bismuth doped calcium tungstate crystals. They discovered that silicate and borate glasses are especially effective in forming glass-ceramic, comprising a glassy matrix and a crystalline material of an alkaline-earth-tungstate, such as calcium tungstate and barium tungstate. They concluded that bismuth was present not as a separated phase, but was incorporated in the structure of the alkaline-earth-tungstate. The glass ceramic samples darken rapidly when exposed to UV light. They fade in absence of UV light. The fading is promoted by heating the sample or exposing it to visible light.

4.3 Copper halide systems

Araujo [28,29] first described transparent photochromic glasses containing both copper halides and cadmium halides in 1979. Araujo used the alkali-aluminoborate glasses. The resulting photochromic glasses were comparable with the best silver halides photochromic glasses. Compared to silver halide systems the advantages of this system are a lower batch price, reduced dependence of photochromic properties on glass temperature and a nearer relationship between the intensity of the incident light and the photochromic darkening induced thereby in the glass.

Kadonno et al. [30] produced CuCl doped aluminoborosilicate and borosilicate based glasses to study the effect of glass composition on precipitation of CuCl crystallites and concluded that phase separation of glass is necessary to grow the crystallites on bulk glasses. After quenching, the glasses were transparent and slightly yellowish. UV-VIS spectra of borosilicate glass annealed at 580 °C showed an absorption peak at 370 nm of CuCl excitons, but no absorption peak of CuCl excitons were found for aluminoborosilicate glasses.

4.4 Introduction of Cd²⁺ as co-activator in copper halide systems

The use of Cd²⁺ as co-activator in the silver halide photographic process is known since 1937. Koch and Wagner [31] devised the incorporation of immobile divalent impurities to control the ionic conductivity in the silver halide crystal.

Mees [32] explains the rule of Cd²⁺ as an inductor of defects at room temperature. The Cd²⁺ occupies an interstitial silver ion place, reducing the concentration of interstitial ions; for each added Cd²⁺ one additional silver ion vacancy must be added to compensate the divalent ion. Using large concentrations of Cd²⁺ will equal the concentration vacancies defects to the Cd²⁺ concentration and the concentration of interstitial defects will tend to zero. Thus, the ionic conductivity can be ruled by the concentration of Cd²⁺ by two different and concurrent processes. The increase in vacancies defect concentration will produce an increase in conductivity due to a larger mobility of vacancy ions (observed for larger amounts of Cd²⁺ impurities). However, addition of small quantities of Cd²⁺ can cause a decrease in conductivity, in this case the increase in the number of vacancies is compensated by the decrease in the number of interstitials. The mobility is only due to interstitial Cd²⁺.

Kriltz [33] compares the influence of Cd²⁺ on the glass composition containing copper halide. The Cd²⁺ ions execute a strong influence on the glass' photochromic effect: glasses without Cd²⁺ do not darken; the addition of increasing Cd²⁺ results in increasing darkening degree and increasing of the

fading velocity of deep darkened glasses ($\text{CdO} = 0.35$ weight %) when compared to glasses with poor Cd^{2+} content ($\text{CdO} = 0.18$ weight%).

The addition of Cd^{2+} increases the precipitation of copper halide crystals on the glass. The presence of CdO/CdS in the glass increases the nucleation forming many small crystals. The presence of too many small crystals decreases the glass viscosity leading to a slow crystal growth.

The gain on crystallite's size has a positive impact on the photochromic effect (deeper darkening degree), However, the expected negative effect on fading velocity is suppressed by the increase of defects caused by Cd^{2+} on copper halide crystals.

4.5 Sol-gel process as a new method of producing bulk glass and glass coatings

The sol-gel process is an alternative low temperature method to synthesize photochromic glasses and coatings.

In general photochromic glasses are synthesized through melting. The melting is followed by a phase precipitation of nanoparticles. This method restricts the use of materials due to the high temperatures involved in the process. Furthermore, it is not possible to synthesize thin films by melting method, due to the high viscosity of the molten glass (2×10^7 dPas for SiO_2 glass at 1600°C)[34]. The sol-gel method can be used to synthesize both bulk glasses and coatings, which can be applied to commercial glasses in order to modify and improve their surface properties.

Back to the silver halide systems, Zayat et al. [35] reported on the first observation the reversibility of SiO_2 sol-gel films doped with AgCl crystallites at room temperature exposed to nitric acid vapours. The films were prepared dissolving silver nitrate and trichloroacetic acid in the precursor sol silica glass based.

Nogami et al. [36] studied CuBr semiconductor crystals in glasses made via sol-gel process. They assume electron hole carriers and excitons to be confined in the deep three-dimensional potential in a glass matrix. They

studied silica glasses doped with CdS, PbS, ZnS and CuCl with sizes between 2 nm and 10 nm and large quantum size effect.

Kriltz et al. [37] who synthesized photochromic bulk glasses containing cuprous halide microcrystals through sol-gel method. CuBr dissolved in CH₃CN, was added to the Al₂O₃ - SiO₂ based sol-gel. Heat-treatments at 280 °C and 410 °C were carried out in order to remove the organics and the following heat-treatment at 700 °C in nitrogen atmosphere reduced Cu⁺ to form CuBr. The achieved photochromic effects on small sol-gel glasses measured under UV irradiation is 24% darkening of the initial transmission and 13% fading in the first 10 min after ceasing the irradiation.

4.6 Photochromic coating with complete reversibility at room temperature and normal atmosphere

Kriltz et al. [38] succeeded for the first time producing glassy coatings via sol-gel process with complete reversibility of photochromic reaction at room temperature and atmosphere. Using a silicon alkoxide based solution containing photoactive components, which were later during heat-treatment precipitated. The photochromic properties were carried out by cuprous halide microcrystals, which have higher absorption coefficients compared with silver halides. This particularity leads to an increase of the darkening intensity. The initial transmission was approximately 57%. After 15 min under UV irradiation, the coatings darkened approximately 50% of initial transmission. The half darkening time was 60 s. The fading started after switching off UV irradiation. After 5 min the transmission increased approximately 10%. The complete fading was achieved after 10 h approximately. They assume that carriers for photochromic effects are cuprous halide microcrystals precipitated on the coating surfaces during a heat-treatment. Both crystallization behaviour and photochromic properties are dependent on coactivating agent contents.

Suyal [39] has used a sol-gel method to synthesize thin films containing CuCl_xBr_{1-x} nanocrystals. The copper was stabilised as Cu⁺ and formed, in the presence of acetonitrile, an acid soluble halocuprate complex in solution. It was confirmed by UV-VIS spectroscopy and XRD measurements that CuX₂⁻ and CuX₃²⁻ complexes decompose with heat-treatment to form CuCl and CuBr.

The sol-gel method is a low temperature process that allows the use of relatively higher concentration of copper precursor to be incorporated in the sol-gel material.

There are some special requirements in order to obtain a photochromic coating: the matrix material around the photochromic microcrystals should be inert – that is no interaction with the products of photochromic reaction; the crystal size should be in the range from 10 to 50 nm in diameter; the crystals should be disordered - insertion of foreign ions or synthesis of mixed crystals [14].

Marquez [40] obtained $\text{CdCl}_2:\text{CuCl}$ photochromic coatings by vacuum deposition of cadmium chloride and copper chloride. Films with 10% CuCl presented a half fading and half darkened times of 5-10 min and 1-3 min respectively and a change of transmittance of 45%.

Natsume [41] prepared zinc oxide films by sol-gel spin-coating method. The films were prepared by 10 cycle spin-coatings on Pyrex glass – drying at 80 °C for 10 min – annealing at 500 °C – 575 °C for 20 min. The films were transparent in the range above 400 nm and hard sharp ultraviolet absorption edges at 380 nm. It is not clear whether cadmium halide crystals or copper halide crystals activate the photochromic process in systems when both are present.

4.7 The aim of this work

The improvement of the photochromic coating based on $\text{CuBr}:\text{CdBr}_2$ mixed microcrystals and a SiO_2 glassy matrix, which is already studied by the work group which involves A.Kriltz, M.Mueller, H, Buerger, R. Fachet and will be mentioned as Kriltz et al. in the following text.

The synthesis will be through the sol-gel method using tetramethoxysilane (TMOS) or tetraethoxysilane (TEOS).

The sol will be applied on a microscope slide (soda-lime glass) using a dip-coating equipment.

The main objective was to improve the darkening and fading rates, increase the change in transmittance (increase the darkening intensity) and the initial

transmittance. During the development of the project various uncertainties about the use of cadmium came up. Would it be possible to substitute the cadmium content for another bivalent ion, which is not hazardous?

The substitution of cadmium concentration through zinc is a main concern today due to stronger environmental legislation such as the Restriction of Hazardous Substances, which banned the use of cadmium in electronics and electrical products sold in the EU that comes into effect on 1st July 2006 [42, 43]. The use of cadmium in Japan dramatically declined following the accident of itai-itai disease in the late 1960s. In Sweden the use of Cd was restricted due to increase of Cd levels in human tissue due to Cd use in phosphate fertilizers. In Australia and several countries the use of Cd in phosphate fertilizers was restricted as well due to Cd transfer to food crops [44].

Another aim of this work is to clarify how the photochromic mechanism acts due to copper and cadmium halides. Is it a cadmium halide crystal with copper acting as co-activator or the other way around? Which roles play Cd^{2+} and Cu^+ in the crystallite during exposition to actinic irradiation and how the addition of Zn^{2+} influences the photochromic effect?

Once knowing the exact role of Cd^{2+} in the photochromic process, it might be possible to find another agent non-hazardous to substitute the cadmium content.

5 EXPERIMENTAL PROCEDURE

This chapter explains all the steps necessary to produce the photochromic coatings by sol-gel method.

It starts with the preparation of the sol-gel solution. The sol-gel process has been known as an efficient, method to produce a three-dimensional network by chemical reaction at a low temperature. The usual starting materials are silicon alkoxides such as tetraethoxysilane (TEOS) and tetramethoxysilane (TMOS) [45]. As silicon alkoxide it was used TMOS, because it showed a better adhesion to the substrate (microscope slide) than TEOS. 3-glycidoxypropyltrimethoxysilane (GPTS) was partially added in order to obtain thicker coatings [46].

The hydrolysis and condensation took place with water addition and ethanol was used as a solvent.

It was not possible to insert Cu^+ ions directly into the solution because they can be oxidized in the presence of water. The precursors used for copper halide photochromic microcrystals were copper(II)nitrate trihydrate ($\text{Cu}(\text{NO}_3)_2 \cdot 3\text{H}_2\text{O}$) for Cu^+ source, and hydrobromic acid for Br^- .

One important problem to solve during the sol-gel process is to stabilize the photoactive components in the sol. In the melting process this problem does not exist because the CuO is easily reduced to Cu^+ due to the high temperatures (~ 1500 °C) of the process.

In the sol-gel process the Cu^+ ions complexation is the key to shift the equilibrium to the Cu^+ side at low temperatures using reducing agents [33].

Cadmium acetate dihydrate ($\text{Cd}(\text{CH}_3\text{COO})_2 \cdot 2\text{H}_2\text{O}$) was added as a source of co-activator Cd^{2+} . As described by Deri et al. [70] the use of any divalent closed d-shell dopants such as Pb^{2+} and Cd^{2+} may increase the photo response of silver halide systems by formation of impurity band by dopant ions at the grain surfaces.

Table 5-1: List of all chemicals used for the preparation of the sol

Compound	Formula	Produced by
Tetramethoxysilane	$\text{Si}(\text{OCH}_3)_4$	Aldrich Chemie
(3-Glycidoxypropyl)-trimethoxysilane	$\text{C}_9\text{H}_{20}\text{O}_5\text{Si}$	ABCR
Ethanol GR for analysis	$\text{C}_2\text{H}_6\text{OH}$	Merck KGaA
Copper(II)nitratetrihydrate GR for analysis	$\text{Cu}(\text{NO}_3)_2 \cdot 3\text{H}_2\text{O}$	Merck
Cadmium(II)acetate dihydrate GR	$\text{Cd}(\text{CH}_3\text{COO})_2 \cdot 2\text{H}_2\text{O}$	Merck
Cadmium(II)acetylacetonate For synthesys	$\text{Cd}(\text{CH}_3\text{COCHCOCH}_3)_2$	Merck Schuchardt
Zinc acetate dihydrate GR for analysis	$(\text{CH}_3\text{COO})_2\text{Zn} \cdot 2\text{H}_2\text{O}$	Merck HGaA
Hydrobromic acid 47% GR for analysis	HBr	Merck KGaA
Acetic acid 85% GR for Analysis	CH_3COOH	Merck

The next step is the coating process, which starts with cleaning of the substrates to be coated. Follows a brief explanation about how important is the cleanliness of a substrate and how it should be done [49].

Then the dip-coating equipment is described and the process divided into 3 steps: the immersion of the substrate in the precursor solution; the substrate's

withdraw from the solution with coating formation; the evaporation of the solvents from the coating.

High viscosities of the solution and high withdraw velocities will give a thick coating in one application comparing to an application where the solution viscosity and withdraw velocity is lower [47]. Many different withdraw velocities were studied in the group [48], the maximum used withdraw velocity was 30cm/min.

The following step is the coating drying in a heating chamber for up to 24 h at temperatures between 50 °C and 100 °C. This step is responsible for the evaporation of solvents and water present inside micro pores of the gel. At this stage the copper halide photochromic microcrystals do not exist.

The last step is the heating treatment of the substrate. Temperatures between 300 °C and 500 °C are sufficient to burn the organic material and form a xerogel that has the same structure of a glass but is also porous. This step is also responsible for the formation of photochromic microcrystals. The glassy structure is formed if heat-treatment is applied over 900 °C eradicating the porosity.

The temperature used however, was not higher than 300 °C because higher temperatures cause the evaporation of photoactive components.

During the heat-treatment, various transformations occur such as evaporation of structural water, solvents (ethanol), and the carbonisation and oxidation of organic groups [33].

The heating treatment used had no heating or cooling stage. The sample is put into the pre-heated furnace as soon as it reaches the desired temperature and is taken out of the furnace as soon as the programmed time is reached. This allows the efficient use of the furnace as there is no need to wait for the furnace to cool and many subsequent treatments can be done.

Temperatures lower than 130 °C need more than 40 min to activate the growth of copper bromide crystals (it will be shown later in the Chapter 7, Fig. 7-6) and higher temperatures (175 °C) activate the copper bromide crystal growth in less than 1 min (see Chapter 7, Fig. 7-7).

5.1 Sol-gel preparation

The glass-matrix chosen to carry the copper halide photochromic crystals is a SiO₂ matrix as used by previous works in our group [48], introduced by the preparation of Si-alkoxide sol-gels.

The copper halide precursors were Cu(NO₃)₂·3H₂O and Cd(CH₃COO)₂·2H₂O, both dissolved in water and bromidic acid respectively.

At the alkoxide sol-gel process, the different needed substances will be mixed in ratios (*r*) relative to the alkoxide content according to the so-called *r_x* -values.

The parameters of water molar ratio (*r_w*), solvent molar ratio (*r_i*) and acid molar ratio (*r_s*) were fixed to 4: 4: 0.5 per mole of alkoxide.

These ratios follow the most successful compositions used in our previous work as mentioned above. These parameters were fixed carefully after extensive trials in order to provide enough water for hydrolysis and condensation of Si-alkoxide, which was sufficient to delay the gelatinisation and enable the deep coating process.

The solution, if stored at room temperature and protected from humidity, would remain stable for more than 4 weeks, with no sign of precipitation or gelatinisation.

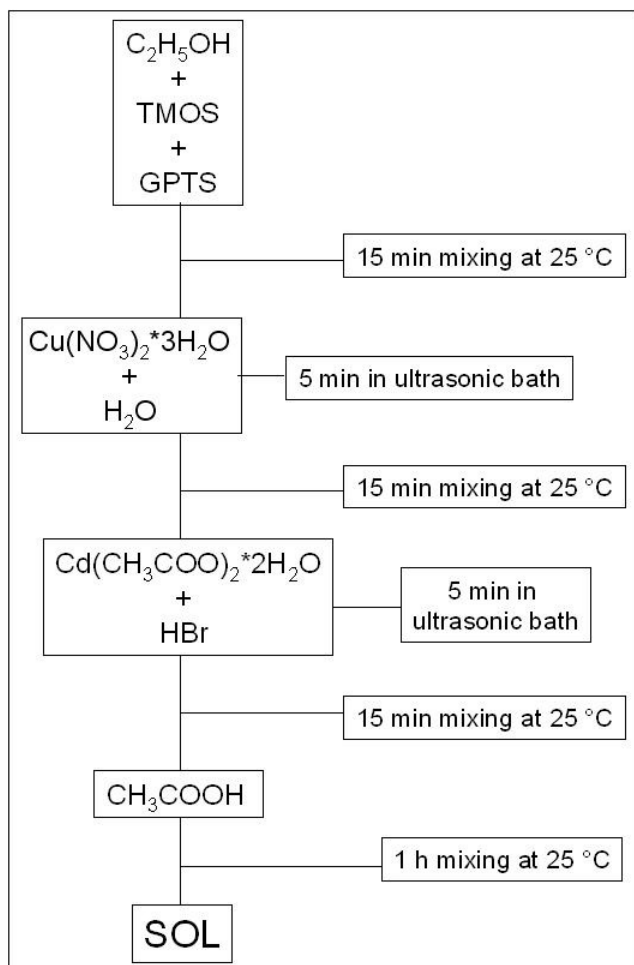


Figure 5-1: Schematic representation of the sol-gel process.

The process consists of stirring 41 mol% Ethanol with drop-wise added 5.1mol% tetramethoxysilane (TMOS) and 5.1mol% (3-glicidoxypropil)-trimethoxysilan (GPTS). All the following components will be added drop-wise to this solution and stirred for 15 min.

Copper(II)nitrate trihydrate was dissolved into water (41 mol% including the water present at used components as HBr and CH₃COOH) before being added to the solution. The compositions had the water and copper(II)nitrate trihydrate content modified between 0.6 mol% to 2.1 mol% and 0.05 to 2 mol%, respectively. Cadmium acetate dihydrate was dissolved into hydrobromic acid and added to the solution. The solution had the cadmium acetate dihydrate content varied between 0 mol% and 1.4 mol%.

The final component to be added is acetic acid which had the percentages altered between 0 mol% and 2.4 mol%.

The complete solution was stirred for up to 1 h and left to rest for another 2h before being used to dip coat the glass substrates.

5.1.1 Co-activators variation

All compositions were listed at Appendix 10-2. The following table displays the main researched compositions and the main results and explanations why they were not followed.

The co-activators were varied according to the following table in order to optimise the CuBr crystal size and precipitation volume.

The addition of $\text{Cd}(\text{CH}_3\text{COO})_2 \cdot 2\text{H}_2\text{O}$, was kept as small as possible because during the heat-treatment CdBr_2 crystals were formed instead of CuBr. This will be explained later by the X-ray diffraction results.

In order to prevent the precipitation of CdBr_2 , cadmium acetate dihydrate was substituted by cadmium(II)acetylacetonate.

Finally zinc acetate dihydrate was introduced in order to substitute cadmium(II) acetate dihydrate.

The hydrobromic acid acts as a hydrolysis catalyser in the sol-gel process. It adds protons to the alkoxyde group which reduces the electron density around the silicon atoms. The hydrolysis water achieve its nucleophilic attack.

The acetic stabilizes the coating in a flaw-free, bubble-free coating. It is responsible for shifting the pH-value to a higher value and increases the silicon-oxygen polyhedrons condensation.

The Table 5.2 displays the most studied compositions and the molar percentage of each component.

Table 5-2: List of the most studied compositions (in Mol%)

Composition code	Cu(NO ₃) ₂ * 3H ₂ O	Cdac ₂ *2H ₂ O #	Cd(acac) #	Znac ₂ * 2H ₂ O #	HBr	Hac #
K26	1	1	-	-	5.1	-
K27	1	2	-	-	5.1	-
K28	1	1.5	-	-	5.1	-
K2	1	0.5	-	-	5.1	-
K1	2	-	-	-	-	-
K7am	0.9	1.4	-	-	4.7	9.3
Z4	1	0.8	-	0.6	4.7	9.3
CDT4	0.9	0.8	0.6	-	4.7	9.3

ac = CH₃COO, acac = acetylacetonate

5.2 Coating process

The coating process is started by vigorously cleaning the substrates to be coated in order to avoid any contamination disturbing the film quality.

To achieve particle removal from the substrate one efficient method is the use of ultrasonic cavitation in an aqueous surfactant solution [49].

The surfactant solution must be diluted properly to avoid formation of gas bubbles because it will absorb cavitation energy and lead to poor cleaning efficiency.

At first the surfactant phosphate based cleaning solution is diluted in deionised water (1% by weight) and poured into a glass beaker. Plastic containers should not be used as they do not properly transmit the ultrasonic energy. The beaker with the substrate inside is placed into an ultrasonic bath. The ultrasonic agitation is activated for 10 min.

The ultrasonic bath operates at a frequency of 40 kHz, it generates a standing wave pattern cleaning the sample vigorously at some spots and leaving others

unaffected. A uniform cleaning can be reached if the beaker is moved from one place to another in the bath.

After rinsing the substrate with deionised water, the beaker is filled again with deionised water for a more effective rinse under ultrasonic agitation for another 10 min. The use of deionised water is important to prevent organic contamination. The organic molecules present at water may deposit on the glass substrate re-contaminating the surface.

Again the substrate is rinsed with deionised water and the beaker is filled for the third time with ethanol 99.99% and the substrate is cleaned for more 10 min by ultrasonic agitation.

The substrate is immediately put into a heating chamber to dry and is ready to be coated.

The substrate used was a microscope slide, which is made of soda-lime-silica glass. It contains approximately 16% sodium oxide. Na^+ can be ion exchanged in water against H_3O^+ and form sodium hydroxide. The reaction can occur in ambient air leading to the formation of a sodium hydroxide film on the glass surface.

The microscope slide is fixed to a vertically sliding arm with mechanically controlled velocity as shown in Fig. 5-2.



Figure 5-2: Dip-coating instrument.

The equipment immerses the substrate perpendicularly to the coating solution surface. After 30 s of immersion, the arm withdraws the substrate at the programmed velocity forming a film on both sides of the microscope slide. The gel formation starts with solvent evaporation. The samples were immediately put in drying chambers to intensify the evaporation of solvent, and to prevent contamination.

The withdrawal velocities were varied between 2 cm/ min to 80 cm/min. Higher withdraw velocities result in thicker coatings because the solution has not enough time to drain off from the substrate.

In order to improve the darkening intensity, two alternatives to produce thicker coatings were used. First increasing the coating withdraw velocity up to 80 cm/min. Double coatings using different withdraw velocities and coating the same sample twice were also tested. The film's thickness varied between 200 nm and 2 μm .

The preferred withdraw velocity was 30cm/min because thinner coatings (withdraw velocities from 2cm/min to 25 cm/min) did not result in desirable darkening intensity. On the other hand, thicker coatings (formed by withdraw

velocities in the range between 40 cm/min and 80 cm/min) had the transparency affected after the heating treatment. Although their darkening intensity was higher, they were opaque and the coating quality was insufficient. The same happened to the double-coated samples. This allows us to discard the double coating process and to use withdraw velocities higher than 30 cm/min.

Table 5-3: List of all studied withdraw velocities and the corresponding visual aspect after drying and heat-treatment for the composition K28

Withdraw velocity (cm/min)	Aspect after coating	Aspect after drying at 100 °C/24 h	Aspect after heat-treatment
2	Transparent	Transparent	Transparent
5	Transparent	Transparent	Transparent
10	Transparent	Transparent	Transparent
15	Transparent	Transparent	Transparent
20	Transparent	Transparent	Transparent
25	Transparent	Transparent	Transparent
30	Transparent	Transparent	Transparent+deepest darkening
50	Transparent	Opaque+ strongly rough	Damaged coating
80	Transparent	Opaque+ strongly rough	Damaged coating
30 (Double)	Transparent	Transparent	Opaque

5.3 Drying stage

The next stage in the production of glass film made from sol-gel technique is the evaporation of solvents, which are occluded in micro-pores formed inside

the three-dimensional silica network gel. Temperatures up to 100 °C are enough to volatilise present solvents.

The samples were dried at 100 °C for 1 h to 24 h. Drying periods longer than 24 h could lead to crystallization and produce an opaque sample. These samples were photochromic. It indicates that the long drying process activated the copper halide crystal growth and that the crystals were large enough to disperse the light and cause opacity.

Some samples were dried at 50 °C from up to 48 h and up to 7 days in order to investigate the effect on photochromic properties. They remain transparent and slightly green coloured. Samples are not sensitive to light when dried at 50 °C.

Table 5-4: Description of used temperatures during drying stage and its consequence to visual aspect

Drying temperature	Time	Aspect
50 °C	24h	Transparent
80 °C	24h	Sometimes slightly opaque
100 °C	1h	Transparent
	24h	Transparent + sometimes slightly opaque
	72h or more	Opaque + photochromic

5.4 Heat-treatment

The heat-treatment is the densification stage. Transformations that occur during the heat-treatment include: vaporization of structural water and structural ethanol; carbonisation and oxidation of organic groups; liberation of water released during network condensation and activation of photochromic crystal growth [48].

Following the same heat-treatment used by our group's last work, the samples were placed in the furnace and heated up to the desired temperature at a rate

of 5K/min. The final temperatures varied between 150 °C and 300 °C. Once the final temperature was reached, it was held for an interval of 10 min up to 1 h. After the holding time, the sample was immediately removed from the furnace.

Considering that the photochromic crystals were growing too large in diameter, even those kept at the lowest temperature and shortest holding time, the heat-treatment had to be modified.

The heating stage was not easy to control as it was time consuming to set the same starting temperature (25 °C) for all treated samples. The variation on the heating stage would influence the crystal growth from sample to sample.

For the purpose of a uniform heating treatment, the samples were placed into the furnace already at the final appropriate temperature without a pre-heating stage. After a cycle that varied between 10 min to 60 min, the sample was promptly removed.

The temperatures altered from 110 °C to 550 °C, not exceeding the holding time of 20 min. Temperatures above 700 °C could not be used, as it drives the evaporation of the photochromic components. Besides, the chosen substrate, (soda-lime-silica glass) does not have such high T_g . To work with substrates with higher T_g is not the purpose of this work since we are interested in coating commercial window glasses. Table 5.2 that follows illustrates the various heat-treatments applied and the immediately visible effect if it produced transparent and photochromic specimens.

Table 5-5: Description of the variation in heat-treatment and resulting effect on photochromic crystal growth.

Composition	Heating rate (K/min)	Temperature (°C)	Time (min)	Transparent	Photochromic
1 Cu:Cd=1:1	5	110	60	Yes	No
		150	60	Yes	No
		200	40	No	Yes
		200	60	No	Yes
2 Cu:Cd=1:2	5	200	40	No	Yes
		200	60	No	Yes
3 Cu:Cd=1:1.5	5	200	40	No	Yes
	10	200	40	No	Yes
6 Cu:Cd=1:1.5	No heating stage	200	60	No	Yes
		200	40	No	Yes
		200	10	Yes	Yes
		350	10	No	No
		450	10	No	No
		550	10	No	No

A second trial of heat-treatment was done in order to enhance the crystal growth: a two-step heating treatment. The temperatures in the first step were fixed at 100, 110, 120 and 130 °C. The holding time was 1h. In the second step, all samples were heated to 160 °C for 1h.

In another test, the first temperature was fixed at 100 °C and the holding time set to 1h. The second temperature used was 160 °C and the holding time altered between 10 min and 50 min. All the heat-treatments produced samples with crystal size larger than 500 nm, which is not the aim of this work.

Another instance was carried out using nitrogen rich atmosphere for heat-treatments at temperatures higher than 280 °C. Samples treated at temperatures higher than 250 °C were completely opaque and dark coloured. A bottle of nitrogen gas was attached to the furnace. The nitrogen flow was at a constant rate, through a tube into the furnace chamber where the samples were placed. After the heat-treatment the samples turned from black colour to a pale white colour except that they were not photochromic. The heat-treatment under nitrogen atmosphere was not suitable.

The most successful heat-treatment was the placement of samples in a furnace already at 250 °C for 20 min and with immediate removal.

Fig. 5-3 below shows the schematic representation of activation of microcrystals formation due to heat-treatment.

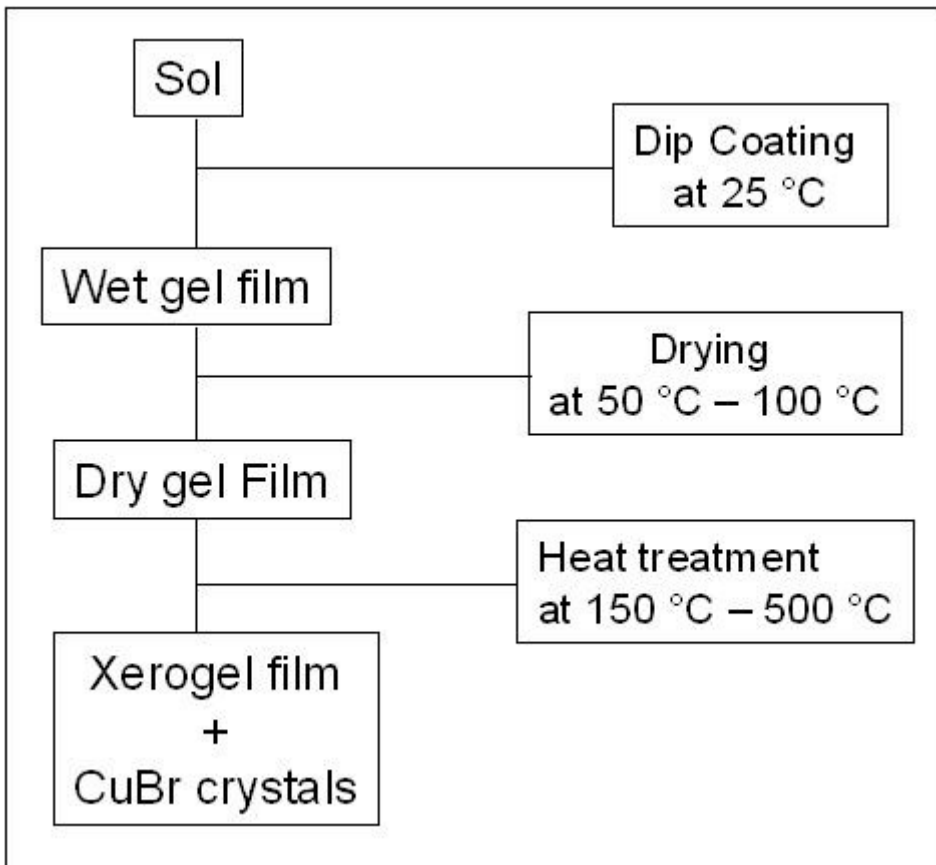


Figure 5-3: Schematic representation of the development from sol-gel to coating containing photochromic microcrystals.

6 METHODS

6.1 X-ray powder diffraction

The X-ray powder diffraction is a powerful tool to investigate crystalline and partial crystalline materials. The powder diffraction pattern (position and intensity of the lines) is characteristic of the substance; each substance in a mixture produces its own pattern (i.e. independently of others); indicate the element's chemical combination state in the material; a small amount is required [50].

The first law of crystallography affirms: "The angle between corresponding faces on crystals of a pure substance is always constant". These angles may serve for identification of the substance, as they are characteristic of the species.

Considering all combinations of symmetry elements consistent with these 14 lattices, there are 230 possible distinct combinations. The 230 different crystallographic groups are listed in *International Tables for X-ray Crystallography* [51].

The distance between neighbouring lattice plans can be calculated by the Bragg Equation:

$$n\lambda = 2d \sin \theta \quad \text{Equation 6-1}$$

Where:

λ = wavelength of used radiation

n = an integer, and $n\lambda$ = is the path difference between waves scattered from adjacent lattice plans with equivalent indices.

d = interplanar spacing for the reflecting planes

θ = complementary of the angle of incidence of the X-ray beam

If the Equation 6-1 is satisfied, thus diffraction maxima occur. The diffraction maxima are observed only for special values of the incidence angle and only if the relation of wavelength, interplanar spacing and angle of incidence is appropriate as to satisfy Equation 6-1.

The X-ray diffraction (XRD) measurements were carried out using a Siemens D5000 diffractometer with CuK_α wavelength (1.5418 Å) radiation.

Because the concentration of photoactive crystals is smaller than 1% in volume, step scanning had to be used to improve the signal-noise ratio. Small angle ranges are analysed in the crystals diffraction pattern's interval. Through repeated measurements the diffraction's signals are increased and the noise levels are decreased.

If the coatings (on glass substrate) are too thin, X-ray grazing incidence on the sample has to be constant at 1°. Just the counter moves towards 2θ . Small grazing incidence causes the X-ray to have a longer path over the thin coating. In this instance, the X-ray is diffracted by a larger number of crystals.

These two methods are time inefficient compared to the standard measurement. For this reason it could not be performed to all samples.

Crystals that are too small produce wide peaks. The crystal size can be calculated based on those wide peaks using the Scherrer's equation (see Equation 6-2).

The interplanar spacing (d) of three strongest lines and the relative intensities of the lines based on the strongest line (100), have to match to identify one compound.

$$L_{hkl} = \frac{K\lambda}{\beta_{\frac{1}{2}} \cos \theta} \quad \text{Equation 6-2}$$

Where:

L_{hkl} = dimension of the crystallite in directions parallel to the planes

$K = 0.89$ (shape factor)

β_{hkl} = breadth of half-maximum intensity (in 2θ units)

λ = wavelength of X-ray

and the error is ($\pm 20\%$)

Determination of the crystal phase through d-values should also match with the relative intensity. If the d-value and relative intensities happen to be very different, models for chemical disorder should be created and the relative intensity calculated. For example, part of Cu^+ of CuBr crystals are substituted against Cd^{2+} , and for each Cd^{2+} present at the crystal one Cu^+ vacancy is created. This has an impact on the relative intensity and through variation of the number of incorporated Cd^{2+} the intensity can be calculated and fit to the measured intensity.

6.2 Ultra violet (UV) and visible (VIS) region absorption spectroscopy

The basic principles of construction of a spectrophotometer are a light source; dispersive element (monochromator with prism or grid); receiver/detector [52].

Two different instruments were used, a single beam and a two beams instrument. A single beam instrument means the reference and measurement cuvette are placed one after another in the path of the light.

The monochromator is responsible for splitting up the measuring light into its constituent wavelengths. In our case, they cover the region between 190 nm to 900 nm. It is the most important instrument of a spectrometer. It can be single or double and the difference between them is that double monochromators have a very small proportion of stray light. Stray light is that from another spectral region which is superimposed on the useful light of the selected for measurement. The quality of the grating monochromators depends on the proportion of scattered light. That means the intensity of light leaving the exit slit with a wavelength in the immediate neighbourhood of the desired light λ_0 .

In the diode array spectrometer the dispersed light of a continuum source is brought to a focus in one plane (the instrument's focal plane). The samples are mounted between the light source and the entry slit of the monochromator.

The diode array spectrometer measures all absorbance values of an absorption spectrum in a selected wavelength region simultaneously. The spectrometer is connected to a computer, which controls it and collects and evaluates the data. See Fig. 6-1.

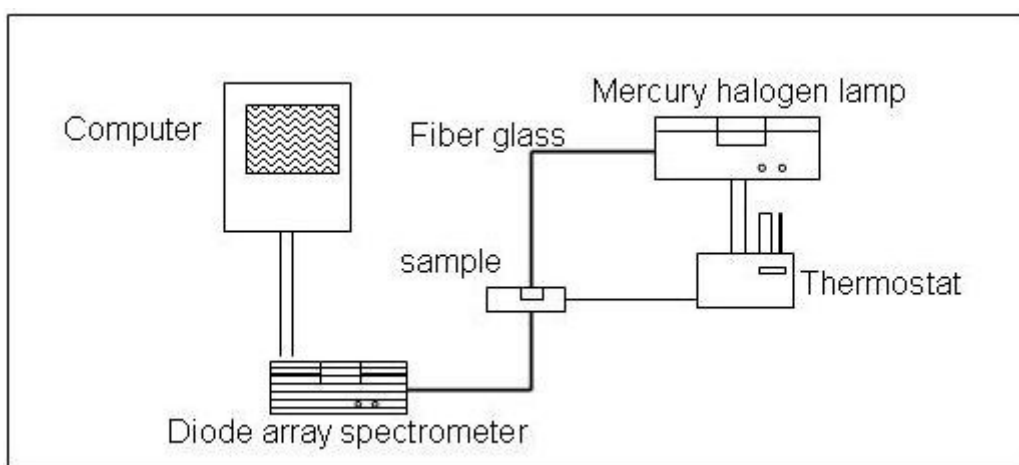


Figure 6-1: Illustration of a diode array spectrometer integrated with mini-furnace.

The UV-VIS spectroscopy is a standard measurement to optical materials.

To measure the absorption behaviour of samples before and after the precipitation of photoactive crystals the Shimadzu UVPC-3101 (two beams) was used. The approximate measurement time is 180 s.

To measure the absorption behaviour of samples during the formation of photoactive crystals *in situ*, a diode array spectrometer (InstaSPEX II, LOT-Oriel) one-beam instrument and a microscope heating table (THMS 600, Linkam) was used. The measurement time is <1 s, which makes dynamic measurements possible.

The light source is a XBO 150 (xenon high pressure lamp); Monochromator Multispec with a 400 lines/mm grid (this makes it possible to measure in a 500 nm wide wavelength range, normally between 300 and 800 nm); diode array receiver with 1.024 Si-photodiode.

The samples measured *in situ* were heated with a constant rate 10K/min up to a desired temperature (150 °C...200 °C), which allows the CuBr crystals to precipitate and grow. After achieving the desired temperature they were kept at that temperature for a certain period of time. The absorption was measured at different temperatures and at different times.

The samples were also measured while under UV irradiation to analyse the absorption during the darkening and during the fading after the UV irradiation was turned off.

The measurement of fading behaviour was problematic because at least for a small amount of time the sample must be irradiated again for the measurement, this causes further darkening.

The calculation of photochromic behaviour (darkening and fading) was evaluated following the values of absorption/transmission at 550 nm as a function of irradiating time and fading time.

The CuBr crystals exhibit two excitons peak absorption. It's absorption coefficient is so high, that it can be observed even if they are present at a very low concentration and very small crystal sizes, which could not be clearly seen by XRD investigations [53]. Observing those characteristic absorption peaks, the formation of CuBr crystals can be followed. The position of those peaks shifts with the size of the crystals (the larger the crystals, the longer the wavelengths the bands will be located). The distance between the two exciton peaks is a measurement for the ratio between Br⁻ and Cl⁻ in the crystals.

Other ions such as Cu⁺; Cd²⁺; and Zn²⁺ do not absorb in the VIS region, only Cu²⁺, at approximately 800 nm.

6.3 Scanning Electron Microscopy

The scanning electron microscope (SEM) produces micrographs of the specimen by scanning its surface with a small beam of electrons synchronously with an electron beam in a cathode ray tube [54]. Fig.6.2 is a schematic representation of a SEM.

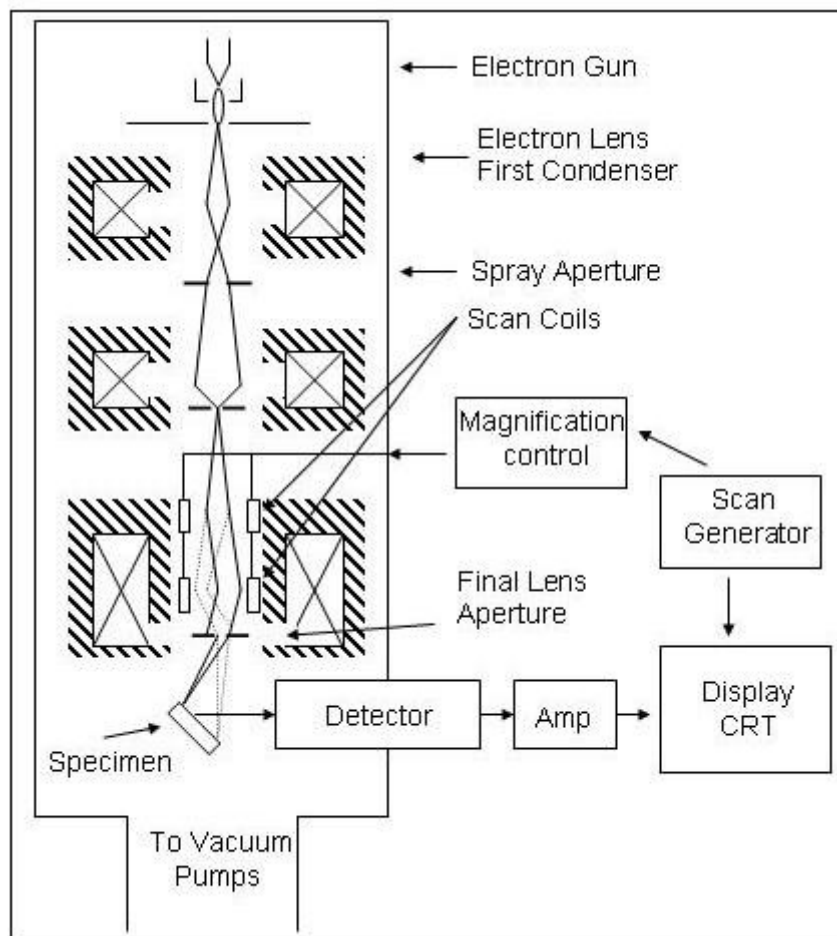


Figure 6-2: Schematic representation of a SEM.

Electrons with energies up to approximately 30 keV are focused into a small spot (a few nm in diameter) by electric and magnetic fields on the surface. Instead of glass lenses in optics, electric coils are used to deflect the charged particles ($\vec{F} = e(\vec{E} + \vec{v} \times \vec{B})$). The resolution of the imaging system is similar to the beam diameter; down to 1.5 nm can be reached. Topographic as well as compositional details can be imaged with a high focus depth.

The SEM image can be formed by any signal generated by the interaction of a finely focused primary beam of electrons as it is scanned over a specimen.

Other products of the specimen- electron beam interaction are backscattered electrons (BSE); Auger electrons; photons; specimen current; characteristic X-rays and Bremsstrahlung.

X-ray spectral measurements can be done by measuring the energy or the intensity distribution of the X-ray signal generated by a focused electron beam.

Quantitative and qualitative information can be achieved. One method detects and measures the energy and the other the intensity distribution of generated X-rays: energy-dispersive spectroscopy (EDS) and wavelength-dispersive spectroscopy (WDS) [55].

In WDS analysis a small portion of the X-ray signal from the specimen infringes on an analysing crystal, which consists of a regular array of atoms. The crystal is oriented such as the selected crystallographic plane of these atoms is parallel to its surface. The X-rays are diffracted and detected by a gas-filled proportional counter and a gas flow counter. Signals from the detector are amplified and converted to a standard pulse size by a single-channel analyser. Later they are counted with a scale or displayed as a rate-meter output.

To perform the chemical analysis along one or more selected elements across a line on a specimen, the line-scan mode was used. The obtained X-ray and beam position information can be superimposed on an electron-image. These data are qualitative since the complete quantitative evaluation leads to conversion of the intensity data to chemical composition [56].

The scanning electron microscope used was DMS 940A (Zeiss) with EDX (eXL10, Oxford Instruments) and WDX (2PC, Microspec).

The preparation of all samples was carried out as follows: the sample is dip-coated in the sol, and then it is dried in a furnace at 100 °C and holding time of 1h, at this stage the layer consists of a dried gel containing active compounds such as Cu^+ ; Cd^{2+} and Br^- . After drying the sample goes for heat-treatment in a furnace at 250 °C and holding time of 10 min where the CuBr photoactive crystals are formed. In order to have a conductive surface, the sample is coated with carbon by spray process.

Wet sol-gel coated sample → drying at 100 °C for 1h → heat-treatment at 250 °C for 10 min → carbon coating → had their surface coated with C after the heat-treatment.

6.4 Atomic force microscopy

The atomic force microscope is a combination of the principals of the scanning tunnelling microscope and the stylus profilometer. It incorporates a probe that does not damage the surface [57].

The AFM is an important tool for imaging surface topography with nanometer resolution [58]. It suits the characterization of coating surfaces.

The AFM utilises a sharp probe, a tip on the end of a cantilever, which bends in response to the force between the tip and the sample.

During the measurement the probe is moved towards the surface at constant velocity until it is brought into contact with the sample up to a predetermined point of maximum load. The direction of motion is reversed and the probe is withdrawn from the sample surface. As the probe withdraws it may stick to the surface due to interactions between them. The magnitude of the measured force between probe and sample created by their proximity forms the image. This force is kept small and at a constant level with a feedback mechanism. When the tip is moved sideways, it will follow the surface contours such as shown in Fig. 6-3.

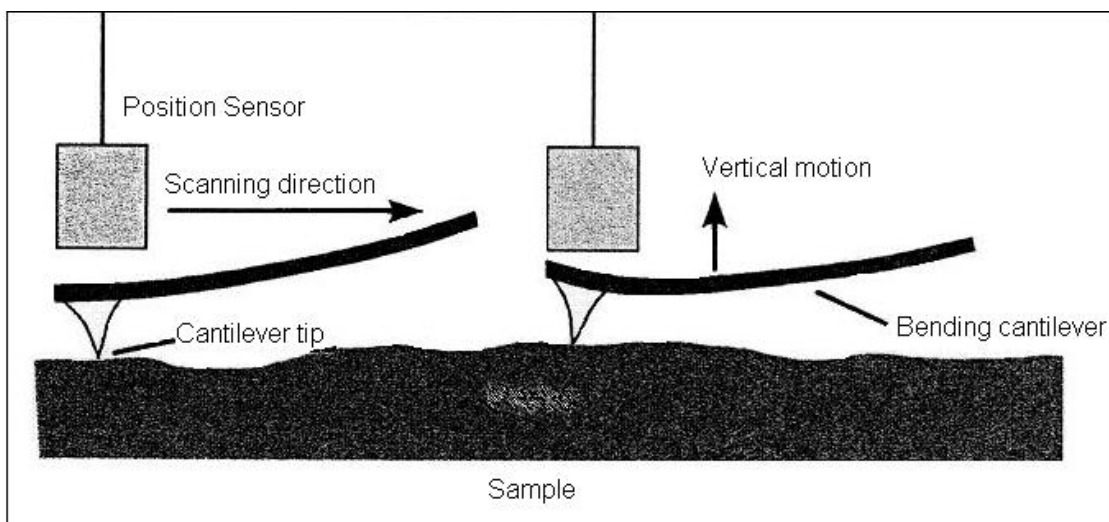


Figure taken from reference [81]

Figure 6-3: Illustration of the principle of operation of an AFM: tip following the surface contour.

The Van der Waals force between the tip and the sample leads to a deflection of the cantilever according to Hooke's law, where the spring of the cantilever is known. The deflection is measured using a laser spot reflected from the top of the cantilever into a diode array as shown in Fig. 6-4[59].

The AFM used was Surface Image Systems - S.I.S. - Ultra Objective.

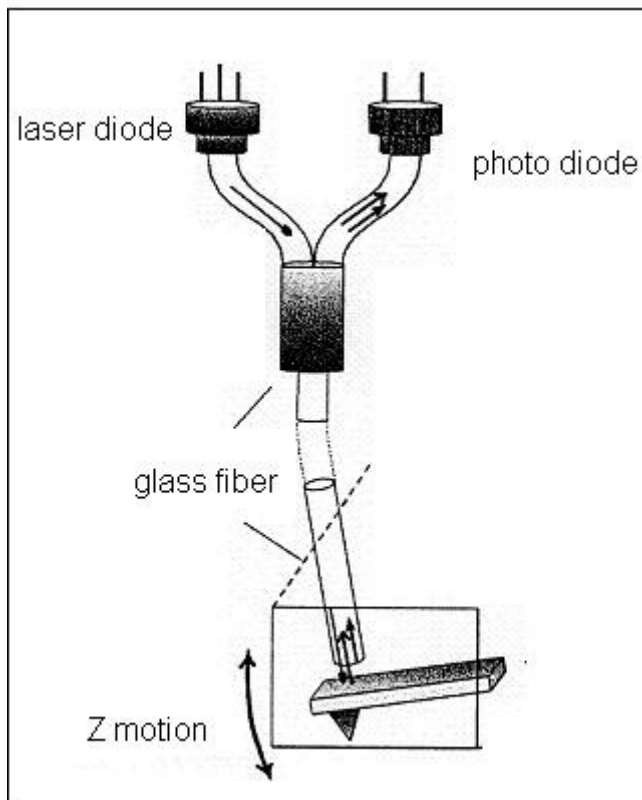


Figure from literature [81]

Figure 6-4: Laser detection system.

6.5 Ellipsometry

The ellipsometry is used to characterize films and interfaces. It is sensitive to several material characteristics such as layer thickness, optical constants (refractive index and extinction coefficient), surface roughness, composition and optical anisotropy. It is an optical technique based on exploiting the polarization transformation that occurs as a beam of polarized light is reflected from or transmitted through the film [60] i.e. the change in polarization state of light reflected from the surface of a sample.

The initial and final ellipses of polarization of a monochromatic or quasi-monochromatic propagating transverse-electric electromagnetic wave (TE-EMW) are measured before and after its interaction with a sample [61].

The ellipsometer consists of five elements: A light source; a polarization state generator (P); a sample; a polarization state detector (A); and a light detector. See Fig. 6-5.

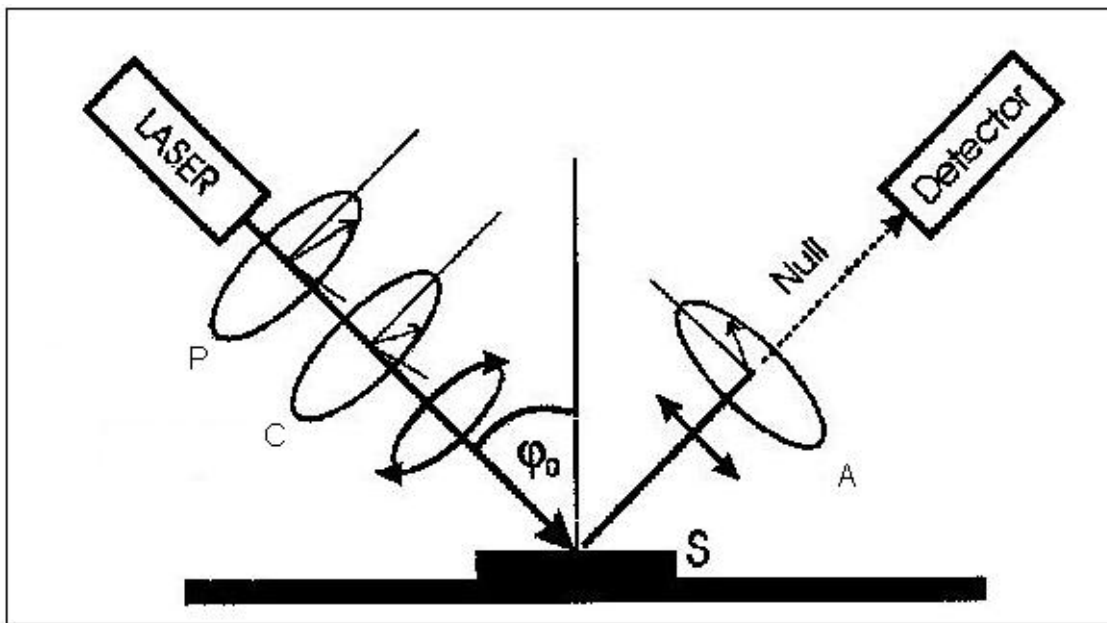


Figure from reference [62]

Figure 6-5: Ellipsometer consisting of light source L; polarizing unit P; compensation unit C; sample S; analysing unit A; light detector D.

The light source can be a monochromatic (from a laser) or white light (from xenon lamp or mercury arc lamp). The P and A consist of polarizers, retarders and photoelastic modulators. The light from P is reflected from the sample surface at a large incidence angle.

Two factors make ellipsometry very attractive: its non-perturbing character; and its remarkable sensitivity to minute interfacial effects. Ellipsometers will only measure the characteristics of reflected light from a sample or transmitted light through the sample, it does not measure the thickness of a film or optical function of materials (refractive index n , absorption coefficient α). These

parameters can be inferred very accurately from the ellipsometric measurements [63].

The ellipsometer used was a SE 400 ellipsometer (SENTECH). It has 2 lasers, 632.8 nm (He/Ne) and 401 nm (CW-laser). The incidence and reflection angles were varied between 40° and 85° (step width 5°). It was used to obtain information about the coatings thickness and roughness.

7 RESULTS

7.1 X-ray powder diffraction

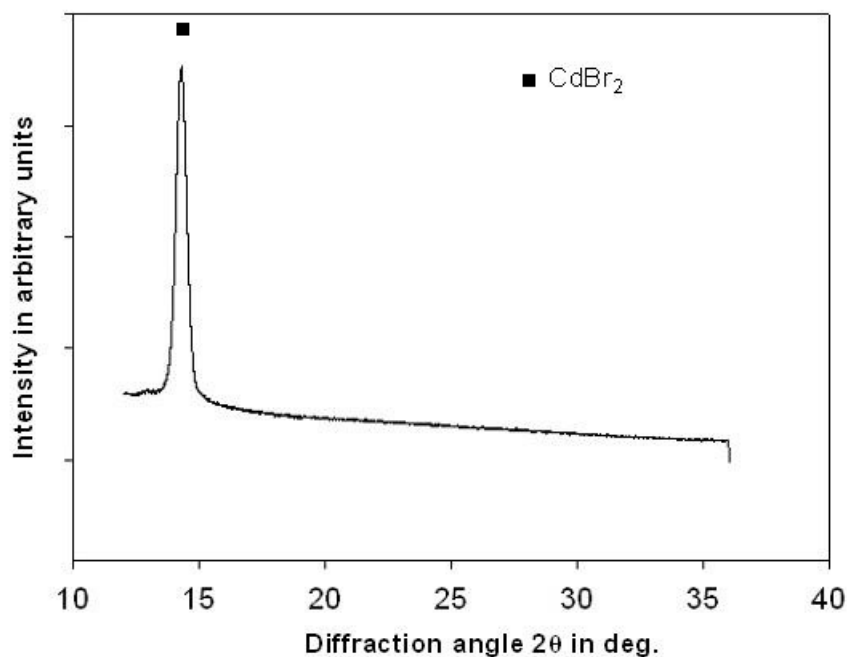


Figure 7-1: X-ray diffraction patterns of sample containing 0.9 mol% $\text{Cu}(\text{NO}_3)_2 \cdot 3\text{H}_2\text{O}$ and 1.4 mol% $\text{Cd}(\text{CH}_3\text{COO})_2 \cdot 2\text{H}_2\text{O}$ before heat-treatment.

Fig. 7-1 shows an X-ray diffraction of a sample before heat-treatment. The sample was coated with a solution containing $\text{Cu}(\text{NO}_3)_2 \cdot 3\text{H}_2\text{O}$ and $\text{Cd}(\text{CH}_3\text{COO})_2 \cdot 2\text{H}_2\text{O}$ in the molar ratio 1:1.5.

The peak at 14.32° is attributable to the hexagonal CdBr_2 phase (JCPDS file No. 3088). The peak can be indexed by (001) diffraction line.

The Table 7-1 highlights the results.

Table 7-1: X-ray diffraction angle for sample containing (a) 0.9 mol% $\text{Cu}(\text{NO}_3)_2 \cdot 3\text{H}_2\text{O}$ and 1.4 mol% $\text{Cd}(\text{CH}_3\text{COO})_2 \cdot 2\text{H}_2\text{O}$ before heat-treatment

Diffraction Angle 2θ (°) JCPDS File 3088	Diffraction Angle 2θ (°) Sample	Crystal Structure	hkl
14.18	14.32	CdBr_2 Hexagonal	001

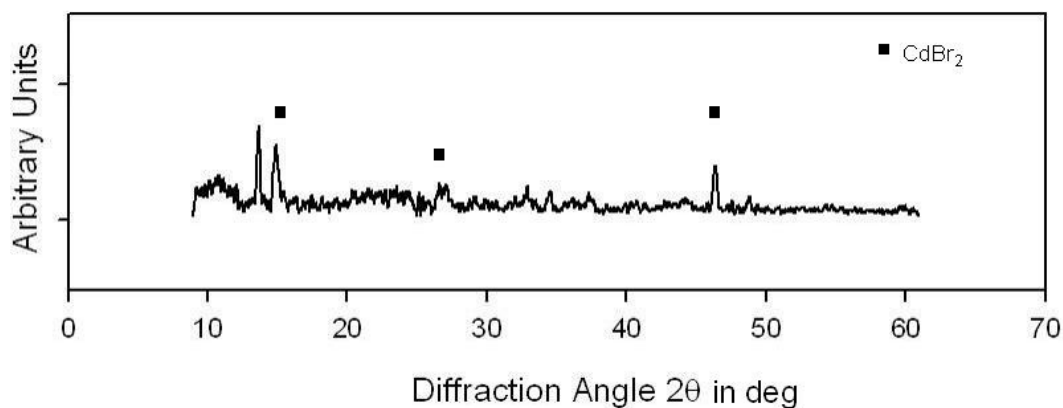


Figure 7-2: X-ray diffraction patterns of sample containing 1 mol% $\text{Cu}(\text{NO}_3)_2 \cdot 3\text{H}_2\text{O}$ and 0.5 mol% $\text{Cd}(\text{CH}_3\text{COO})_2 \cdot 2\text{H}_2\text{O}$ after drying at 100 °C for 12h.

The cadmium (II) acetate dihydrate content was reduced from 1.4 mol% to 0.5 mol% so that the crystal growth prior to heat-treatment would be inhibited.

Fig. 7-2 shows that CdBr_2 crystals did exist before the heat-treatment. This time two peaks at 12.72 ° and 13.98° were visible. Two other peaks appeared, one at 28.24° and another one at 45.41°.

According to JCPDS file No. 3088 those peaks could be equivalent to the description of hexagonal CdBr_2 phase with peaks at 14.18°; 28.49° and 45.79° relative to planes (001); (002) and (100) respectively.

Table 7-2 summarizes these results.

Table 7-2: Sample after drying for 12h at 100 °C; Ratio Cu:Cd = 1:0.5

Diffraction Angle 2θ (°) JCPDS File 3088	Diffraction Angle 2θ (°) Experimental	Crystal Structure	hkl
14.18	13.98	CdBr ₂ Hexagonal	001
28.49	28.24	CdBr ₂ Hexagonal	002
45.79	45.41	CdBr ₂ Hexagonal	100

The next samples contained 1 mol% of Cu(NO₃)₂·3H₂O and 0.5 mol% of Cd(CH₃COO)₂·2H₂O were heat treated at different temperatures varying between 110 and 170 °C.

The diffraction patterns in Fig. 7-3 showed the formation of CdBr₂ crystals along with CuBr crystals.

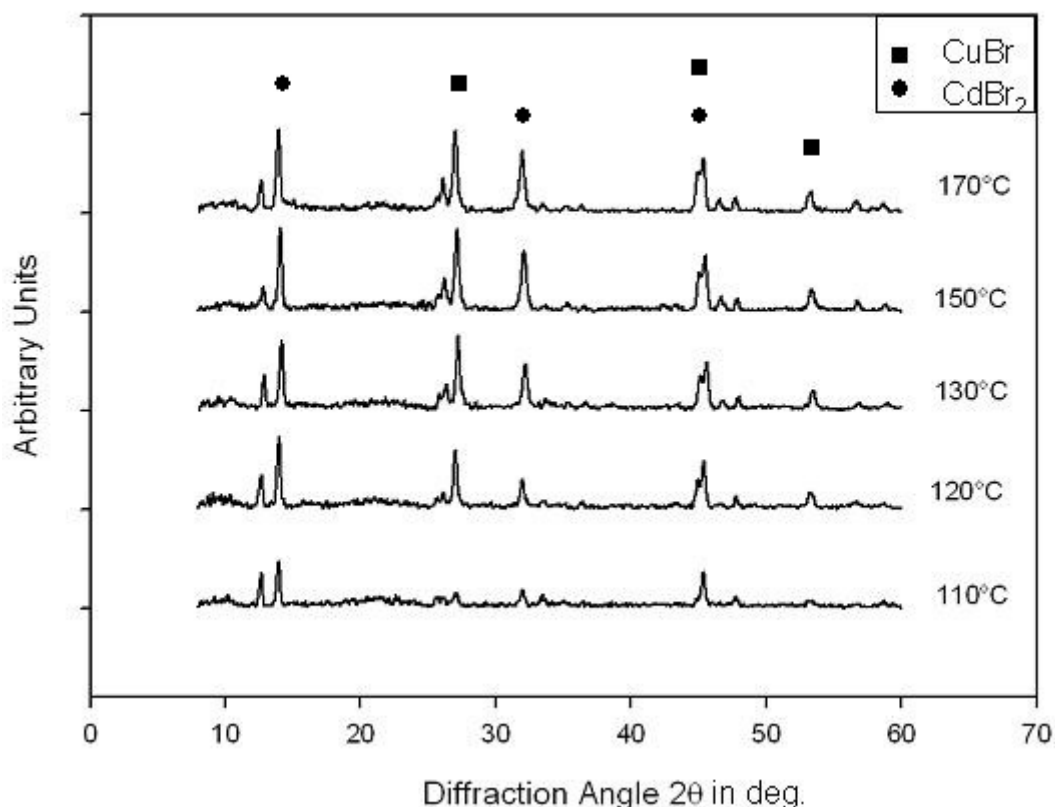


Figure 7-3: X-ray diffraction patterns of samples containing 1 mol% $\text{Cu}(\text{NO}_3)_2 \cdot 3\text{H}_2\text{O}$ and 0.5 mol% $\text{Cd}(\text{CH}_3\text{COO})_2 \cdot 2\text{H}_2\text{O}$. Heat treatment at different temperatures. Presence of crystal phases: CuBr and CdBr₂.

The experimental results showed peaks at 27°; 45.38° and 53.40° that could be attributed to cubic gamma-CuBr. The indexed diffraction lines were (111), (220) and (311). The relative intensities were 100; 60 and 35% respectively, as found in previous literature [33, 36] and at JCPDS file No. 60292.

Peaks at 14.03 °; 32.93°, 45.38° resembled the CdBr₂ rhombohedral phase with relative diffraction lines (003), (104), and (110) and relative intensities of 100; 20 and 40% respectively as found on the JCPDS file No. 100438.

In the literature, Nogami et al. [36] observed CuBr nanocrystals precipitated in sol-gel glass under a nitrogen atmosphere. The most frequently observed coordination group of Cu⁺ ions in CuBr crystals was the group of four square-coplanar neighbours with two more distant neighbours completing a distorted octahedron. The XRD patterns for samples heated in nitrogen atmosphere revealed relatively diffuse peaks at $2\theta \approx 27^\circ$, 45° and 53° corresponding to

cubic CuBr crystals and (111), (220), (311) diffraction lines (JCPDS file n° 60292). This was the same results found in our experimental research, although the heat-treatment was not carried out under nitrogen atmosphere.

Table 7-3 compares the diffraction angles 2θ in degrees found on experimental results and the literature.

Table 7-3: Identified crystals in experimental data and literature in samples heated from 110 °C up to 170 °C.

Diffraction Angle 2θ (°) JCPDS	Diffraction Angle 2θ (°) Experimental	Crystal Structure	hkl
14.11	14.03	CdBr ₂ Rhombohedral	003
32.11	31.93	CdBr ₂ Rhombohedral	104
45.47	45.38	CdBr ₂ Rhombohedral	110
27.12	27	Cubic Gamma-CuBr	111
45.02	45.38	Cubic Gamma-CuBr	220
53.34	53.40	Cubic Gamma-CuBr	311

With the purpose of substituting Cd²⁺ against Zn²⁺, samples containing 0.9 mol% of Cu(NO₃)₂·3H₂O; 0 to 1.4 mol% of Cd(CH₃COO)₂·2H₂O and 0 to 1.4 mol% of Zn(CH₃COO)₂·2H₂O were dried at 100 °C for 12 h.

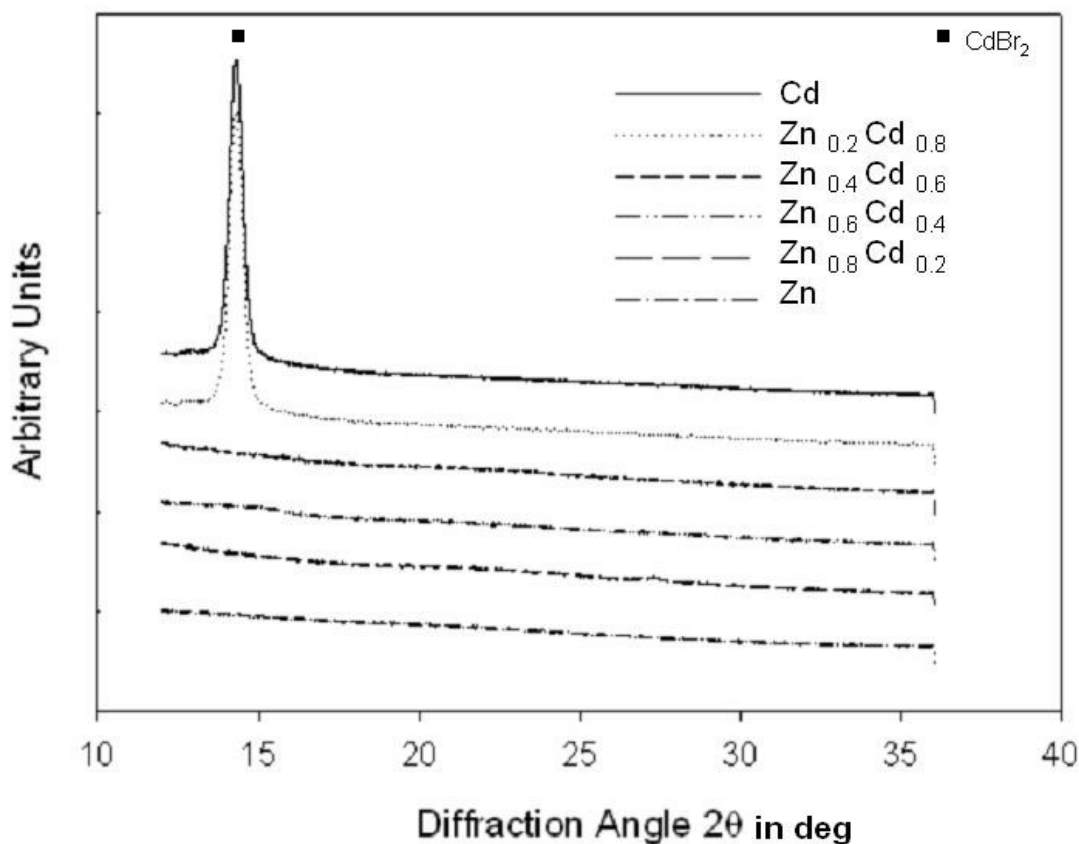


Figure 7-4: X-ray diffraction patterns of samples dried at 100 °C and holding time of 12 h and variable Cd²⁺ substituted against Zn²⁺

In order to decrease the Cd(CH₃COO)₂·2H₂O content, a portion of it was substituted by Zn(CH₃COO)₂·2H₂O. The effect of this substitution can be seen in Figs. 7-4 and 7-5 for samples before and after heat-treatment respectively.

Fig. 7-4 provides evidence of the formation of CdBr₂ crystals during the drying stage at 100°C for the two samples containing respectively 1.4 mol% and 1.1 mol% of Cd(CH₃COO)₂·2H₂O. According to JCPDS File Nr. 10438 and Nr. 3088, the diffraction angle 2θ at 14° as described before, is attributed to hexagonal CdBr₂.

Fig.7-4 made it clear that the CdBr₂ is no longer visible, if at least 40% Cd²⁺ were substituted against Zn²⁺.

The precipitation of crystals before the heat-treatment could explain the opaque colour of samples after the drying stage (for those heated to 100°C for more than 12 h). The narrow and large peak is characteristic of large crystals.

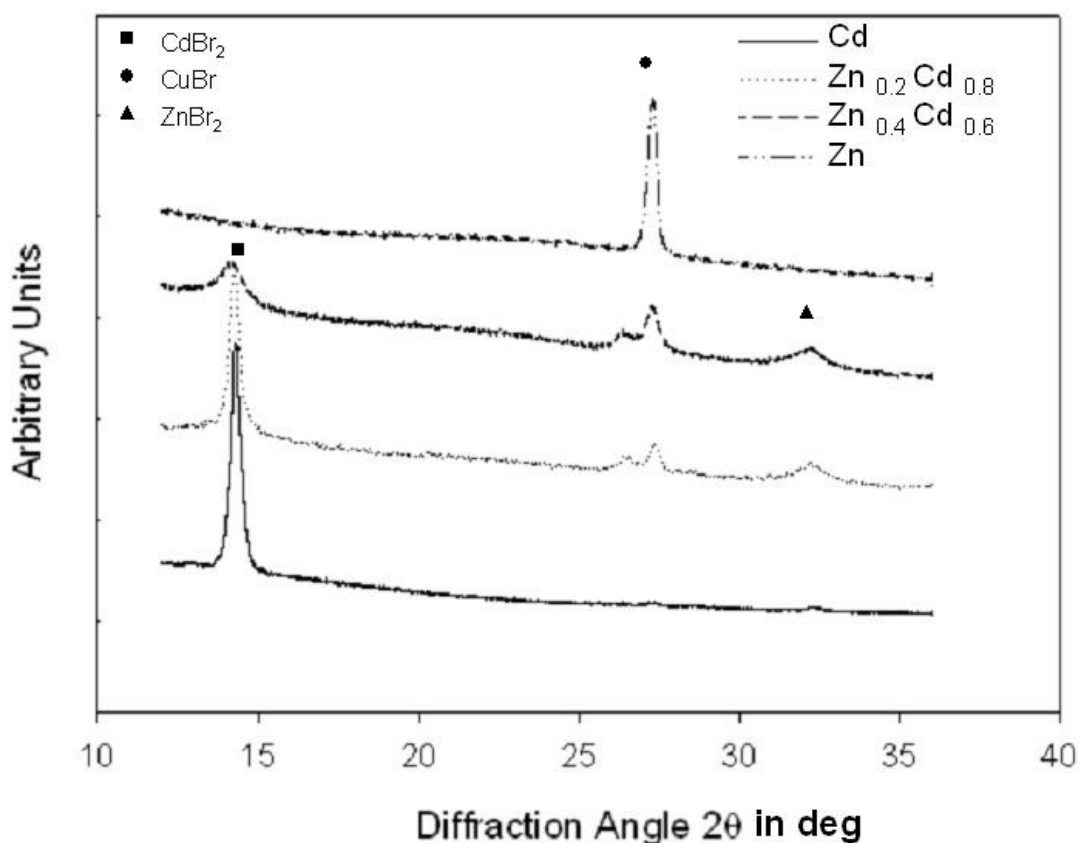


Figure 7-5: X-ray diffraction patterns of samples containing $\text{Zn}(\text{CH}_3\text{COO})_2 \cdot 2\text{H}_2\text{O}$ after heat treatment at 250 °C and holding time of 20 min.

The X-ray diffraction patterns of samples heat treated at 250 °C for 20 min are shown in Fig. 7-5.

The increase of $\text{Zn}(\text{CH}_3\text{COO})_2 \cdot 2\text{H}_2\text{O}$ content, caused the growth of CuBr and ZnBr₂ crystals and inhibited the CdBr₂ crystal growth.

The narrow and high peaks at 14° were due to large CdBr₂ crystals. The size of CdBr₂ crystals decreased with the increase of the $\text{Zn}(\text{CH}_3\text{COO})_2 \cdot 2\text{H}_2\text{O}$ content. This could be observed by the change in the peak width.

The crystallite's size was calculated in accordance with Scherrer's equation (Equation 7-1):

$$D_{111} = \frac{0,89\lambda}{\beta_{1/2} \cos \theta}$$

Equation

7-7-1

Table 7-4 shows the results obtained after calculating the crystal size with the equation above.

Table 7-4: Crystallite size variation with increasing Zn(CH₃COO)₂.2H₂O content

Zn(CH ₃ COO) ₂ .2H ₂ O Content	CdBr ₂ Crystallite Size	CdBr ₂ Crystallite Size
	20 min at 250 °C	20 min at 350 °C
0%	46 nm	67 nm
20%	37 nm	46 nm
40%	19 nm	32 nm

The opposite occurred for CuBr crystals, with increasing Zn(CH₃COO)₂.2H₂O content, the crystal size increases.

Table 7-5 compares the peaks present in Fig. 7-5 and the respective crystals from literature.

Table 7-5: Crystal structure present for samples containing $\text{Zn}(\text{CH}_3\text{COO})_2 \cdot 2\text{H}_2\text{O}$; experimental and literature data comparison.

Crystal Structure	JCPDS		hkl	Diffraction Angle 2θ (°)			
	Diffraction Angle 2θ (°)	Intensity		0%Zn	20%Zn	40%Zn	100%Zn
CdBr ₂ Hexagonal	14.18	100	001	14.28	14.30	14.24	
	28.49	40	002	28.58	28.60	28.60	
CdBr ₂ Rhombohedral	14.11	100	003	14.28	14.30	14.24	
	32.11	20	104	32.30	32.28	32.36	
	26.19	10	101	26.46	26.42	26.44	
	28.40	10	104	38.58	28.60	28.60	
Cubic	27.12	100	111	27.34	27.34	27.32	27.38
Gamma-CuBr	31.40	4	200				
ZnBr ₂ Hexagonal	15.40	18	001				
	32.33	100	101	32.30	32.28	32.36	
ZnBr ₂ Tetragonal	14.14	20	112		14.30	14.24	
	18.74	10	211				
	22.09	20	213				
	27.21	20	312		27.34	27.32	27.38
	28.54	100	224		28.60	28.60	
	33.02	40	400		32.28	32.36	

Experiments were made with samples containing $\text{Zn}(\text{CH}_3\text{COO})_2 \cdot 2\text{H}_2\text{O}$ in order to determine the influence of its addition during heat-treatment. More results will be shown in the Section 7.6.1.4.

Fig.7-6 shows that the peak intensity at $2\theta \approx 14^\circ$, which is relative to CdBr_2 crystals, decreases with increasing $\text{Zn}(\text{CH}_3\text{COO})_2 \cdot 2\text{H}_2\text{O}$ content. The CuBr peak at $2\theta \approx 27^\circ$ is present at all samples.

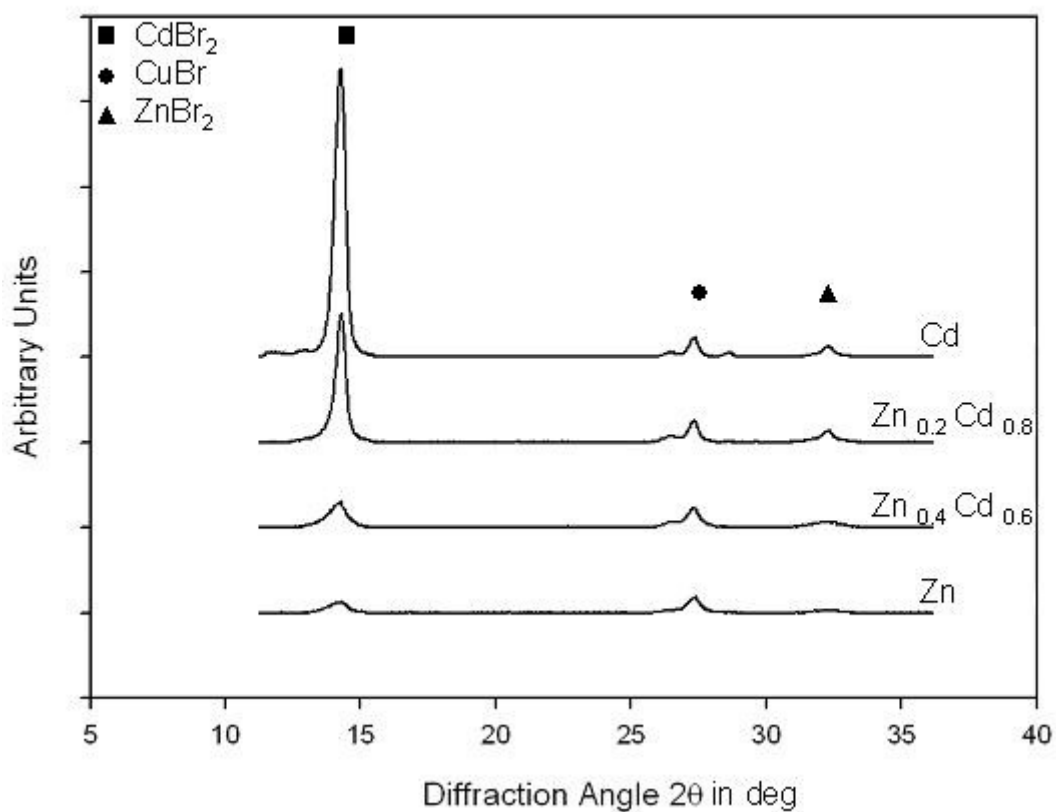


Figure 7-6: X-ray diffraction patterns of samples with increasing $\text{Zn}(\text{CH}_3\text{COO})_2 \cdot 2\text{H}_2\text{O}$ content, after heat-treatment at 250°C and holding time of 1h.

7.2 Polarizing microscopy

Some samples were viewed with a Zeiss Jenapol Interphako polarizing microscope. The crystals represented in Fig. 7-7 have an average size of approximately 1 μm . This sample was made of a sol-gel with Cu:Cd ratio equal to 1:2. The coating was heat treated at 200 $^{\circ}\text{C}$ for 60 min. In this example we have 3 factors that could contribute to the excessive growth of crystals: the high temperature; long term of heat-treatment and high ratio of co-activator concentration. Notice that the signed crystal has a clear octahedral shape just as described before in previous works in our research group [33,48].

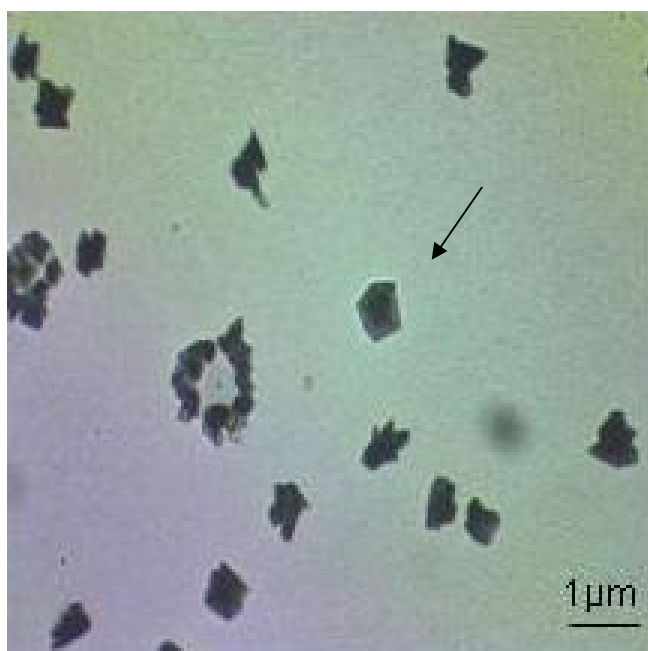


Figure 7-7: Polarizing microscope, sample containing 1mol% of $\text{Cu}(\text{NO}_3)_2 \cdot 3\text{H}_2\text{O}$ and 2 mol% of $\text{Cd}(\text{CH}_3\text{COO})_2 \cdot 2\text{H}_2\text{O}$.

7.3 Atomic force microscopy

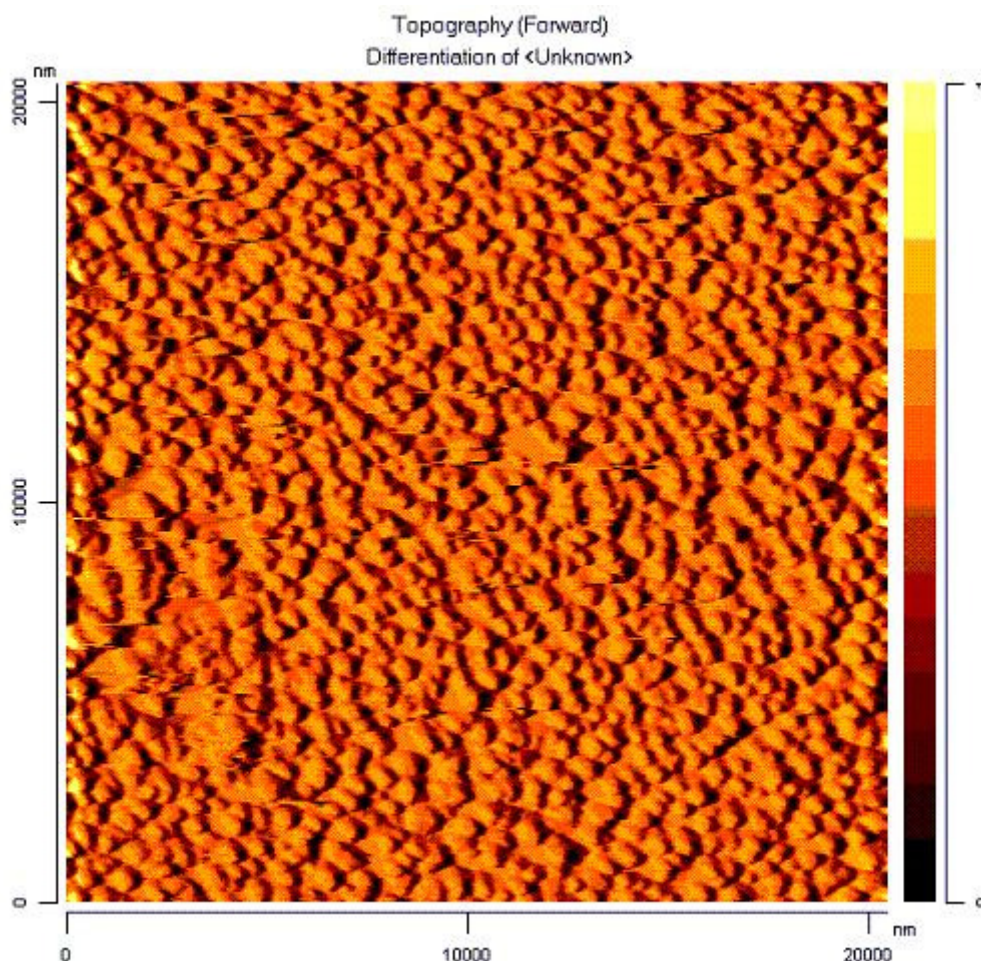


Figure 7-8: AFM of a coating surface of sample containing 1 mol% of $\text{Cu}(\text{NO}_3)_2 \cdot 3\text{H}_2\text{O}$ and without co-activator (Cd^{2+}) heat-treated at 130 °C and holding time of 3h.

Fig. 7-8 shows the texture surface of a coated sample. This sample was prepared from a sol-gel without cadmium acetate dihydrate and 1 mol% of copper (II) nitrate trihydrate. This sample has no co-activators. The heating treatment was done at 130 °C and a holding time of 3 h. Notice that the crystals occupied almost the entire surface, the glassy matrix was poorly observed. The average crystal size was approximately 200 nm and some crystals jutted out from the coating surface approximately 200 nm.

Similar crystal precipitation could be achieved by rising the temperature for example at 200 °C and holding time of 1 h.

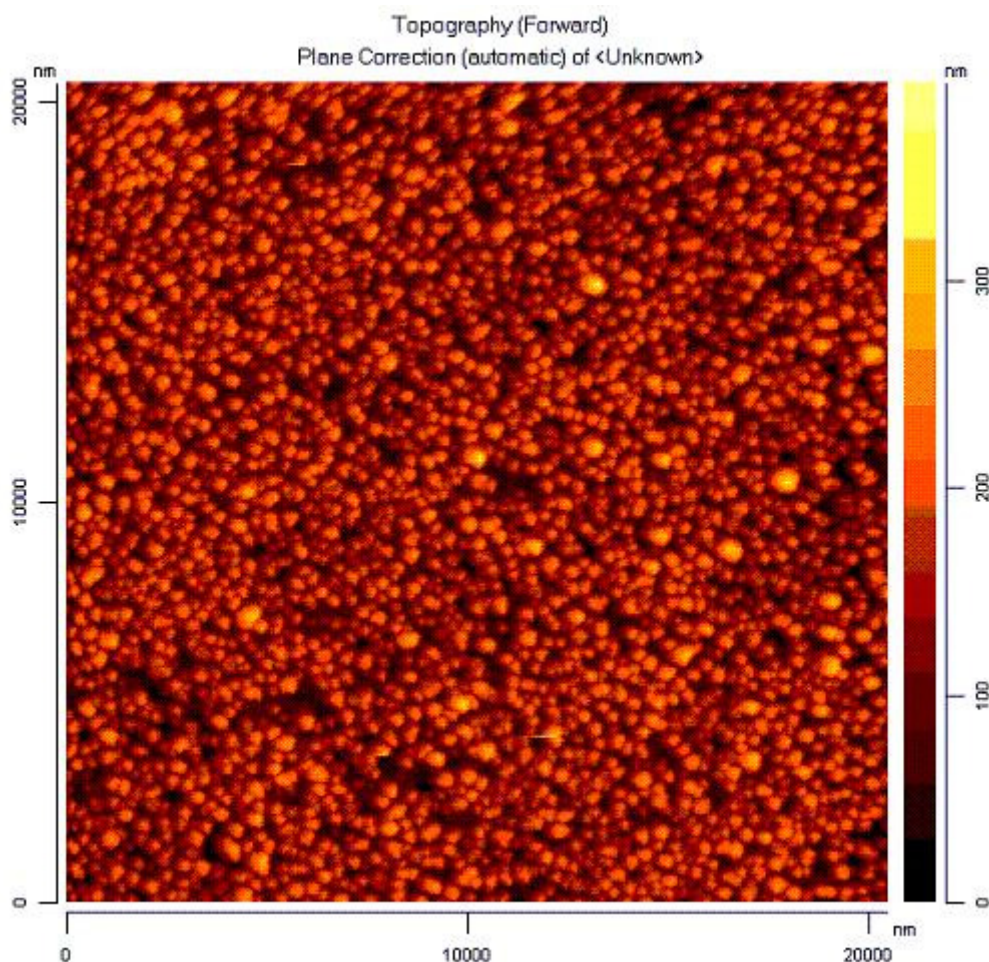


Figure 7-9: AFM of a coating surface of sample containing 1 mol% of $\text{Cu}(\text{NO}_3)_2 \cdot 3\text{H}_2\text{O}$ without co-activator (Cd^{2+}) heat treated at 200 °C and holding time of 1h.

Fig. 7-9 shows a micrograph of a sample with the same formulation. It provides evidence of not only the increment in crystal volume precipitation, but also of the crystal size. These crystals had an average size of 321 nm and jutted out approximately 290 nm from the coating surface. Both samples Fig. 7-8 and Fig. 7-9 were not photochromic (as explained later).

It will be discussed later in Chapter 8 how the co-activation with Cd^{2+} is necessary to produce photochromic crystals.

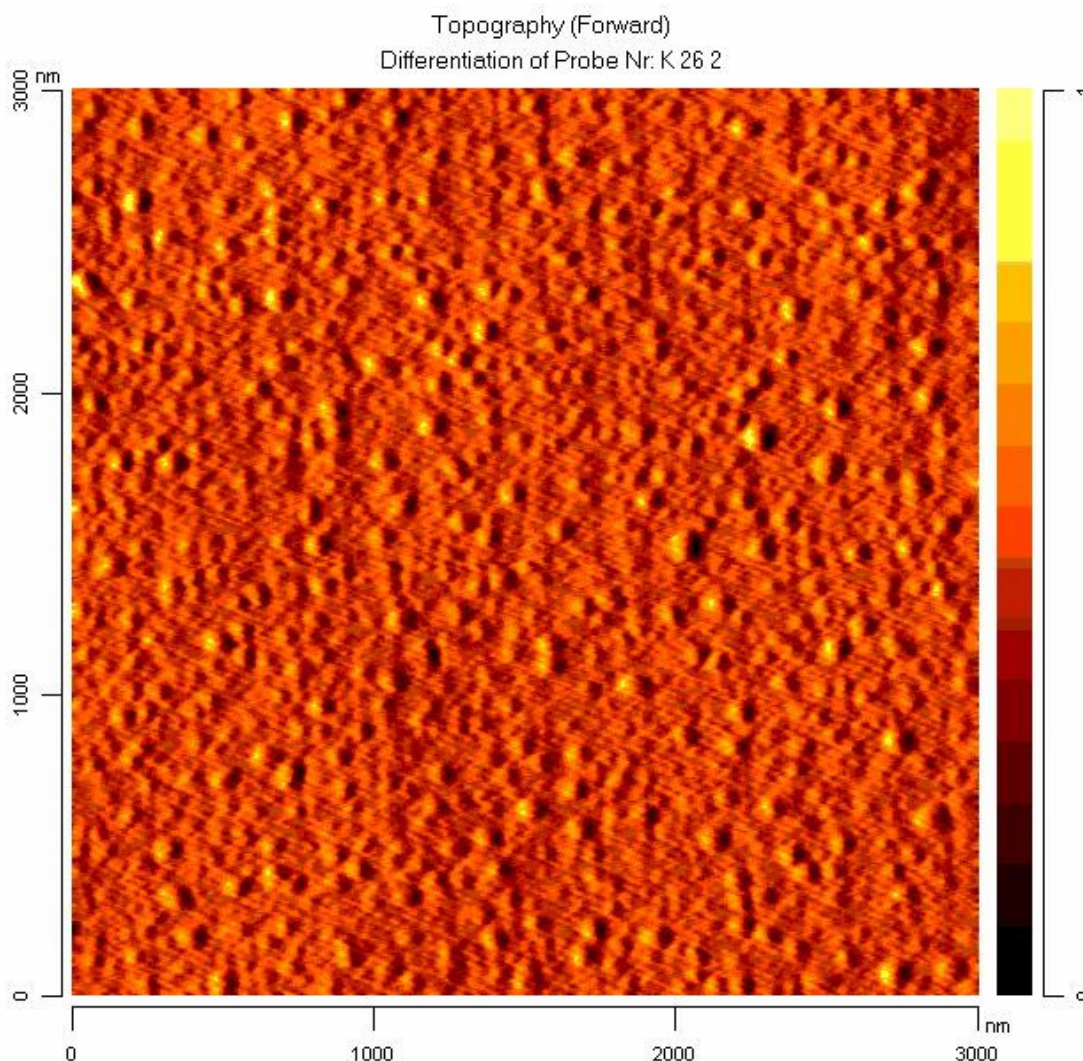


Figure 7-10: AFM of a coating surface of sample containing 1mol% $\text{Cu}(\text{NO}_3)_2 \cdot 3\text{H}_2\text{O}$ and 1mol% $\text{Cd}(\text{CH}_3\text{COO})_2 \cdot 2\text{H}_2\text{O}$ heat treated at 200 °C and holding time of 40 min.

Adding co-activating agents during the sol-gel synthesis can make a significant difference in the surface crystallization [33, 48].

Fig. 7-10 illustrates a sample which contained 1 mol% of copper(II)nitrate trihydrate and 1 mol% of cadmium acetate dihydrate. The heat-treatment was at 200 °C for 40 min. The average crystal size was approximately 30 nm and the crystals juttred out approximately 20 nm from the coating surface. The presence of a co-activator agent inhibited the crystal growth. The glassy matrix was completely covered by crystals. The glassy matrix was not observed

although the crystal size is of one order smaller. They were photochromic. Increasing the co-activator content increased the crystal size.

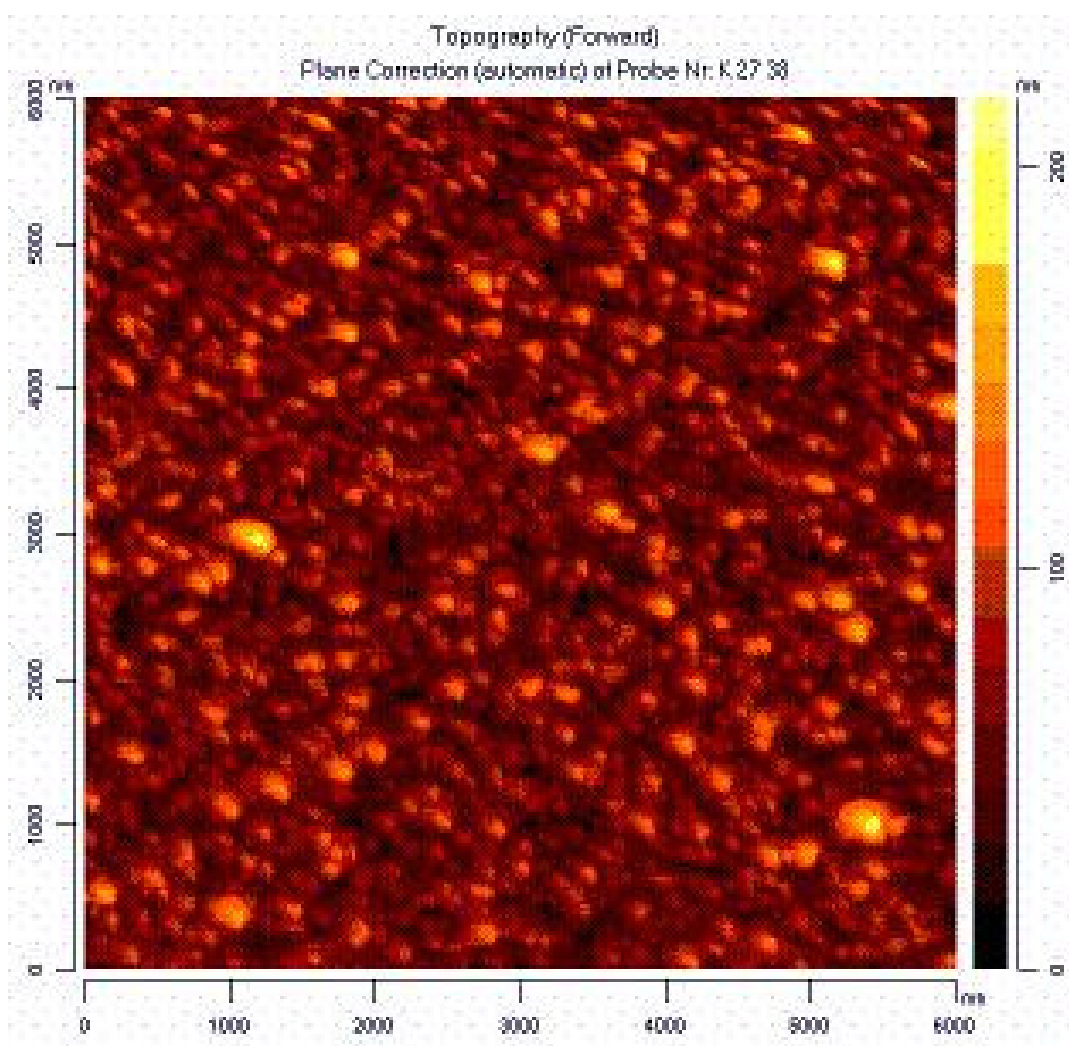


Figure 7-11: AFM of sample surface containing 1mol% $\text{Cu}(\text{NO}_3)_2 \cdot 3\text{H}_2\text{O}$ and 2mol% $\text{Cd}(\text{CH}_3\text{COO})_2 \cdot 2\text{H}_2\text{O}$ heat treated at 200 °C and holding time of 40 min.

Fig. 7-11 exhibits another sample also heat treated at 200 °C and holding time of 40 min. The average crystal size was approximately 200 nm and the crystals seems to be placed in more than one layer of crystals one over another. The crystal did not jut out the coating surface more than 100 nm high. This sample had 2 mol% of cadmium(II)acetate dihydrate.

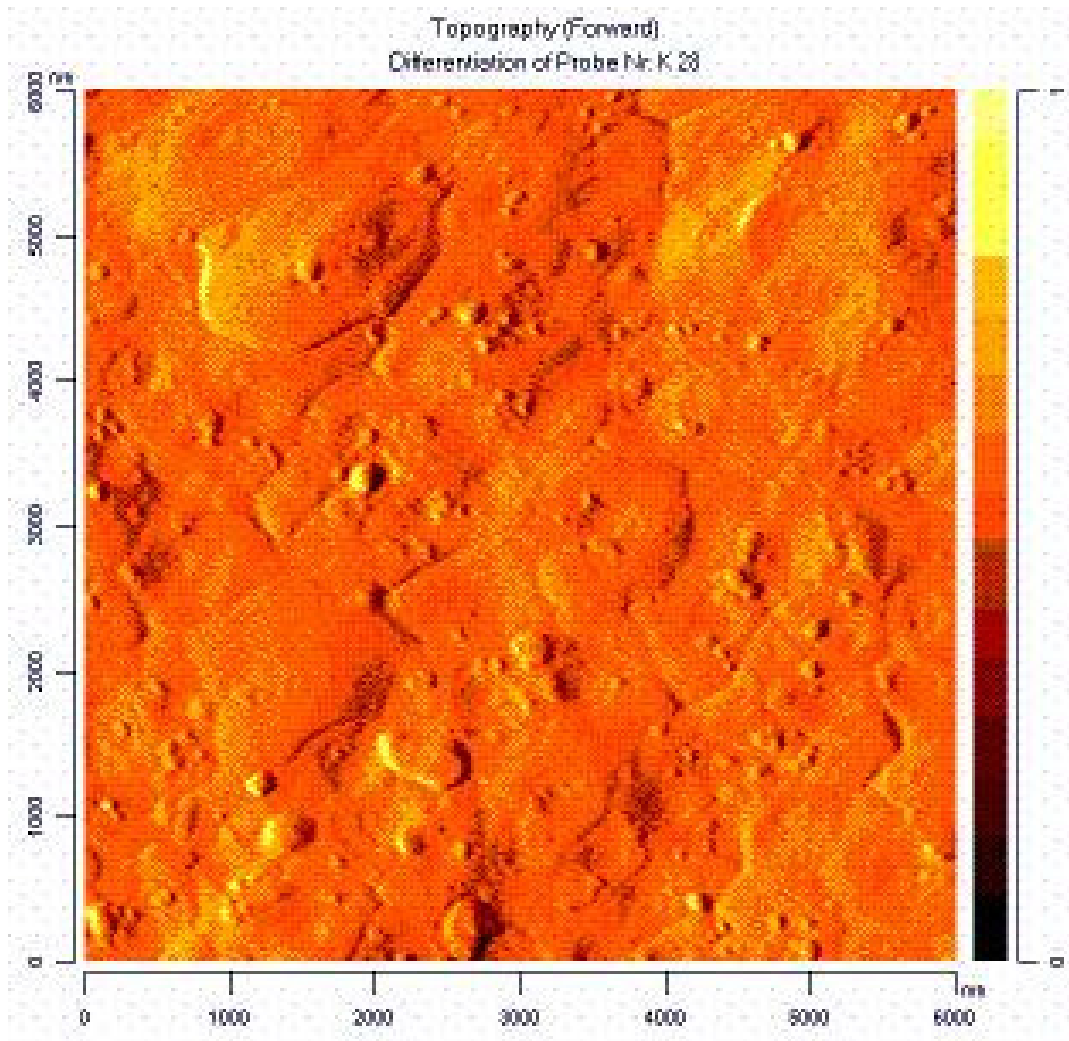


Figure 7-12: AFM of sample surface containing 1mol% $\text{Cu}(\text{NO}_3)_2 \cdot 3\text{H}_2\text{O}$ and 1.5mol% $\text{Cd}(\text{CH}_3\text{COO})_2 \cdot 2\text{H}_2\text{O}$ heat treated at 200 °C and holding time of 40 min.

Decreasing the co-activator content to 1.5 mol% had an interesting result. The sample was heat-treated at 200 °C for a holding time of 40 min. After the heat-treatment, the surface is densely crystallized as seen on the micrograph in Fig. 7-12. The average crystal size was approximately 450 nm and there was no indication of the glassy matrix surface.

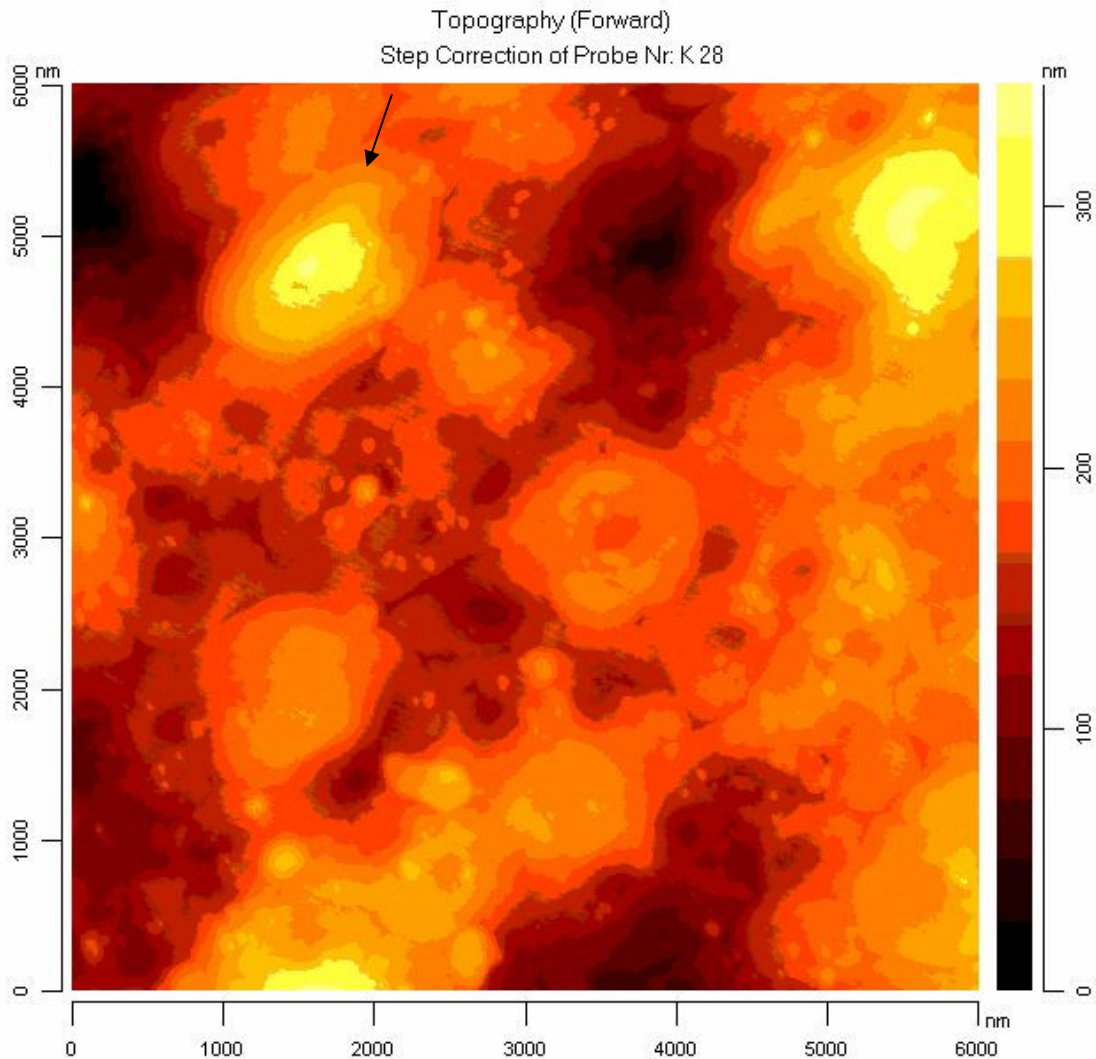


Figure 7-13: Surface structure of a sample containing Cd^{2+} and its spirally grown crystals. Sample containing 1mol% $\text{Cu}(\text{NO}_3)_2 \cdot 3\text{H}_2\text{O}$ and 1.5mol% $\text{Cd}(\text{CH}_3\text{COO})_2 \cdot 2\text{H}_2\text{O}$ heat treated at 200 °C and holding time of 40 min.

Other previous works in the group [33, 48] described the spirally crystal growth and Fig. 7-13 provides evidence of the same kind of crystal growth. Fig. 7-13 represents the step correction of the figure above. Note that at the left upper corner of the micrograph, one concentric pattern of crystal growth appears. The crystals grow with one or more growth centres and they might be convex (on the micrograph they are represented by a lighter spot in the centre) or concave (they have a dark centre). The average distance between the crystal periphery and centre is 150 nm.

Table 7-6 compares the data obtained in this work and the previous work [48].

Table 7-6: Average crystallite size compared to the literature

Composition	Crystallite average size	Previous crystallite average size*
1 Cu:Cd = 1:1	20 nm 30 nm high	
2 Cu:Cd= 1:2	200 nm 100 high	150 nm distance periphery- centre (spiral crystal)
3 Cu:Cd=1:1.5	450 nm – diameter spiral crystal 150 nm distance periphery- centre	
5 Cu:Cd = 2:0	200 nm 200 nm high	1.2 μm 200 nm high

Data from reference [48]

7.4 Scanning electron microscopy

Scanning electron microscopy has long been a standard technique for surface morphology characterization.

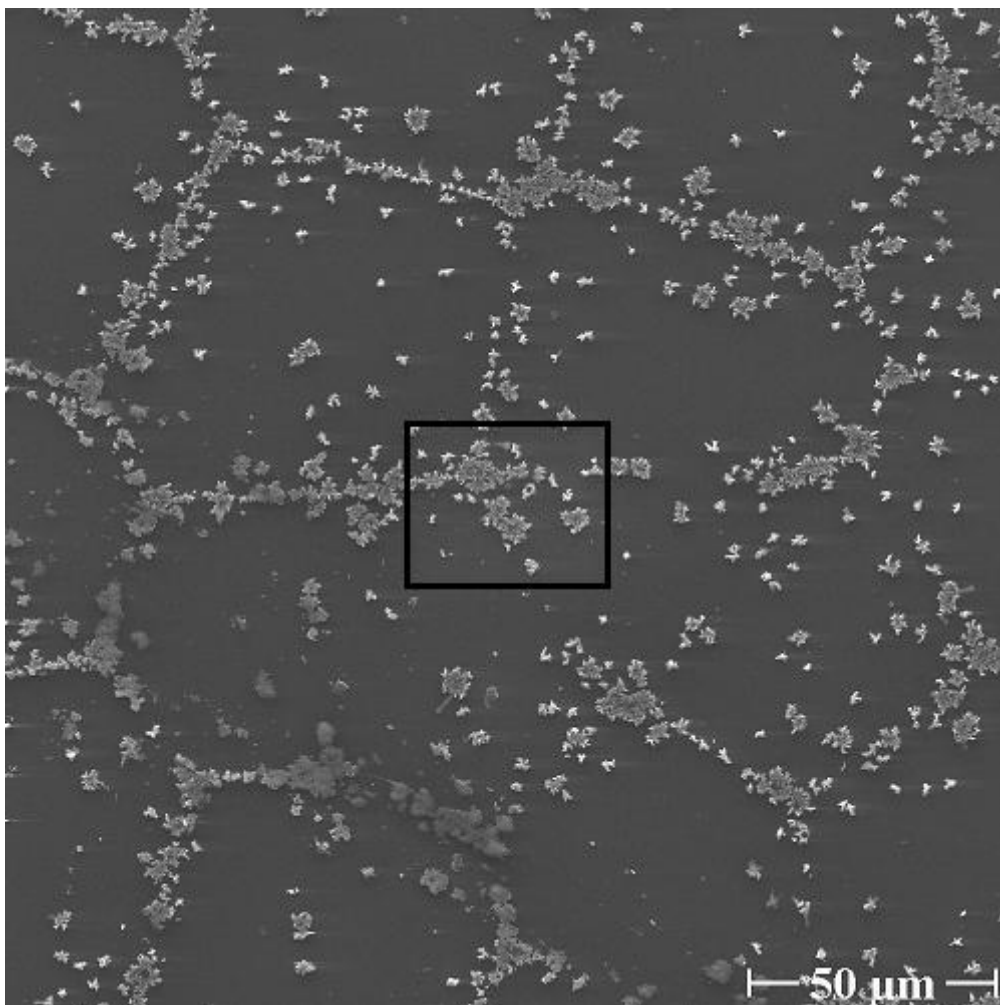


Figure 7-14: SE micrograph of a sample containing 0.9 mol% $\text{Cu}(\text{NO}_3)_2 \cdot 3\text{H}_2\text{O}$; 0.8 mol% $\text{Cd}(\text{CH}_3\text{COO})_2 \cdot 2\text{H}_2\text{O}$ and 0.6 mol% $\text{Zn}(\text{CH}_3\text{COO})_2 \cdot 2\text{H}_2\text{O}$.

Fig. 7-14 illustrates a sample prepared from a sol containing 0.9 mol% $\text{Cu}(\text{NO}_3)_2 \cdot 3\text{H}_2\text{O}$; 0.8 mol% $\text{Cd}(\text{CH}_3\text{COO})_2 \cdot 2\text{H}_2\text{O}$ and 0.6 mol% $\text{Zn}(\text{CH}_3\text{COO})_2 \cdot 2\text{H}_2\text{O}$.

Notice that the crystals were dispersed in a glassy matrix and partially connected to each other in a network forming a polygonal pattern. The junction

points between the polygons usually connected three of them. The junction point in detail is an exception connecting four polygons. The diameter of the polygons was approximately 50 μm .

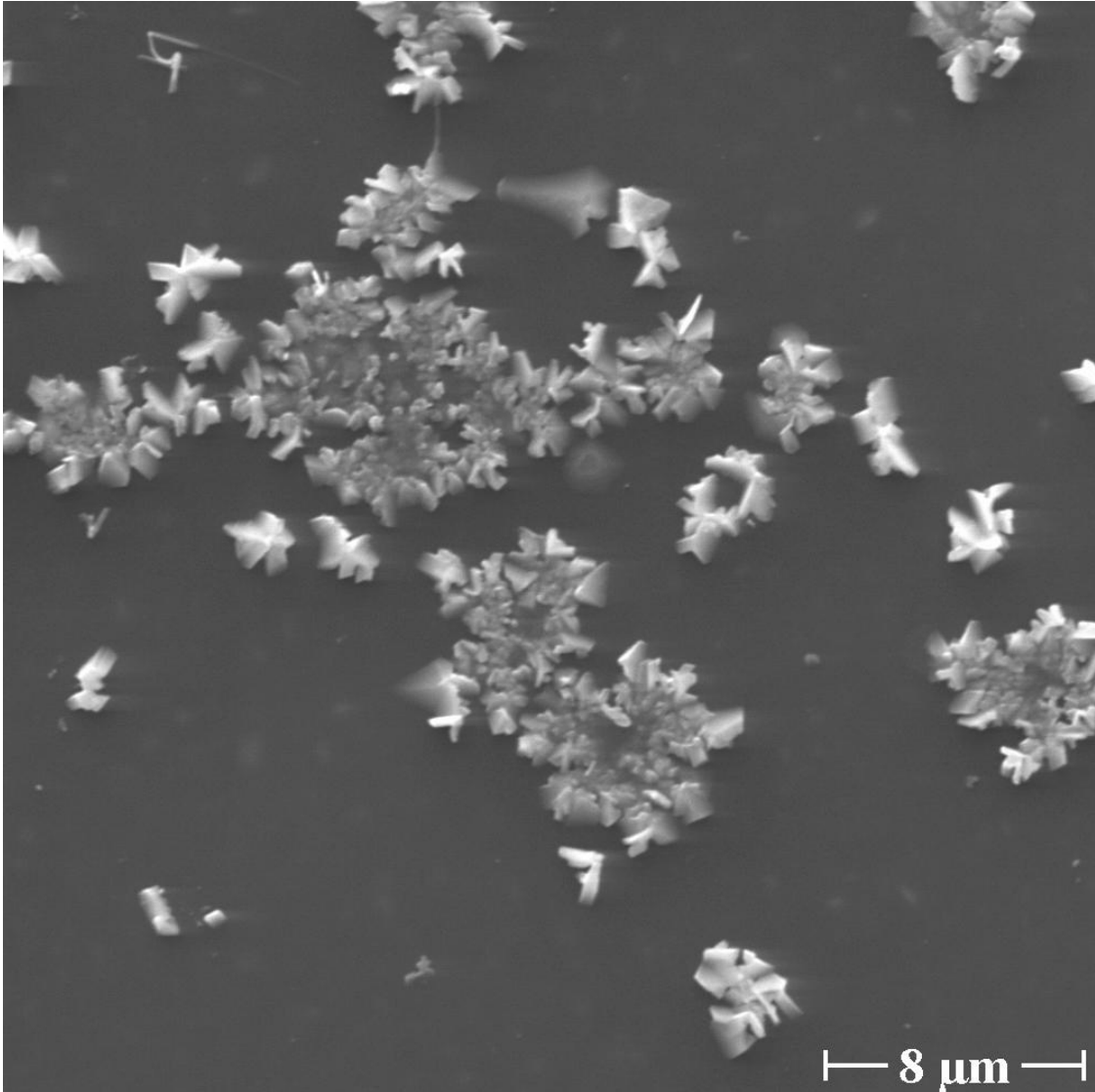


Figure 7-15: SE micrograph of a sample containing 0.9 mol% $\text{Cu}(\text{NO}_3)_2 \cdot 3\text{H}_2\text{O}$; 0.8 mol% $\text{Cd}(\text{CH}_3\text{COO})_2 \cdot 2\text{H}_2\text{O}$ and 0.6 mol% $\text{Zn}(\text{CH}_3\text{COO})_2 \cdot 2\text{H}_2\text{O}$.

In Fig. 7-15, the crystal agglomerates could be better observed. The nodal point of four polygons can be viewed in detail. Crystals around 1 μm in diameter formed the agglomerates. The agglomerates were approximately 8 μm in diameter. The small crystals were actually the top of agglomerates that are located one level below the measured level.

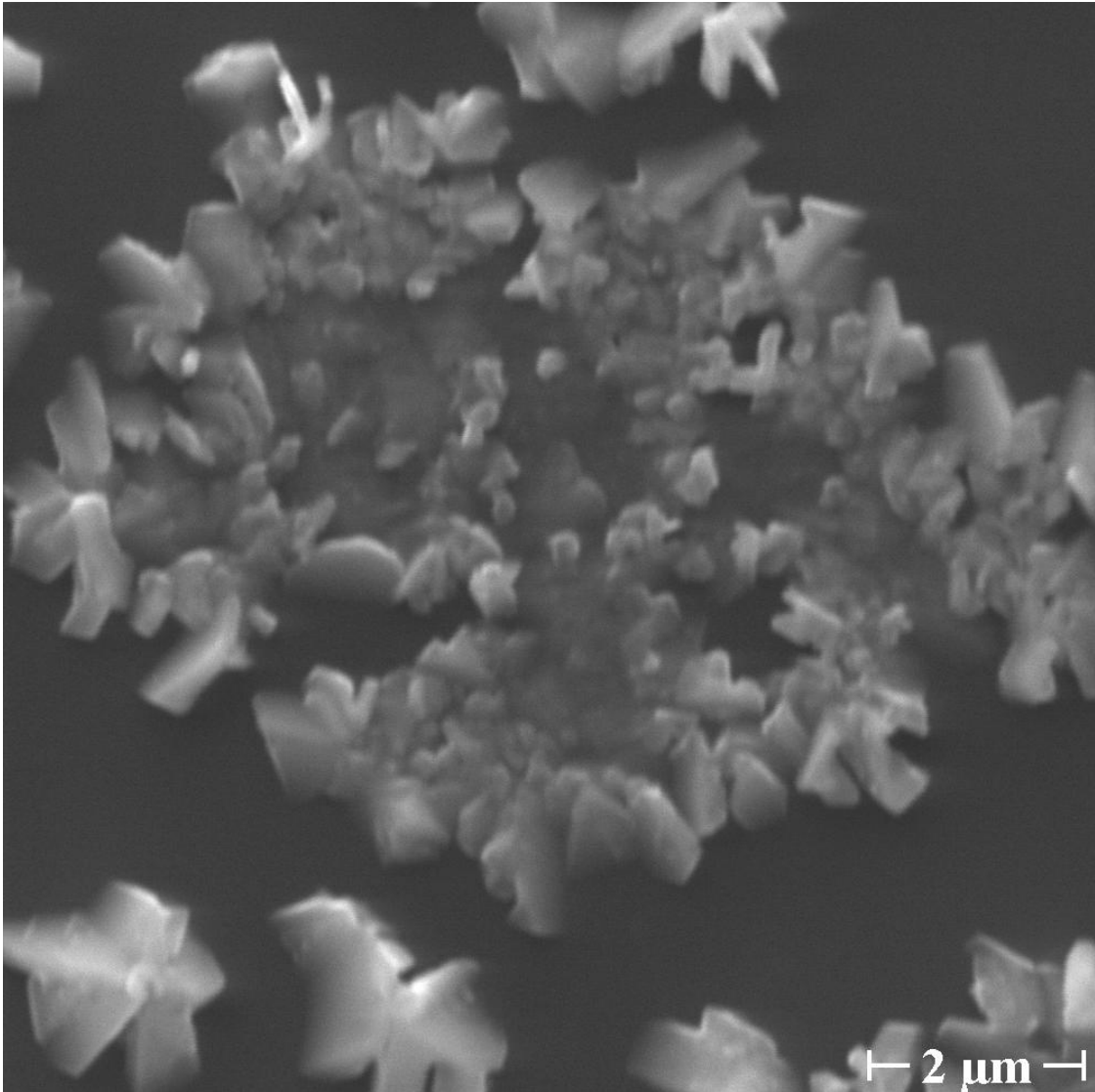


Figure 7-16: SE micrograph of a sample containing 0.9 mol% $\text{Cu}(\text{NO}_3)_2 \cdot 3\text{H}_2\text{O}$; 0.8 mol% $\text{Cd}(\text{CH}_3\text{COO})_2 \cdot 2\text{H}_2\text{O}$ and 0.6 mol% $\text{Zn}(\text{CH}_3\text{COO})_2 \cdot 2\text{H}_2\text{O}$.

In the micrograph, Fig. 7-16, the plaque like crystals were shown in detail. The crystals looked like small and flat tiles linked one to another by one common plane, making angular shapes, like L-shaped, V-shaped or W-shaped as well as combinations of more than one of these shapes.

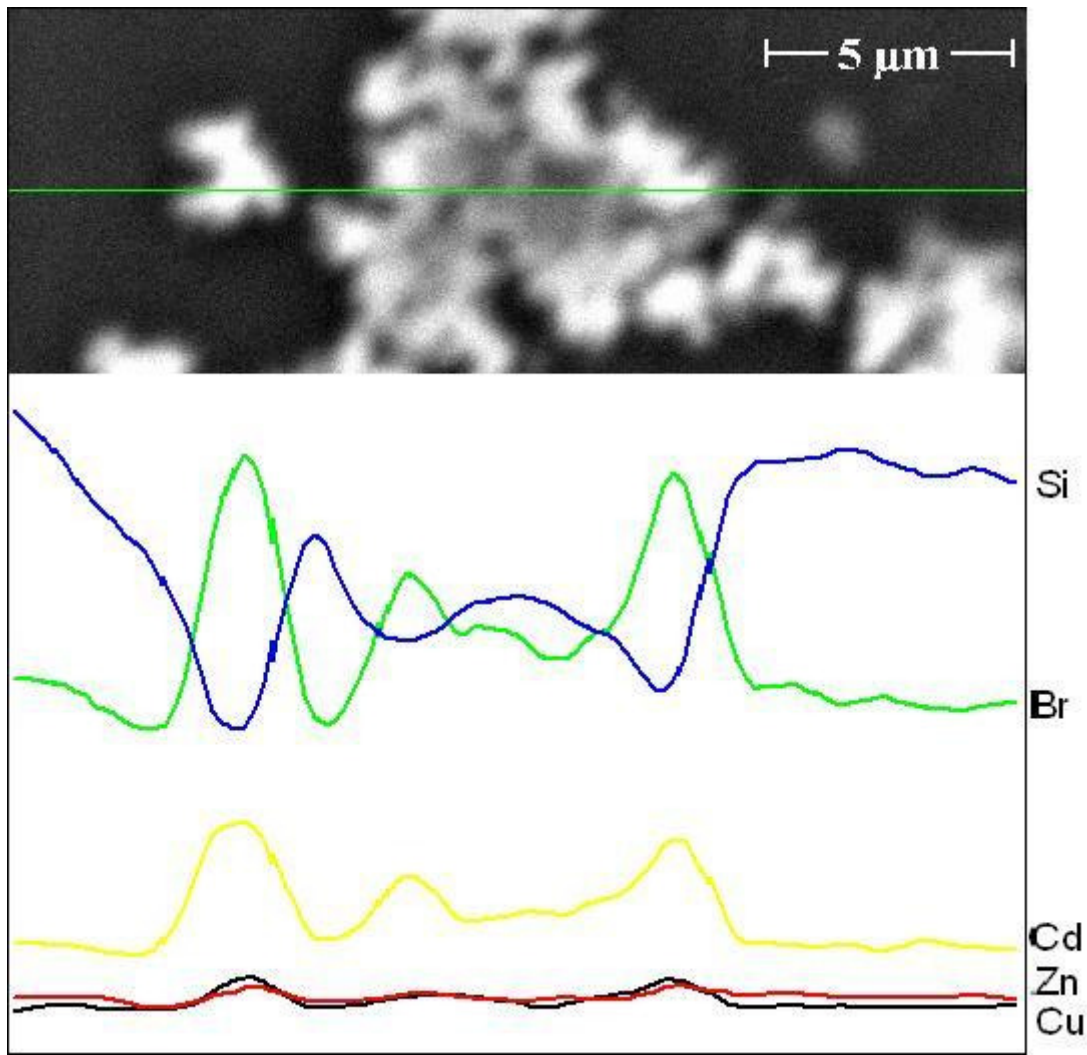


Figure 7-17: BSE micrograph of a sample containing 0.9 mol% $\text{Cu}(\text{NO}_3)_2 \cdot 3\text{H}_2\text{O}$; 0.8 mol% $\text{Cd}(\text{CH}_3\text{COO})_2 \cdot 2\text{H}_2\text{O}$ and 0.6 mol% $\text{Zn}(\text{CH}_3\text{COO})_2 \cdot 2\text{H}_2\text{O}$. X-ray emission signals for Br, Cu, Cd and Zn along a line scan.

Fig. 7-17 is a BSE image of the surface of a 5 μm sized agglomerate. Below the micrograph, is shown the X-ray emission signals for Br, Cu, Cd and Zn along a line scan (green) intersecting the micrograph.

The micrograph could be divided in 4 regions along the scan line. Beginning on the left side of the figure, on the first dark region (that will be called the matrix), the content of Si was much higher compared to all other analysed elements (Br, Zn and Cd).

The second region (the first white region) is the first crystal on the left. Note that emission signals for Si dropped dramatically and the signals for Cd, Br, Zn

increased. The content of Cd and Br was higher than the Cu and Zn contents. It illustrates that these elements were present at the crystal constitution.

A third region represented by the larger crystal agglomerate in the middle of the micrograph, showed different intensity of the signals for all elements including Si. This was not expected. The X-ray emission signals increased for the elements in the following order: Zn; Si; Cu; Br; Cd.

Finally the fourth region of amorphous matrix is represented by the dark patches of the micrograph and by higher emission signals for Si.

The signal for Zn remained almost constant along the green line. A relatively remarkable peak could be seen only in the second region.

The presence of Si could be attributed to the glass surrounding a very small crystal (smaller than 2 μm). The X-ray generation volume is approximately 2-3 μm in diameter and depth. If the crystal is smaller and/or is positioned above this depth, it is possible that signals from the glass are measured instead of the crystal caused by a superposition of the X-rays from the crystal and the matrix.

7.5 Ellipsometry

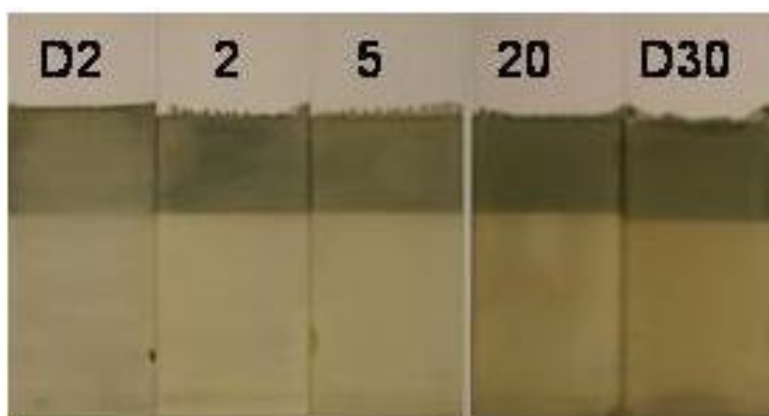


Figure 7-18: Samples coated at 2 (double), 2, 5, 20 and 30 (double) cm/min.

Thickness of the samples varied between 200 nm and 500 nm. The thickest samples were coated twice with a withdraw velocity of 30 cm/min each. It is possible for the increase of withdraw velocity up to 30 cm/min to increase the

thickness. Samples coated with withdraw velocities higher than 30 cm/min did not display wrinkle-free and uniform surface.

The roughness of the samples varied between approximately 5 nm to 30 nm. Thicker samples resulted in less roughness and vice-versa. Fig. 7-18 illustrates photochromic coatings with different withdraw velocities. From the left side, the first sample was coated twice with a velocity of 2 cm/min. The following samples marked with 2, 5 and 20, were coated at these velocities, and the last one to the right was double coated at 30 cm/min withdraw velocity.

The samples were also partially exposed to UV light, which corresponds to the darkened upper part of each sample in Fig. 7-18. Note that the samples after heat-treatment have a yellow/brown colour and the colour intensity enhances with increasing coating thickness (this is relative to withdraw velocity). The thinnest sample was 200 nm thick and corresponds to the second sample, coated at 2 cm/min. The thicker sample in the picture below was the last one (right), 500 nm thick which was coated twice at 30 cm/min.

7.6 UV-VIS spectroscopy

7.6.1 The formation of photochromic crystals

In order to investigate the crystal formation, UV-VIS absorption spectrometric measurements were made on dried samples during the heating treatment.

The results of the measurements described at Chapter 6.1. are found below.

It can be seen that the CuBr crystals show two exciton absorption bands around 400 nm. The position of the peaks can shift in accordance with some crystal characteristics such as crystal size [64].

Although the absorption spectra are more meaningfully expressed as a function of wave number (cm^{-1}), the most commonly used quantity is wavelength (nm), which will be used in the following figures.

7.6.1.1 Samples with no cadmium (II) acetate dihydrate

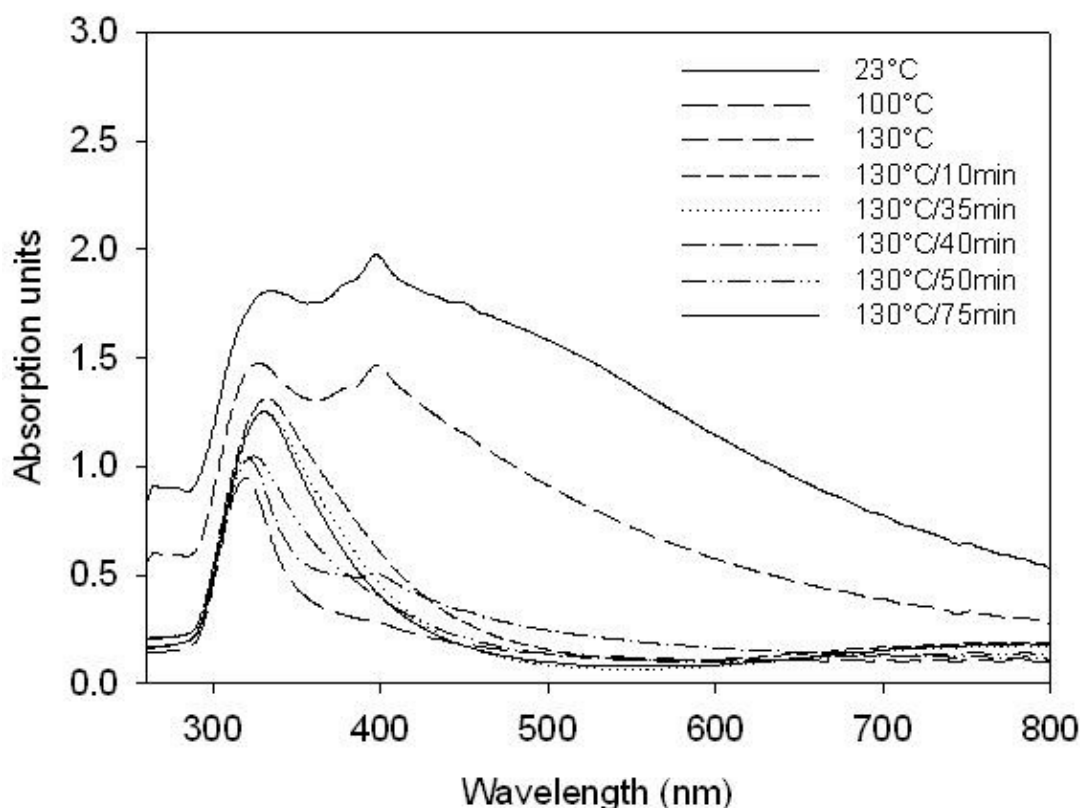


Figure 7-19: Sample containing 2 mol% $\text{Cu}(\text{NO}_3)_2 \cdot 3\text{H}_2\text{O}$, without $\text{Cd}(\text{CH}_3\text{COO})_2 \cdot 2\text{H}_2\text{O}$, heated up to 130 °C and holding time by 130 °C was 75 min.

Fig. 7-19 shows a broad absorption band centred near 350 nm. A sharp increase in absorption at wavelength near 390 nm and 400 nm can also be observed.

The first absorption band (350 nm) is due to Cu^+ and Br^- ions in the gel. During the heat-treatment this absorption decreases as the temperature increases from room temperature to 130 °C. This happens because those insoluble bromocuprate ions precipitate forming CuBr crystals.

The two other absorption bands (390 nm and 400 nm) start to take shape after 35 min at 130 °C. These bands are due to CuBr excitons absorption, which means that this band confirms the presence of CuBr crystals. In this instance, it might be affirmed that the formation of CuBr crystals begins at 130 °C after 35 min.

It should be noted that these samples do not contain cadmium acetate dihydrate in the formulation and they are not photochromic.

The absorption between 500 nm and 700 nm increases with time under UV exposure because the sample turns pale opaque, but it does not darken.

These findings are evidence that the formation of pure CuBr crystals is not sufficient to activate the photochromic effect.

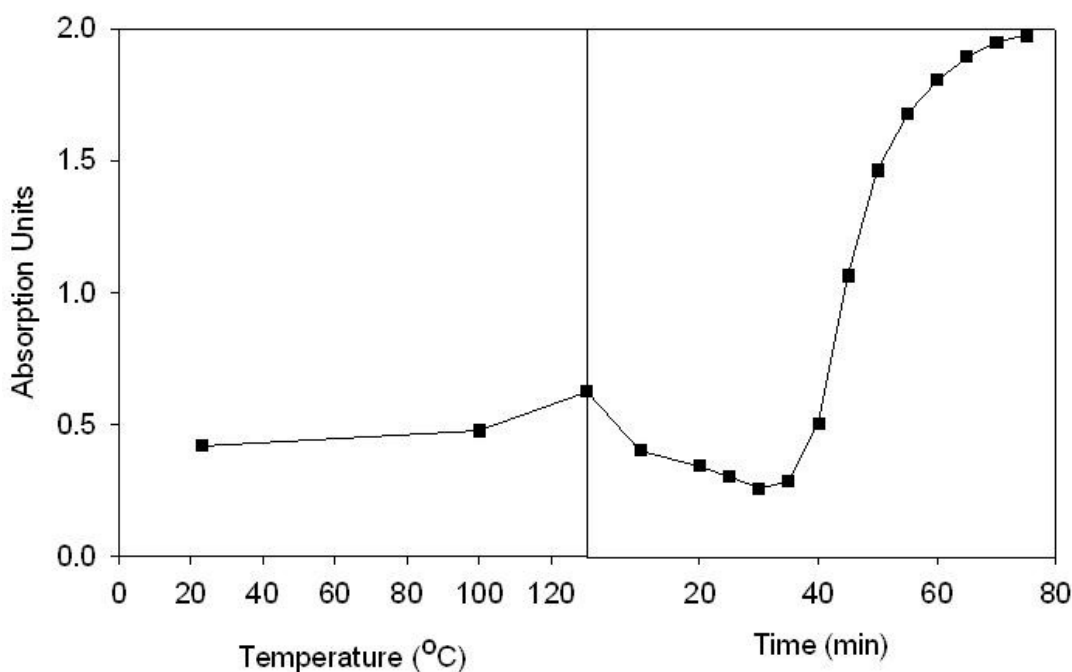


Figure 7-20: Absorption behaviour at 400 nm (CuBr exciton absorption band) during heat-treatment: heating and holding time at 130 °C of sample containing 2 mol% $\text{Cu}(\text{NO}_3)_2 \cdot 3\text{H}_2\text{O}$, without $\text{Cd}(\text{CH}_3\text{COO})_2 \cdot 2\text{H}_2\text{O}$.

Fig. 7-20 shows that the absorption at 400 nm is increased slightly during the heating stage (10 K/min) and dropped again when achieved the holding temperature (130 °C). During the holding time of 75 min, the absorption increased abruptly. At this stage, all insoluble Cu^+ and Br^- ions existing in the gel gain mobility and start forming CuBr crystals. This process increases the absorption as shown in Fig.7-20. At the end of this stage the absorption tends to stabilize as there are no more Cu^+ and Br^- ions to crystalize.

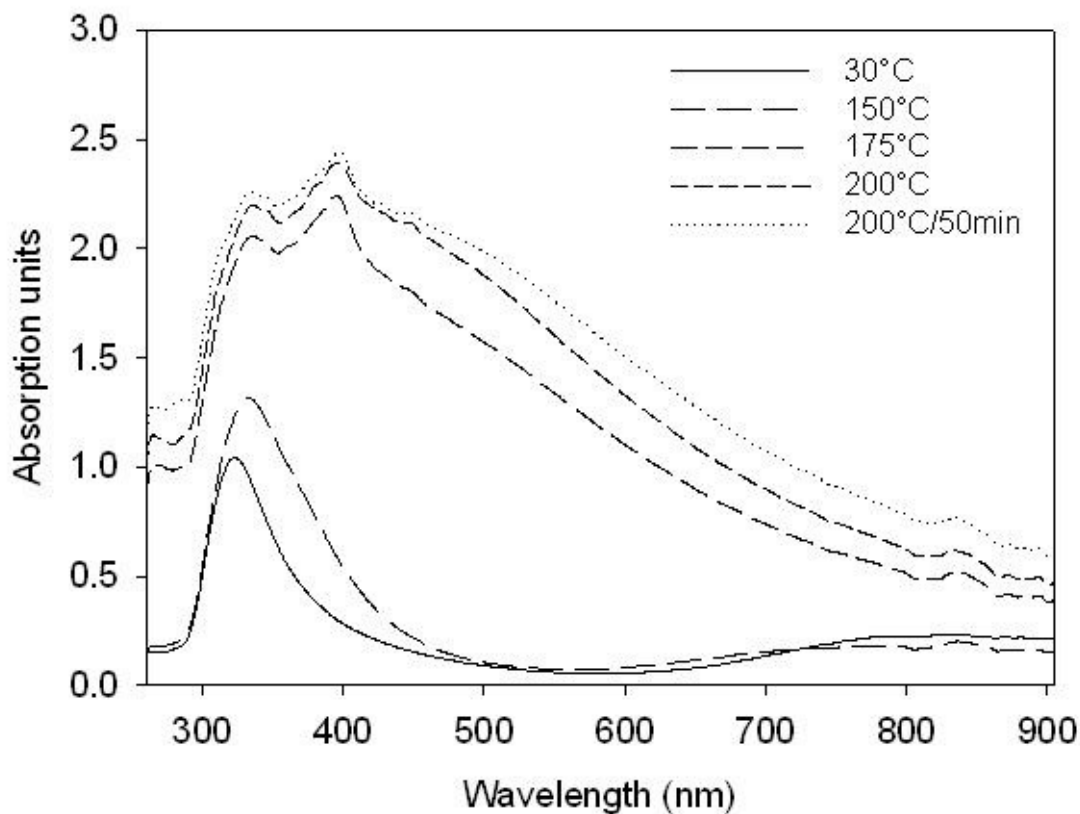


Figure 7-21: Sample containing 2 mol% $\text{Cu}(\text{NO}_3)_2 \cdot 3\text{H}_2\text{O}$, without $\text{Cd}(\text{CH}_3\text{COO})_2 \cdot 2\text{H}_2\text{O}$, heated up to 200 °C with 50 min of holding time.

Fig. 7-21 shows that the CuBr formation can happen at higher temperatures.

In this case, the CuBr formation started at 175 °C before the holding time began, set to 200 °C.

A smooth shift to the left of the Cu^+ absorption band at 390 nm can be noticed. That shift suggests the crystals are slightly smaller than those in the previous Fig. 7-19. The reason is that it was not given enough time for crystal growth when they are first generate at 175 °C (the heating rate was 5K/min).

At 840 nm another peak can be noticed. This is attributed to Cu^{2+} ions.

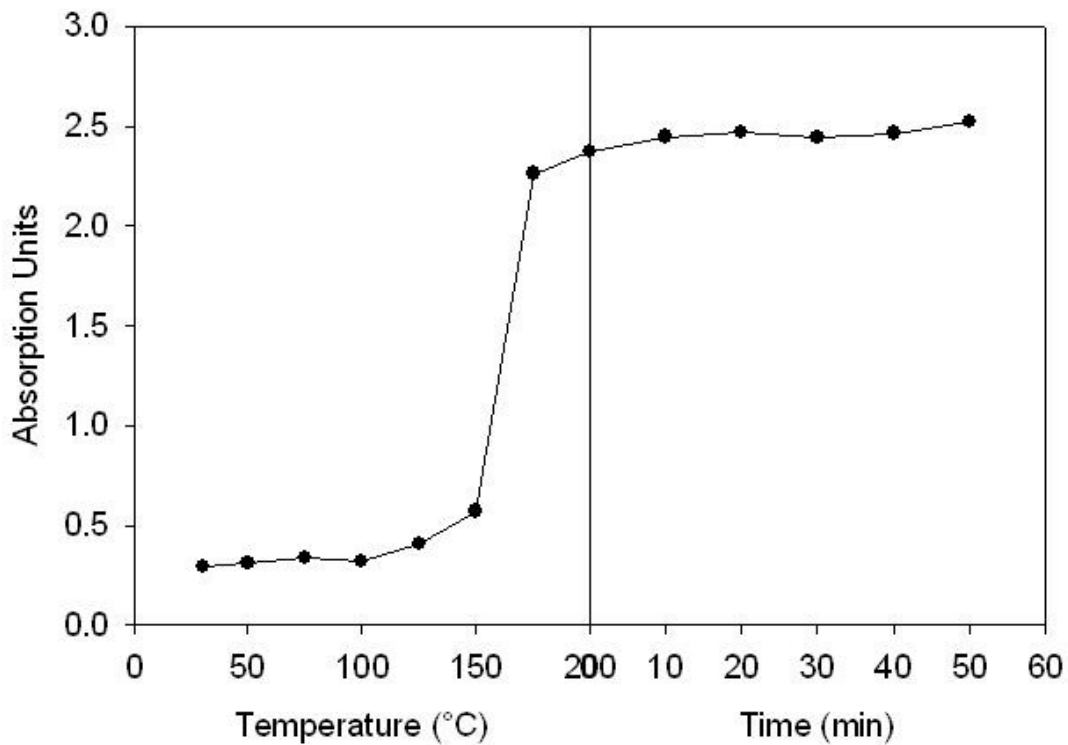


Figure 7-22: Absorption behaviour at 397 nm (CuBr exciton absorption band) for sample containing 2 mol% $\text{Cu}(\text{NO}_3)_2 \cdot 3\text{H}_2\text{O}$, without $\text{Cd}(\text{CH}_3\text{COO})_2 \cdot 2\text{H}_2\text{O}$, heated up to 200 °C with 50 min of holding time.

Fig. 7-22 shows that an intense increase in absorption happened between 150 °C and 175 °C. As described before, this is a sign for CuBr crystals formation from Cu^+ and Br^- ions existing in the gel. The crystals are generated during the heating stage in this example. Once the holding temperature was achieved, the absorption remained stable. This suggests the most of insoluble Cu^+ and Br^- ions already precipitated in the glass.

Table 7-7 shows the summary of resulting absorption bands for the composition K1 (see Appendix 10-2) where the copper halide crystallites had no effect of co-activator (Cd^{2+}), as the heat-treatment gradually occurred.

Table 7-7: Enumeration of occurring absorption bands during heat-treatment at various temperatures and comparison with literature

Heat-treatment		Bromocuprate complexes Absorption bands (nm)	Cu ⁺ excitons Absorption bands (nm)	
Temperature (°C)	Time (min)			
100	< 1	310	-	-
130	30	310	-	-
130	40	310	390	400
130	75	310	390	400
150	< 1	310	-	-
175	<1	310	-	-
200	<1	310		410
200	50	310		410
800 Literature [36]	120		380	390
150 Literature [39]	60 +UV irradiation	310	391	410

7.6.1.2 Samples with 0.5 mol% of cadmium(II)acetate dihydrate and the influence of heat-treatment in transmission behaviour

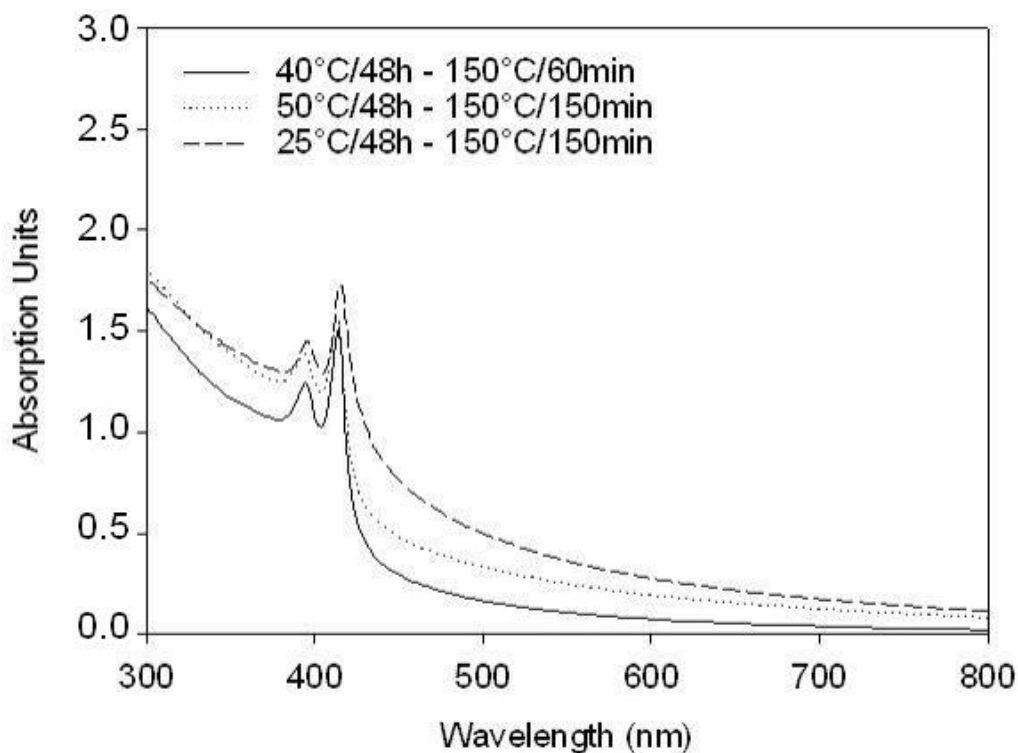


Figure 7-23: Absorption behaviour of samples containing 1 mol% $\text{Cu}(\text{NO}_3)_2 \cdot 3\text{H}_2\text{O}$ and 0.5 mol% $\text{Cd}(\text{CH}_3\text{COO})_2 \cdot 2\text{H}_2\text{O}$ dried and heat treated at variable temperatures.

Fig. 7-23 shows samples with 0.5 mol% $\text{Cd}(\text{CH}_3\text{COO})_2 \cdot 2\text{H}_2\text{O}$ and different heat-treatments.

They had different drying temperatures (25 °C; 40 °C and 50 °C) but the same time (48 h). After the drying process, they were heat treated at 150 °C and different holding times (60 min and 150 min).

The results show that the samples dried at 50 °C have higher transmission percentage at wavelengths above 400 nm. These samples were heat treated at 150 °C for 60 min and 150 min. The sample heat treated at 150 °C for 60min had a higher transmission percentage and the narrowest width of the absorption peak, which is evidence of smaller crystal sizes distribution.

The sample dried at room temperature and heat treated for 150 min had the lowest transmission percentage at 550 nm. The sample dried at 40 °C and heat treated for 60 min had the highest transmission percentage at 550 nm.

These results clarify that those drying temperatures (25 °C and 50 °C) do not influence the final crystal size. The peak widths in those curves (dots and slashes) do not change significantly between the two samples. The value of transmissions for both curves at 550 nm does display a significant change (28%), however.

The larger crystal size distribution of the samples heat treated for 150 min is illustrated by the width peak that appears at ~410 nm (dots and slashes) compared to the sample heat treated for 60 min (line). However, they are not photochromic.

The following table displays the resume of transmission behaviour for the composition K2 (see Appendix 10-2).

Table 7-8: Samples with different drying temperatures and heat-treatments and their influence on transmission behaviour at the visible light range (wavelength at which the human eye is most sensitive)

Drying temperature (48h)	Heat-treatment (150 °C)	Cu⁺ Absorption bands	Initial transmission at 550 nm
25 °C	150 min	410 nm*	35 %*
40 °C	60 min	410 nm*	78 %*
50 °C	150 min	410 nm*	45 %*

*Values are approximated.

7.6.1.3 Samples with 1 mol% of cadmium acetate dihydrate

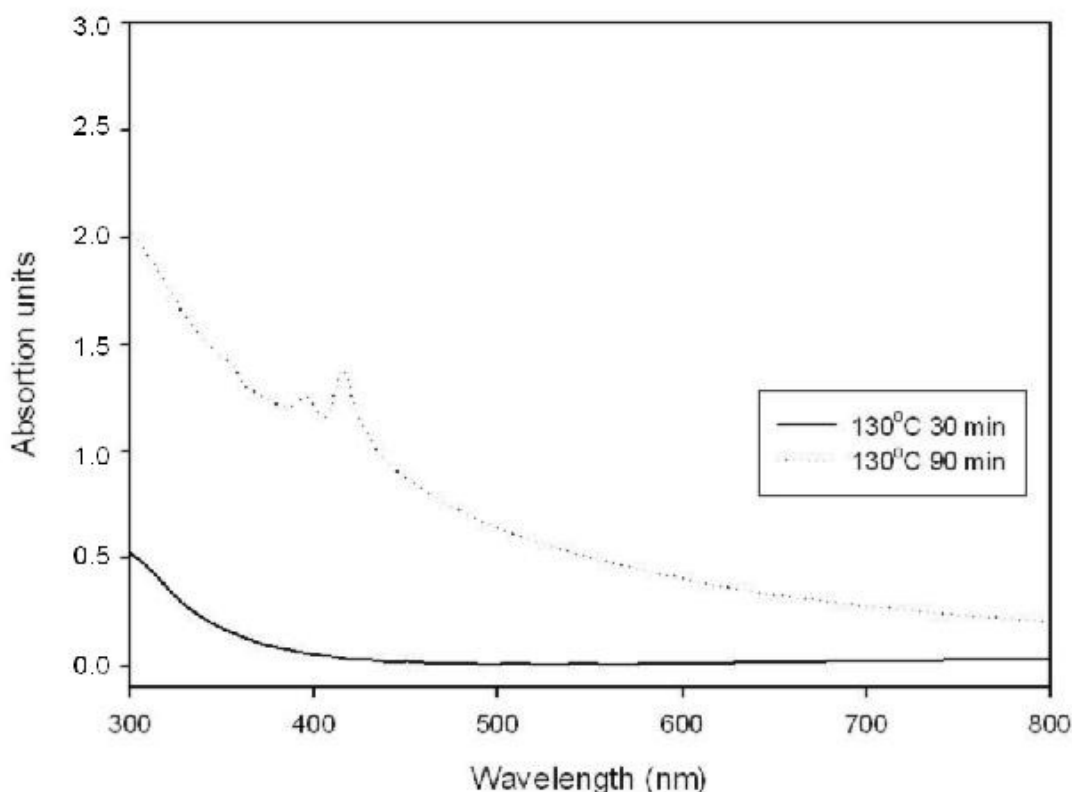


Figure 7-24: Absorption behaviour of samples containing 1 mol% $\text{Cu}(\text{NO}_3)_2 \cdot 3\text{H}_2\text{O}$ and 1 mol% $\text{Cd}(\text{CH}_3\text{COO})_2 \cdot 2\text{H}_2\text{O}$.

Fig. 7-24 shows two samples heat treated at 130 °C and holding time of 30 min and 90 min respectively, both of them containing 1 mol% of copper(II)nitratetrihydrate and 1 mol % of cadmium(II)acetate dihydrate.

The first sample was heated to 130 °C for 30 min (line) and did not have enough time to precipitate and grow the CuBr crystals. This sample does not show the characteristic CuBr absorption band at 400 nm.

Recalling the discussion in section 7.2.1.1, Fig. 7-19 showed that the CuBr crystal precipitation and growth at 130 °C started after 35 min holding on that temperature (for samples without Cd^{2+}). The conclusion was that the presence of Cd^{2+} delays the CuBr precipitation.

The second sample, heated with a holding time of 90 min at 130 °C, showed the absorption band around 400 nm.

This sample on the other hand, is sensitive to UV irradiation. It clearly darkens under irradiation.

After heat-treatment the sample had a 30% initial transmission at 550 nm. The sample is visibly opaque. This is a sign that the crystals are too large and they scatter the light instead of transmitting it.

Temperatures as low as 130 °C needed more than 40 min to activate the CuBr crystals precipitation and growth.

The sample heat treated for 90 min, did have the CuBr excitons absorption band relative to CuBr crystallites but they were extremely large.

We can therefore conclude that in order to obtain copper bromide crystallites the heat-treatment should be at higher temperatures rather than longer heat-treatments at lower temperatures to avoid excessive crystal growth that causes opacity.

The table below illustrates the influence of heat-treatment in crystal growth and transmission.

Table 7-9: Influence of heat-treatment on the CuBr crystal precipitation in transmission

Heat-treatment (130 °C)	CuBr absorption bands	Initial transmission at 550 nm
30 min	-	95%
90 min	410 nm	30 %

7.6.1.4 Samples with 1.5 mol% of cadmium acetate dihydrate

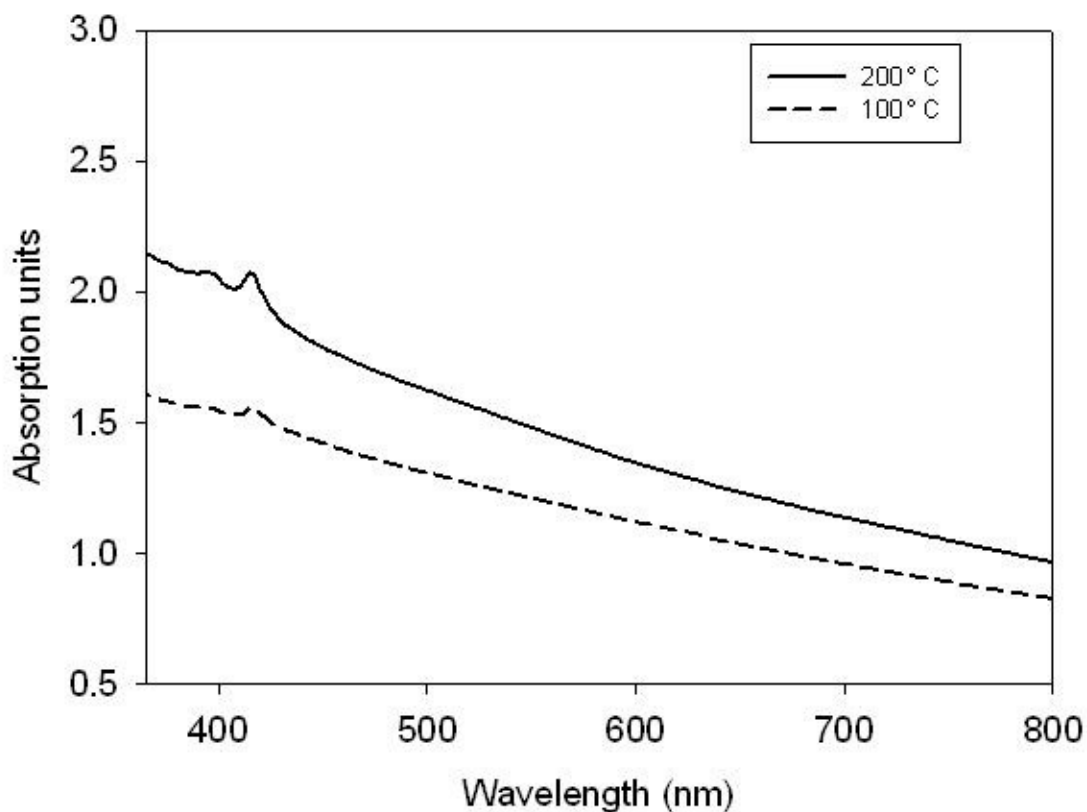


Figure 7-25: Absorption behaviour of samples containing 1 mol% $\text{Cu}(\text{NO}_3)_2 \cdot 3\text{H}_2\text{O}$ and 1.5 mol% $\text{Cd}(\text{CH}_3\text{COO})_2 \cdot 2\text{H}_2\text{O}$.

Fig. 7-25 illustrates two samples containing 1.5 mol% $\text{Cd}(\text{CH}_3\text{COO})_2 \cdot 2\text{H}_2\text{O}$. The absorption level was higher than that of samples containing 1 mol% $\text{Cd}(\text{CH}_3\text{COO})_2 \cdot 2\text{H}_2\text{O}$ (compare with Fig.7-24). The sample dried at 100 °C for 30 days showed the beginning of the peak at 400 nm.

7.6.1.5 Samples with 40% of cadmium acetate dihydrate content substituted by zinc acetate dihydrate

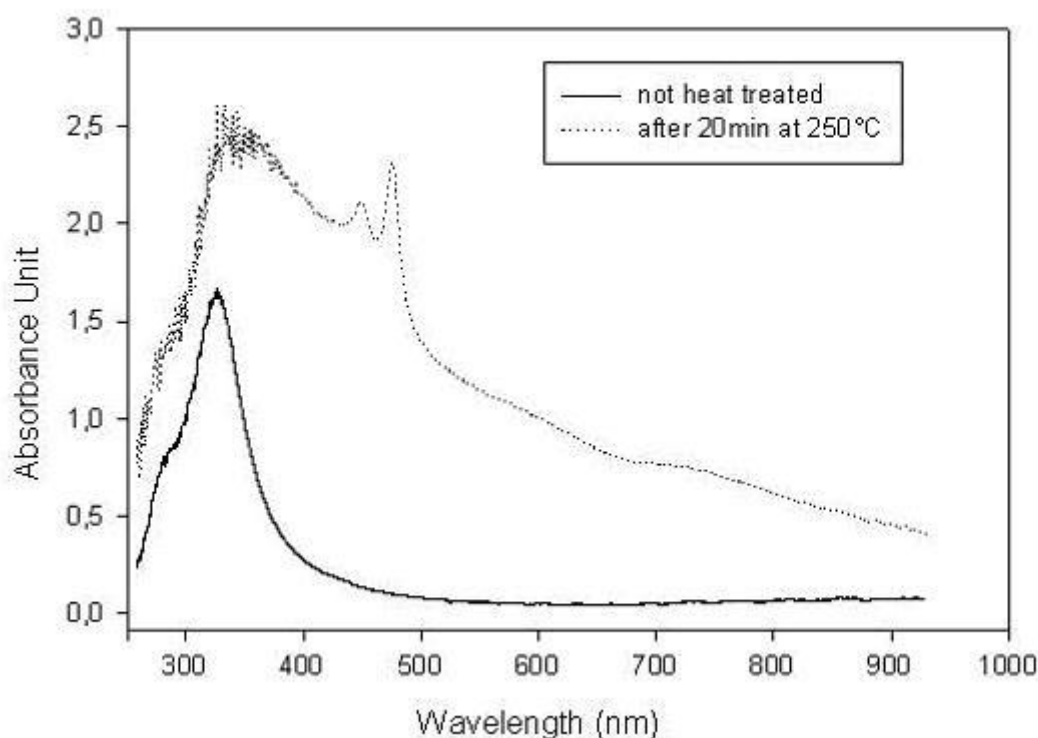


Figure 7-26: Absorption behaviour of samples containing 0.9 mol% $\text{Cu}(\text{NO}_3)_2 \cdot 3\text{H}_2\text{O}$; 0.8 mol% $\text{Cd}(\text{CH}_3\text{COO})_2 \cdot 2\text{H}_2\text{O}$ and 0.6 mol% $\text{Zn}(\text{CH}_3\text{COO})_2 \cdot 2\text{H}_2\text{O}$.

After setting the best composition to be the one with 1.5 mol% $\text{Cd}(\text{CH}_3\text{COO})_2 \cdot 2\text{H}_2\text{O}$, Fig. 7-26 shows two samples with 40% of $\text{Cd}(\text{CH}_3\text{COO})_2 \cdot 2\text{H}_2\text{O}$ substituted against $\text{Zn}(\text{CH}_3\text{COO})_2 \cdot 2\text{H}_2\text{O}$.

After one sample was heat treated at 250 °C and holding time of 20 min, the measurement revealed two absorption peaks between 450 nm and 500 nm caused by the CuBr excitons. The bromocuprate complexes could also be observed at absorption peak around 325 nm.

This measurement was made before and after the heat-treatment to illustrate the absence of photochromic crystals (CuBr) before the heat-treatment and its formation characterized by the absorption peak around 490 nm.

The sub-sequential table associates the results of absorption bands for the composition Z4 (see Appendix 10-2). This sample was sensitive to UV light, in that it darkens when exposed. Its photochromic behaviour was measured and will be discussed in more detail in section 7.6.1.4 below. Samples heat-treated at higher temperatures such as 350 °C for 20 min were not photochromic. This is probable because at this temperature the photoactive elements evaporate.

Table 7-10: Copper halide absorption bands containing both Zn²⁺ and Cd²⁺ as co-activator

Composition	Cu⁺ excitons absorption bands (nm)
Z4	450 nm 500 nm

7.6.2 Darkening and fading measurements

The next measurement of the photochromic effect (darkening and fading) was described by Veit [13]. The transmission behaviour of a sample during exposure to irradiation was measured. A XBO lamp 150 W (xenon lamp) provided a continuous spectrum at the visible range and daylight colour temperature of approx. 6000K. One SiO₂ fibre cable connected the lamp and was placed 1cm above the sample. A SiO₂ fibre connected the transmitted light to the monochromator and diode array detector. The wavelength range was between 300 to 800 nm. The transmitted light was measured 10 times in 0.2 s.

The sample was then irradiated by the xenon lamp for 5 min. The photochromic samples would darken while under activation irradiation. The transmission was measured 5 times during this irradiation period to characterize the darkening behaviour. When the irradiation stopped the sample was placed under a protective dark cover so that it could recover the initial transmission. To measure the fading process the transmission was measured at the same spot after 5 and 10 minutes and every 30 minutes until the sample recovered the initial transmission.

In accordance with Hoover [65] the human eye is highly sensitive to wavelengths of 550 nm. To measure the darkening and fading effect, the transmission alteration at 550 nm was plotted.

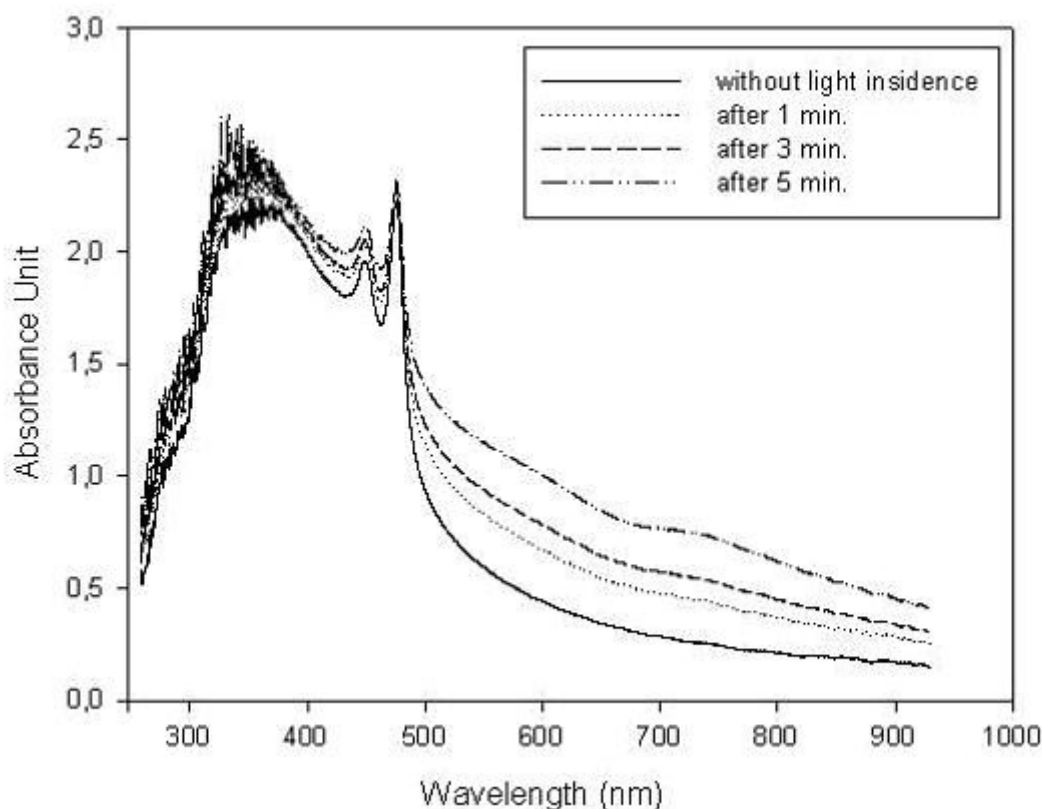


Figure 7-27: Darkening behaviour of sample containing Zn^{2+} irradiated for the duration of 5 min.

The sample shown in Fig. 7-27 was measured while under UV irradiation. The first curve (lowest line) was done before any exposure to UV radiation, and the following 3 measurements after 1 min (dots), 3 min (slashes) and 5 min (dot-slashes), while under UV irradiation. In this instance, it is possible to see how the sample modified its initial absorbance due to the darkening process.

The CuBr excitons absorption created two bands at approximately 449 nm and 475 nm. These bands already existed before the irradiation started. After 1 min under UV light radiation, formation of copper colloids could be seen on the surface of the CuBr crystals. This could be seen by Cu colloids absorption bands approximately at ~ 590 nm and ~ 730 nm [48].

The following table describes the existing absorption peaks and their relative excitons.

Table 7-11: Absorption peaks formed during irradiation compared to the literature.

Sample	UV irradiation	Absorption peaks	
		CuBr	Cu ⁰
Z4	< 1 second	449	
		475	
Z4	After 5 minutes	449	590
		475	730

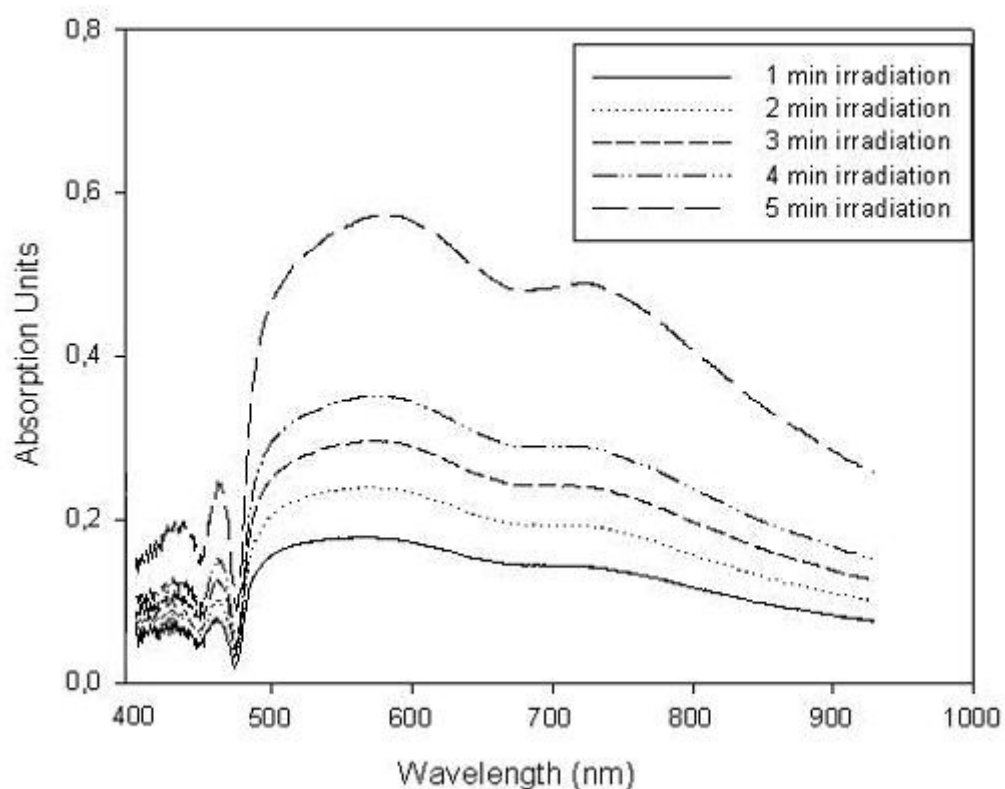


Figure 7-28: Absorption behaviour of sample containing Zn²⁺ irradiated for the duration of 5 min. Subtracted spectra for different exposure times.

Fig. 7-28 provides evidence of the bands due to colloids Cu^0 and ions Cu^{2+} respectively $\sim 590 \text{ nm}$ and $\sim 730 \text{ nm}$. Each curve was plotted after subtracting the curve before exposure to UV light. Marquez et al. attributed the peak at 590 nm to Cu^0 colloids [40].

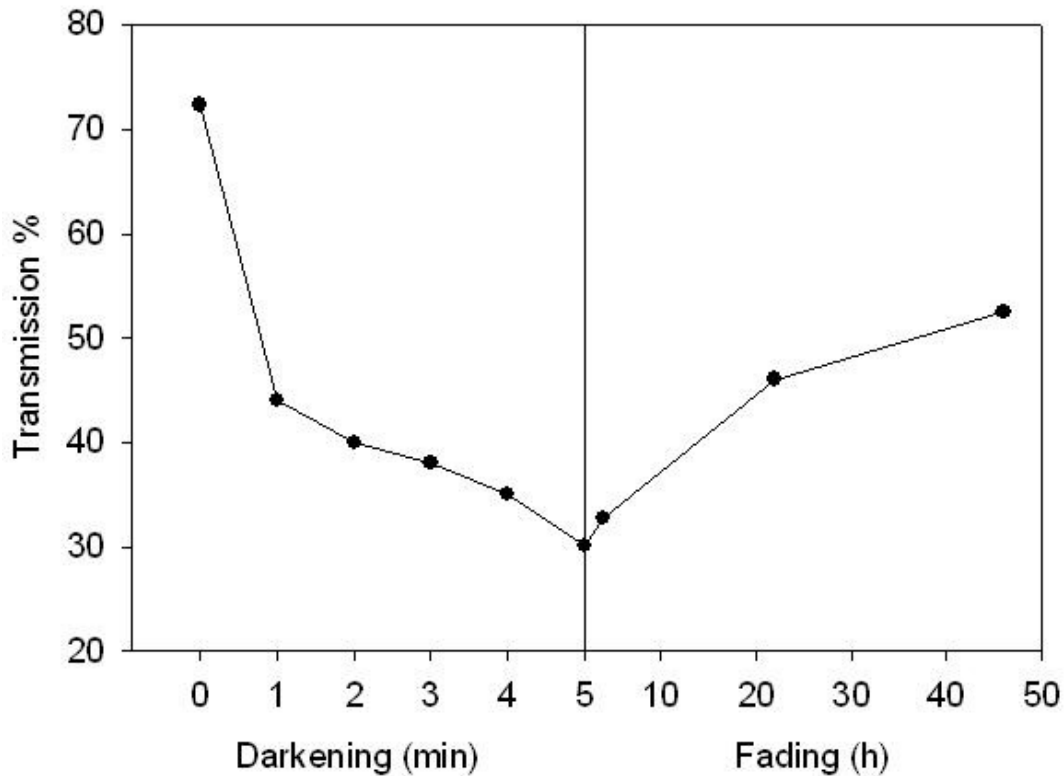


Figure 7-29: Darkening and fading behaviour of sample containing 0.9 mol% $\text{Cu}(\text{NO}_3)_2 \cdot 3\text{H}_2\text{O}$; 1.1mol% $\text{Cd}(\text{CH}_3\text{COO})_2 \cdot 2\text{H}_2\text{O}$ and 0.3mol% $\text{C}_{10}\text{H}_{14}\text{CdO}_4$.

Fig. 7-29 shows the transmission changes at 550 nm of a sample which contained 20% of cadmium(II)acetate dihydrate substituted against cadmium acetylacetonate. This substitution was done in order to prevent CdBr_2 crystals precipitation. The acetylacetonate was a complexation agent, that means it made a complex with the Cd^{2+} ion, inhibiting the CdBr_2 formation [66].

After 5 min of irradiation (first part of the graph) the degree of darkening at wavelength of 550 nm was approximately 0.42, while the half-life time of darkening was around 60 s and half-life of fading was approximately 1200 min.

Table 7-12 describes the results above.

Table 7-12: Darkening and fading characteristics for sample containing 0.9 mol% $\text{Cu}(\text{NO}_3)_2 \cdot 3\text{H}_2\text{O}$; 1.1 mol% $\text{Cd}(\text{CH}_3\text{COO})_2 \cdot 2\text{H}_2\text{O}$ and 0.3 mol% $\text{C}_{10}\text{H}_{14}\text{CdO}_4$

Initial transmission	73%
Darkening degree	0.42
Darkening half-life	60s
Fading half life	1200min

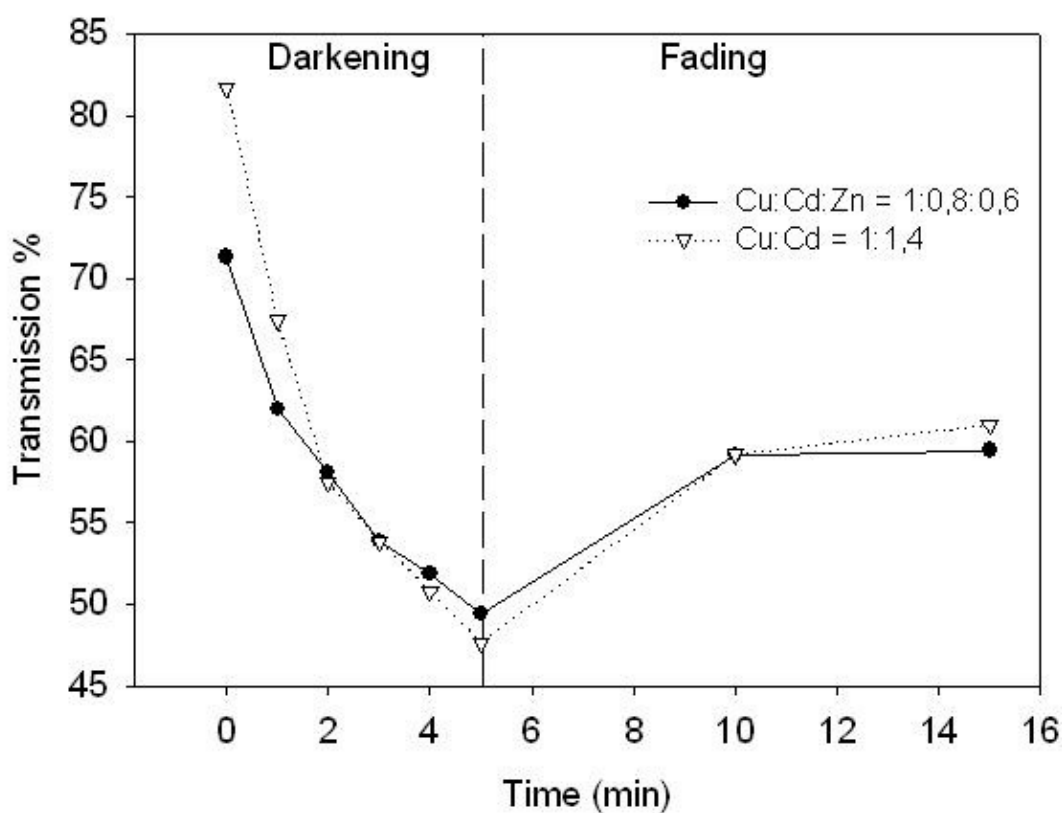


Figure 7-30: Darkening and fading behaviour of samples containing (line) 0.5 mol% $\text{Cu}(\text{NO}_3)_2 \cdot 3\text{H}_2\text{O}$; 0.4 mol% $\text{Cd}(\text{CH}_3\text{COO})_2 \cdot 2\text{H}_2\text{O}$ and 0.3 mol% $\text{Zn}(\text{CH}_3\text{COO})_2 \cdot 2\text{H}_2\text{O}$ and (dots) 0.5 mol% $\text{Cu}(\text{NO}_3)_2 \cdot 3\text{H}_2\text{O}$; 0.4 mol% $\text{Cd}(\text{CH}_3\text{COO})_2 \cdot 2\text{H}_2\text{O}$ and 0.3 mol% $\text{C}_{10}\text{H}_{14}\text{CdO}_4$.

Fig. 7-30 shows two samples with different compositions.

The dotted curve is attributed to a sample containing cadmium acetylacetonate substituting 20% of the cadmium acetate dihydrate content. This sample did not contain Zn^{2+} . The initial transmission was 82%. After 5 min of irradiation

the degree of darkening was approximately 0.34, while the half-life time of darkening was around 70 s and half-life of fading was approximately 900 s.

The other curve (line) was a sample with zinc acetate dihydrate substituting 40% of cadmium acetate dihydrate.

The initial transmission was 72%. Notice that after 5 min of irradiation the degree of darkening was approximately 0.22, the half-life time of darkening was around 70 s and half-life of fading was approximately 600 s.

Between these two samples, the one without Zn^{2+} darkened more intensely but displayed a longer half-time fading.

Table 7-13 describes these results in more detail.

Table 7-13: Darkening and fading characteristics Darkening and fading of samples containing (line) 0.5 mol% $Cu(NO_3)_2 \cdot 3H_2O$; 0.4 mol% $Cd(CH_3COO)_2 \cdot 2H_2O$ and 0.3 mol% $Zn(CH_3COO)_2 \cdot 2H_2O$ and (dots) 0.5 mol% $Cu(NO_3)_2 \cdot 3H_2O$; 0.4 mol% $Cd(CH_3COO)_2 \cdot 2H_2O$ and 0.3 mol% $C_{10}H_{14}CdO_4$

Sample	0.5 mol% $Cu(NO_3)_2 \cdot 3H_2O$; 0.4 mol% $Cd(CH_3COO)_2 \cdot 2H_2O$ and 0.3 mol% $C_{10}H_{14}CdO_4$	0.5 mol% $Cu(NO_3)_2 \cdot 3H_2O$; 0.4 mol% $Cd(CH_3COO)_2 \cdot 2H_2O$ and 0.3 mol% $Zn(CH_3COO)_2 \cdot 2H_2O$
Initial transmission	82%	72%
Darkening degree	0.34	0.22
Darkening half-life	70s	70s
Fading half-life	900s	600s

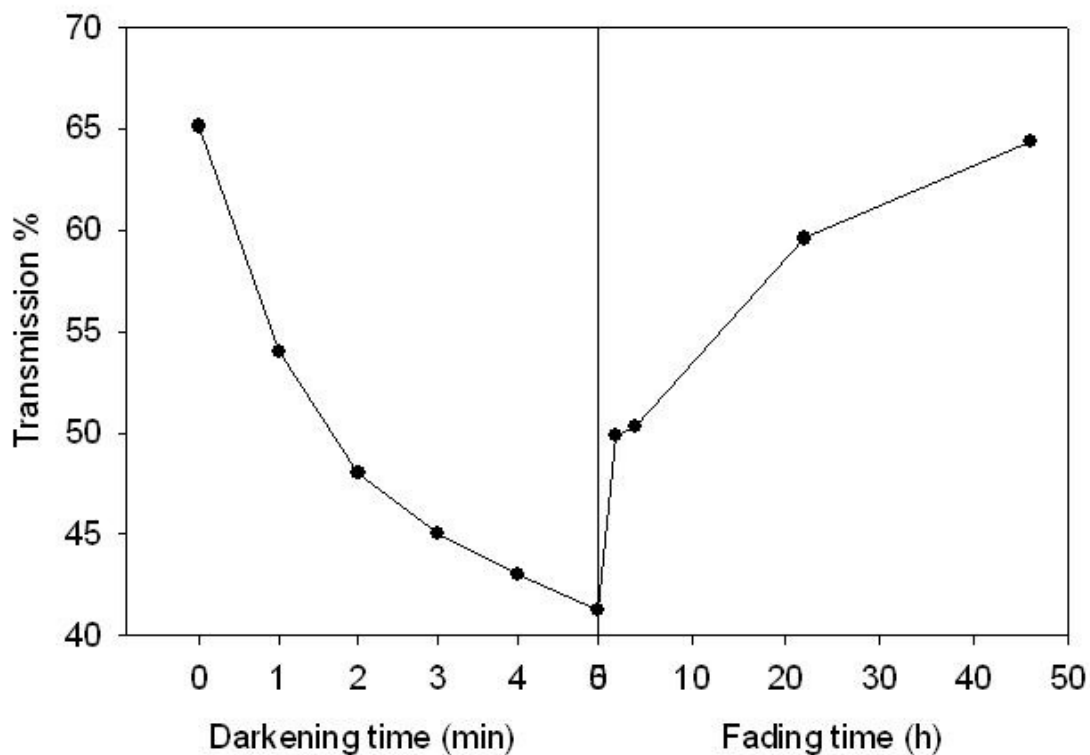


Figure 7-31: Darkening and fading behaviour of sample containing 0.5 mol% $\text{Cu}(\text{NO}_3)_2 \cdot 3\text{H}_2\text{O}$; 0.4mol% $\text{Cd}(\text{CH}_3\text{COO})_2 \cdot 2\text{H}_2\text{O}$ and 0.3mol% $\text{Zn}(\text{CH}_3\text{COO})_2 \cdot 2\text{H}_2\text{O}$ dried at 50 °C and holding time of 24h and heat treated at 200 °C for 20 min.

Fig. 7-31 shows the best-obtained result.

The sample contain 0.5 mol% $\text{Cu}(\text{NO}_3)_2 \cdot 3\text{H}_2\text{O}$; 0.4mol% $\text{Cd}(\text{CH}_3\text{COO})_2 \cdot 2\text{H}_2\text{O}$ and 0.3mol% $\text{Zn}(\text{CH}_3\text{COO})_2 \cdot 2\text{H}_2\text{O}$.

It was dried at 50 °C and using a holding time of 24h and heat treated at 200 °C for 20 min. In this sample it was possible to measure the return to initial transmission during the 40 h fading time.

Table 7-14 displays the results above.

Table 7-14: Darkening and fading characteristics for sample containing 0.5 mol% $\text{Cu}(\text{NO}_3)_2 \cdot 3\text{H}_2\text{O}$; 0.4mol% $\text{Cd}(\text{CH}_3\text{COO})_2 \cdot 2\text{H}_2\text{O}$ and 0.3mol% $\text{Zn}(\text{CH}_3\text{COO})_2 \cdot 2\text{H}_2\text{O}$ dried at 50 °C and holding time of 24h and heat treated at 200 °C for 20 min.

Initial transmission	65%
Darkening degree	0.24
Darkening half-life	60 s
Fading half life	9000s

One interesting effect was observed during the next fading measurements. The UV beam irradiated the samples for less than one second to measure the transmission. This small amount of time was enough to reactivate the darkening on the same spot already irradiated/darkened faster than it would take to darken a new spot. Note that the changes of curve inclination in Fig. 7-30.

The consequence of this is that the fading measurements will hardly achieve the initial transmission and one might draw the false conclusion that the samples do not recover their initial transmission after irradiation stops. This phenomenon of easy re-activation is well known for photochromic glasses (memory effect).

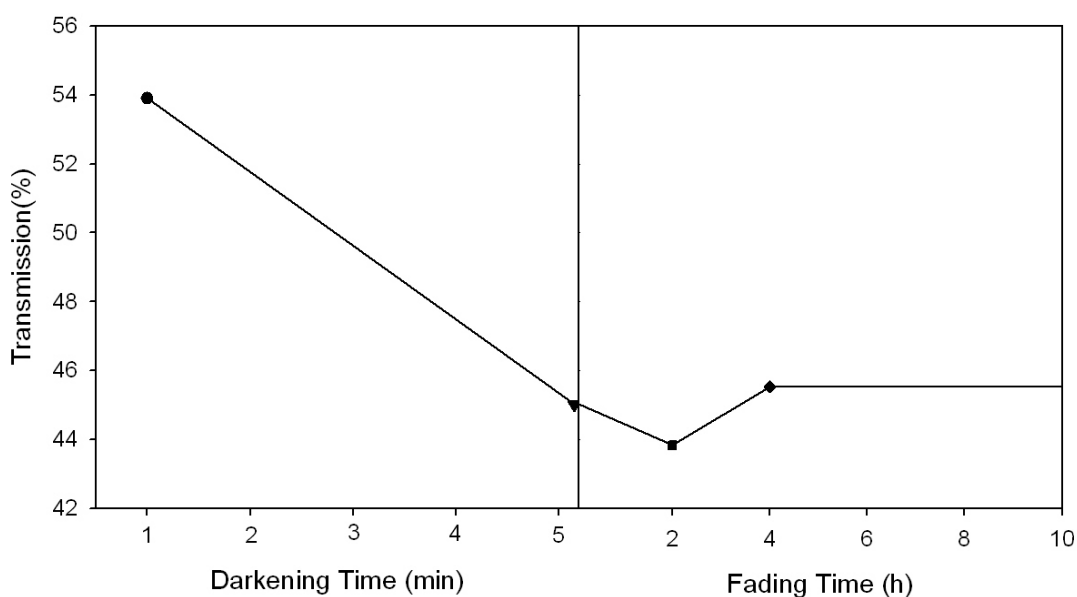


Figure 7-32: Darkening and fading behaviour of sample with memory effect.

Fig. 7-32 reveals such a sample with strong memory effect. Five measurements were made, the first one before irradiation started; the second one 5 min after continuous irradiation; the third measurement made 2 h after irradiation stopped. The short irradiation (less than 1s) of Xenon lamp was sufficient to cause further darkening on the sample during the third measurement. This sample contained 40% of $\text{Zn}(\text{CH}_3\text{COO})_2 \cdot 2\text{H}_2\text{O}$ in substitution of $\text{Cd}(\text{CH}_3\text{COO})_2 \cdot 2\text{H}_2\text{O}$. The total content of $\text{Cd}(\text{CH}_3\text{COO})_2 \cdot 2\text{H}_2\text{O}$; $\text{Cu}(\text{NO}_3)_2 \cdot 3\text{H}_2\text{O}$ and HBr was reduced by the half part in order to achieve smaller crystals.

Considering this, the last results in Fig.7-28, where a sample recovered its original transmission after 40 h, could actually have a smaller fading time.

All samples containing a partial substitution of $\text{Cd}(\text{CH}_3\text{COO})_2 \cdot 2\text{H}_2\text{O}$ against $\text{Zn}(\text{CH}_3\text{COO})_2 \cdot 2\text{H}_2\text{O}$ were photochromic. Previous to the heat-treatment these samples were not photochromic. It might be considered that the CdBr_2 crystals have a strong role for the photochromic effect, as the samples without CdBr_2 were not photochromic as well. Samples with CdBr_2 and no CuBr are not photochromic. Samples with CdBr_2 and CuBr are photochromic. Samples with CdBr_2 , CuBr and ZnBr_2 are photochromic. Samples with CuBr and ZnBr_2 are not photochromic.

8 DISCUSSION

8.1 Crystalline structure of CuBr; CdBr₂ and ZnBr₂

The X-ray powder diffraction results showed the presence of three different crystallites: CdBr₂; CuBr and ZnBr₂.

The crystalline phases relative to these crystals are displayed in Table 8-1.

Table 8-1: Crystallites present on the coatings identified by X-ray powder diffraction

Crystallite	Angle of diffraction in 2 θ		Crystallographic Phase
	JCPDS	Experimental	
CdBr ₂	14°; 28°; 45°	14°; 28°; 45°	Hexagonal
CdBr ₂	14°; 32°; 45°	14°; 32°; 45°	Rhombohedral
γ -CuBr	27°; 45°; 53°	27°; 45°; 53°	Cubic
ZnBr ₂	33°	32°	Tetragonal

The two CdBr₂ crystallographic phases, hexagonal and rhombohedral can be easily confused, as the only significant difference is the peak at 28°, present at the hexagonal phase and the peak at 32°, present at the rhombohedral phase. The X-ray results showed the hexagonal phase appeared only in samples dried at 100° C before heat-treatment. (see Fig 7.1 and Fig. 7.2; Table 7.1 and Table 7.2). After heat-treatment over 120° C the rhombohedral CdBr₂ phase appears (see Fig.7.3 and Table 7.3). We could assume that after heat-treatment the hexagonal CdBr₂ phase changes to rhombohedral CdBr₂.

The presence of ZnBr₂ is also uncertain. ZnBr₂ and CdBr₂ have a diffraction peak at 33° and 32° respectively and as the average error of this X-ray diffraction powder is ± 0.6 %. It is not possible to determine whether the peak is relative to CdBr₂ crystal or ZnBr₂ crystal when both Cd(CH₃COO)₂.2H₂O and Zn(CH₃COO)₂.2H₂O are present at the composition.

The presence of $\text{Zn}(\text{CH}_3\text{COO})_2 \cdot 2\text{H}_2\text{O}$ inhibits (but not extinguish) the formation of CdBr_2 crystals before heat-treatment. This could also be explained by the decrease in content of $\text{Cd}(\text{CH}_3\text{COO})_2 \cdot 2\text{H}_2\text{O}$, due to its substitution against $\text{Zn}(\text{CH}_3\text{COO})_2 \cdot 2\text{H}_2\text{O}$.

Samples without $\text{Zn}(\text{CH}_3\text{COO})_2 \cdot 2\text{H}_2\text{O}$ and a 0.5 mol% of $\text{Cd}(\text{CH}_3\text{COO})_2 \cdot 2\text{H}_2\text{O}$ was analysed and the presence of CdBr_2 crystals prior to heat-treatment could confirm that the $\text{Zn}(\text{CH}_3\text{COO})_2 \cdot 2\text{H}_2\text{O}$ does inhibit the formation of CdBr_2 crystals.

The γ -CuBr cubic structure is formed at temperatures $\approx 200^\circ \text{C}$. The X-ray results confirm this statement.

There was one series of measurements carried out with samples without both $\text{Zn}(\text{CH}_3\text{COO})_2 \cdot 2\text{H}_2\text{O}$ and no CH_3COOH . It was not clear whether the origin of the peak at 45° is attributed to cubic γ -CuBr or to rhomboedral CdBr_2 as both crystals diffract in this 2θ position.

Why do the Cd^{2+} and Zn^{2+} ions replace Cu^+ ions to form a chemical disorder in CuBr crystals?

The similarity between CuBr and CdBr_2 is the fact that in both cases the Br^- ions are cubic face centred.

In CdBr_2 crystals, the Cd^{2+} ions occupy one half of the octahedral positions surrounded by Br^- and they form a layered structure due to the double charged Cd^{2+} (see Fig. 8-1).

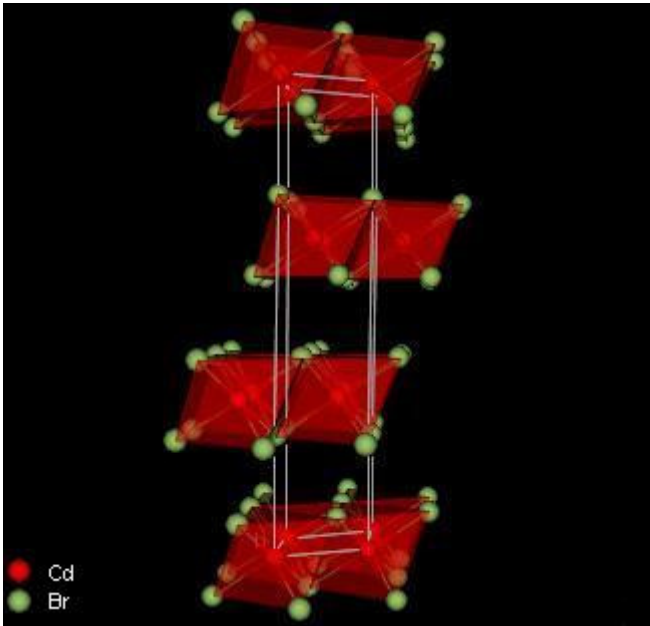


Figure taken from reference [67]

Figure 8-1: Illustration of a CdBr₂ crystal.

In analogy, in ZnBr₂ crystals, the Zn²⁺ ions occupy one half of the tetrahedral positions surrounded by Br⁻ and they form a layered structure due to the double charged Zn²⁺ (see Fig. 8-1).

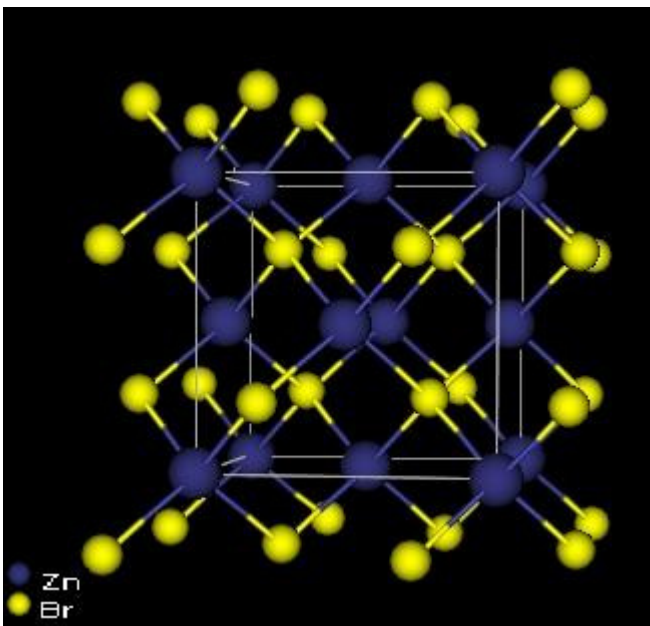


Figure taken from reference [67]

Figure 8-2: Scheme of a ZnBr₂ crystal.

In the CuBr crystal, the Cu^+ occupies the FCC position surrounded by Br^- ions. When one Cd^{2+} substitutes one Cu^+ , it will occupy an octahedral position due to its larger size compared to Cu^+ (see Fig. 8-3).

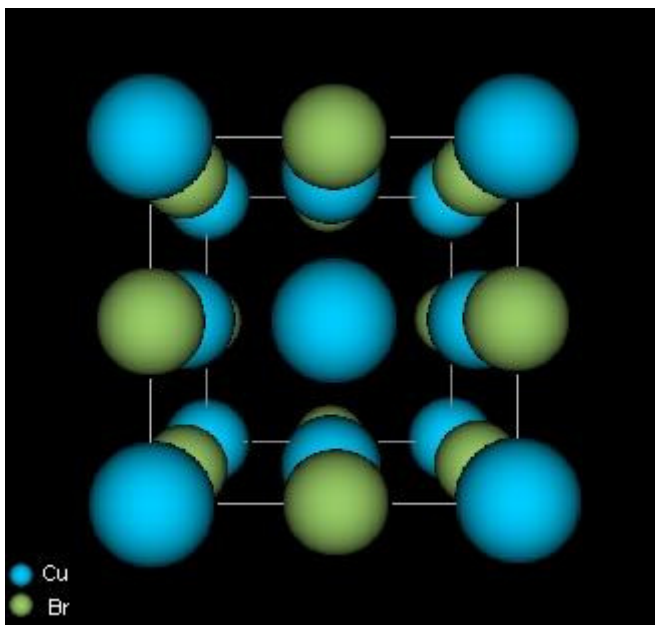


Figure taken from reference [67]

Figure 8-3: Schematic representation of γ -CuBr cubic.

8.2 All studied compositions and the effect of its variations

8.2.1 Hydrobromic acid

The decrease of hydrobromic acid in the compositions O2 and O4 affects the darkening behaviour of the sample. As already shown in Chapter 7, Section 7.7.2, the sample containing half the hydrobromic acid content presents the lowest light transmission (54% - see Fig.7-29). Furthermore, the sample has a very fast darkening in the regions where it was once activated by light (memory effect).

The chemistry of alkoxides (TEOS and TMOS) varies in function of the pH. For an aqueous solution with $\text{pH} \approx 2.5$, the silicate particles are not chemically charged [9]. However, when the pH is decreased ($\text{pH} < 2.5$) varying the content of hydrobromic acid, the solution turns quite acidic and the silicate particles are negatively charged. The hydrolysis reaction is catalysed by the

high concentration of protons. This means more protons H^+ will attack the alkoxide CH_2O-Si bond, forming siloxane $Si-OH$ groups, while less $Si-O-Si$ silica groups will be formed by condensation.

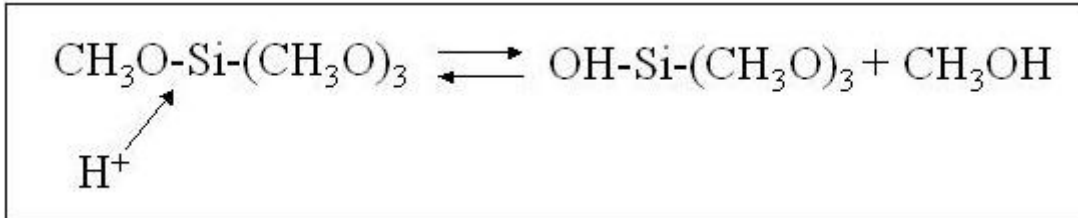


Figure 8-4: Hydrolysis reaction in acid sols.

In the other hand, the addition of a base in the composition causes a shift of the pH-value > 2.5 . In this instance the silanol groups are deprotonated. They build siloxane bridges by a mechanism that involves intermediary complexes with penta coordinated silicons. If the pH becomes larger than 4, the condensation rate is not only proportional to the concentration of OH^- but also superior to that of hydrolysis. Furthermore, since the reticulation inside the silicon polymers is more developed than when conditions for acidic catalysis are used, denser solids are obtained.

During the heat-treatment, the content of Br^- ions will affect the crystallization. In accordance with Volmer [68] the nucleation rate increases with the super-saturation.

$$I = A \cdot \exp \left(\frac{-B\sigma^3}{\ln \left(\frac{c}{c_0} \right)} \right) \cdot RT \qquad \text{Equation 8-1}$$

A and B are constants; σ is the surface tension between crystallite and glass matrix; $\frac{c}{c_0}$ is the super-saturation.

Fig. 8-5 shows how the HBr content influences the darkening and fading behaviour. The sample containing less HBr, shows a lower transmission level

before irradiation. The difference in the darkening rate is easily noticeable. The darkening degree is much lower for the sample with lower acetic acid content and the half-life of darkening and fading are as follows.

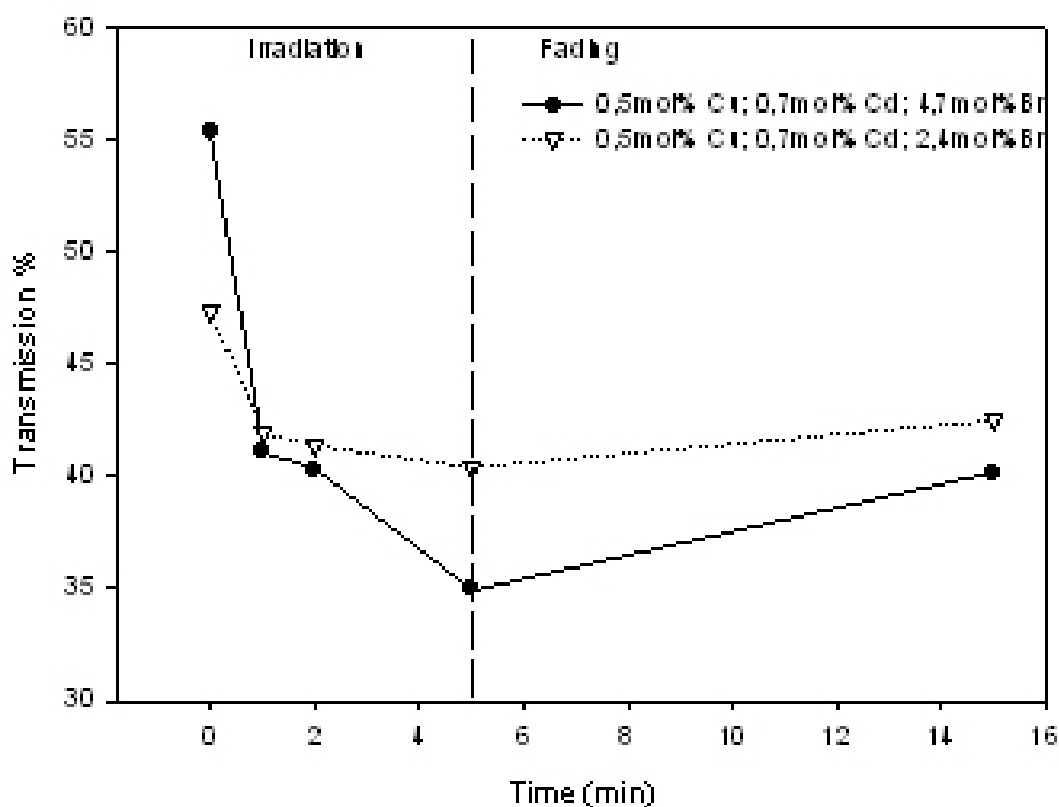


Figure 8-5: Darkening and fading behaviour of samples showing the influence of HBr content.

8.2.2 Acetic acid

Both the addition of acetic acid and simultaneous decreasing of HBr content cause the shift of the pH value to a more basic sol. This is relevant to the coating formation and its quality. If the equilibria of hydrolysis and condensation reactions are shifted towards the condensed products, the viscosity of the sol will be higher. This allows withdrawal giving a smoother, flaw free coating.

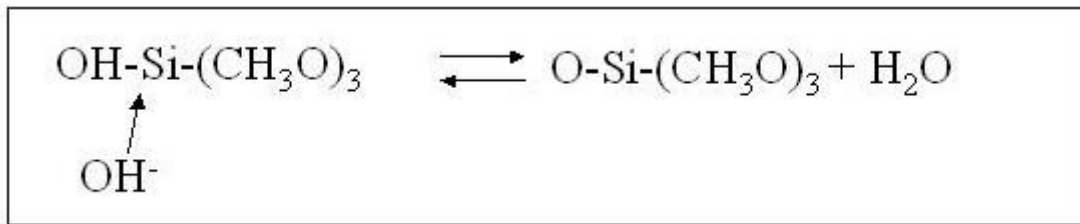


Figure 8-6: Condensation reaction in basic sols.

The acetic acid was responsible not only for better coating quality during the sol-gel and coating process, but also for the transparency of the coating. The next figure shows how the light transmission is better for the sample containing acetic acid.

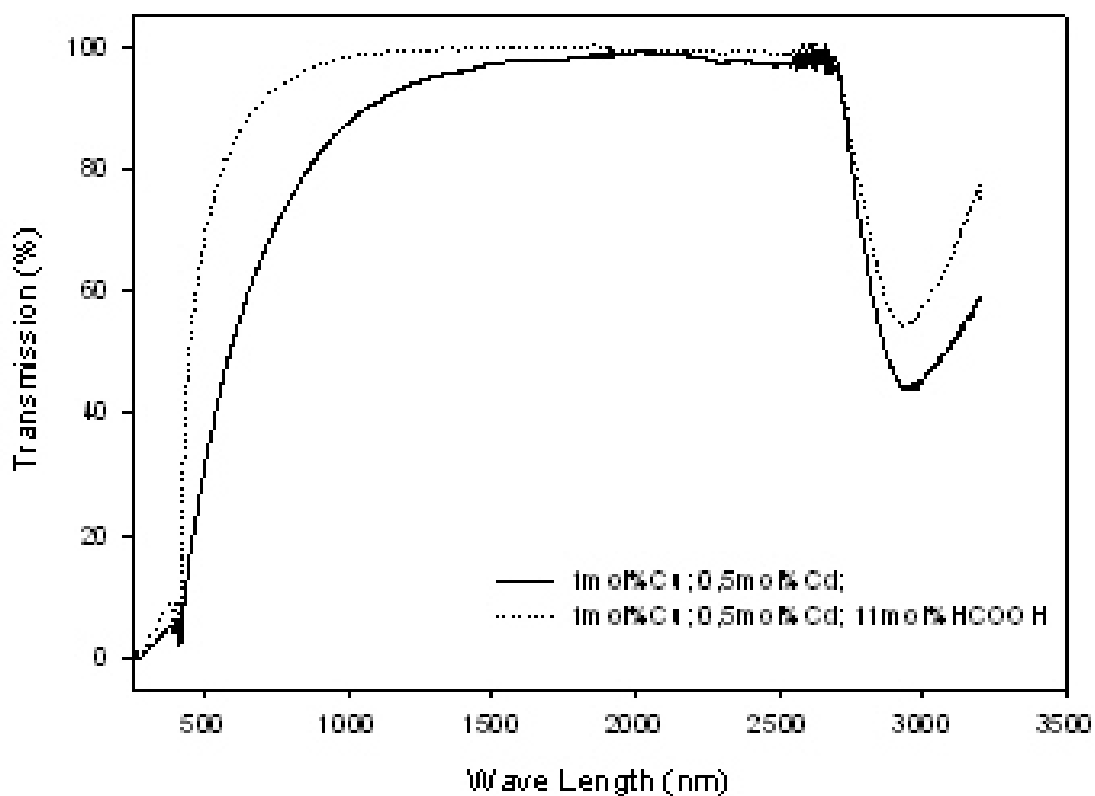


Figure 8-7: Transmission behaviour of sample showing the effect of acetic acid addition.

8.2.3 Copper Bromide - CuBr

The use of CuBr instead of $\text{Cu}(\text{NO}_3)_2 \cdot 3\text{H}_2\text{O}$ as stated in the composition K3B (see list Appendix 10-2) was done in order to prevent the formation of CdBr_2 microcrystals prior to heat-treatment. These experiments were not successful. During the sol-gel preparation, the CuBr precipitated in the sol and as the coating solution is pre filtered, the samples were not photochromic after coating and subsequent heat-treatment. Probably the CuBr was removed by filtering process.

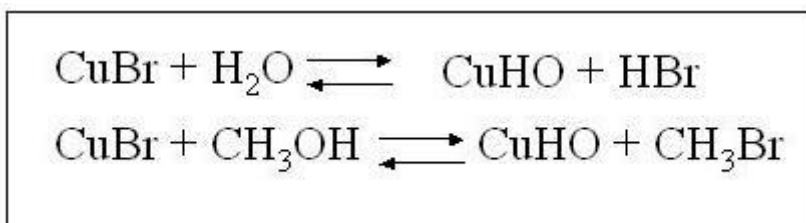


Figure 8-8: CuBr precipitation reactions during sol-gel preparation.

8.2.4 Cadmium acetylacetonate

In order to form a complex that would inhibit the formation of CdBr_2 prior to heat-treatment, part of the $\text{Cd}(\text{CH}_3\text{COO})_2 \cdot 2\text{H}_2\text{O}$ was substituted, by Cadmium acetylacetonate ($\text{C}_{10}\text{H}_{14}\text{CdO}_4$). The idea was to build a strong interaction between molecules and transition metals such as Cd^{2+} during the sol-gel preparation so that the formation of CdBr_2 , prior to heat-treatment, is prevented [65].

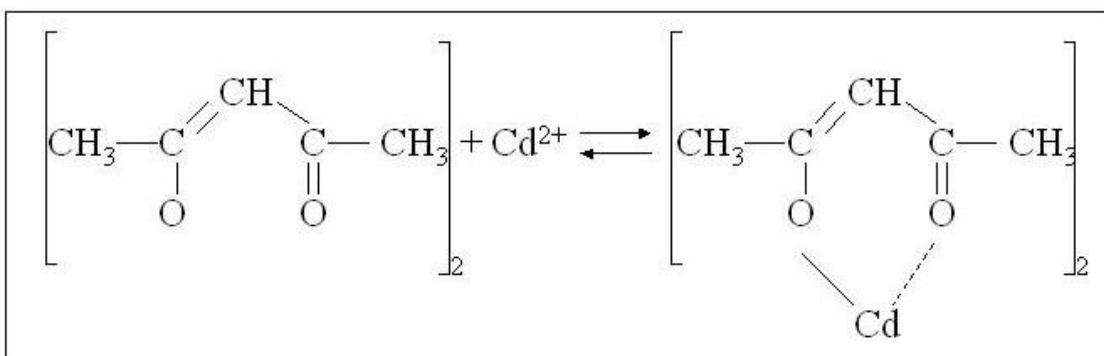


Figure 8-9: Reaction of Cd complexation during sol-gel preparation.

The sample CTD4 (0.6 mol% $C_{10}H_{14}CdO_4$) presented the highest percentage of light transmission before excitation with UV light, comparing to samples containing only $Cd(CH_3COO)_2 \cdot 2H_2O$ (see Fig. 7-27).

Fig. 8-10 shows the darkening and fading behaviour for a sample CDT2 containing 0.3 mol% $C_{10}H_{14}CdO_4$. The samples produced excellent results. The darkening degree is 0.34; the half-life darkening is 70s and the half-life of fading is approximately 900s

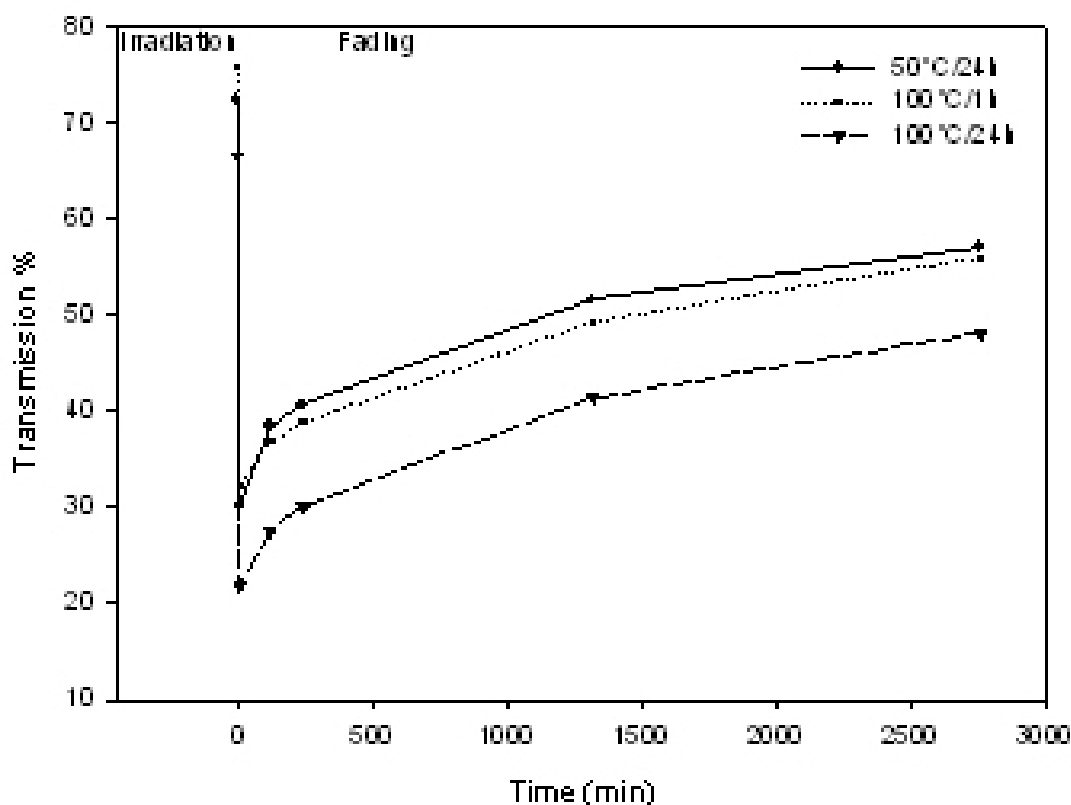


Figure 8-10: Darkening behaviour of samples containing $C_{10}H_{14}CdO_4$ with different drying temperatures.

Fig. 8-10 also facilitates another observation, the drying temperature. It should be noted that the samples were dried at 50° C for 24 h and at 100° C and holding time of 1 h or 24 h. The sample dried at 100° C for 24 h, shows the lowest light transmission before irradiation (67%). The sample dried at 50° C for 24 h shows the highest light transmission (78%). Their fading curve is quite similar in shape.

The best results for light transmission due to the drying stage, shows that the preferred temperature for drying is 50° C, rather than 100° C.

8.2.5 Silver nitrate

In order to find a additional component that would allow improved darkening and fading characteristics, Ag(NO₃) was introduced to the system. The idea was to disturb the crystalline order of the CuBr crystallites so that a deep darkening would be possible without the need of growing larger crystals and that the small crystals would provide a fast fading after the irradiation stopped. A very small amount (0.01 mol%) of Ag(NO₃) was introduced during the sol-gel preparation on samples NP (see Appendix 10-2) but precipitation occurred right away as the silver bromide is the most insoluble compound compared to CuBr, CdBr₂ and ZnBr₂.

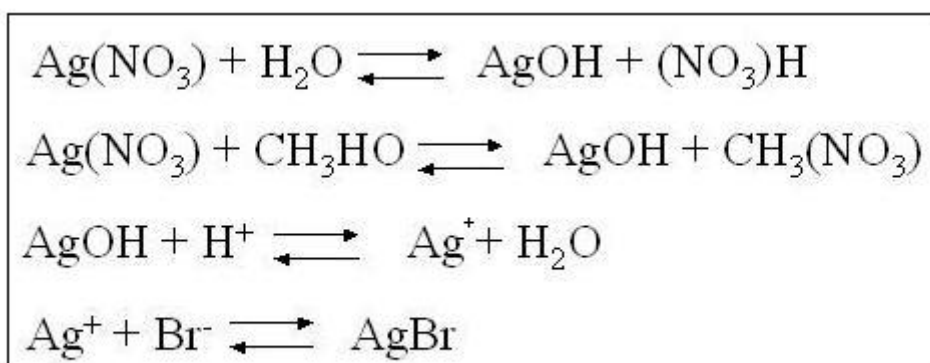


Figure 8-11: Precipitation of silver during the sol-gel preparation.

8.2.6 TEOS versus TMOS

The samples K2 had their composition alternated by the use of TEOS and TMOS. The samples with TEOS resulted in opaque samples, after heat-treatment. They exhibit a light transmission lower than the TMOS containing sample. See Fig. 8-12.

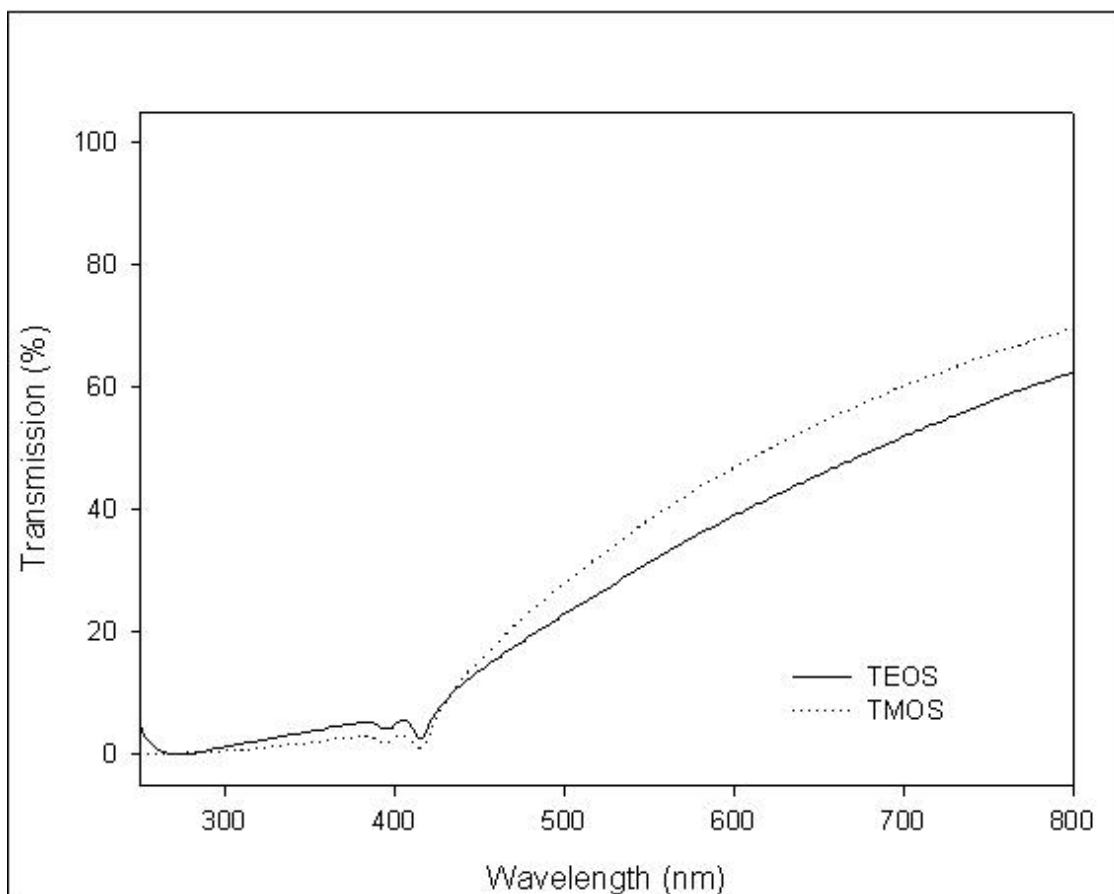


Figure 8-12: Transmission behaviour of samples heat treated at 130 °C for 60min. Comparison between a TEOS and a TMOS containing sample.

8.3 Co-activators

8.3.1 Cadmium acetate dihydrate

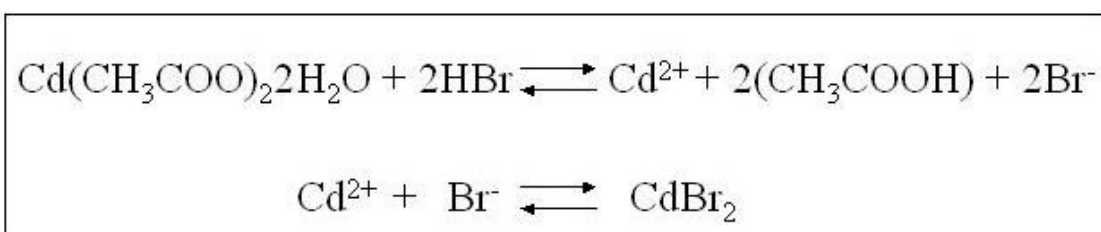


Figure 8-13: Reaction of CdBr₂ formation.

The induced crystal defects in CuBr crystals are essential for the photochromic behaviour. CuBr crystals without a chemical disorder caused by Cd^{2+} do not darken.

With Increasing Cd^{2+} content, the tendency to darken increases. The precipitated volume of CuBr crystallites also increases with increasing Cd^{2+} content. The Cd^{2+} content also influences the CuBr crystallite size.

The Cd^{2+} content influences the photochromic effect in two ways: increasing the CuBr crystal size (larger crystals reach deeper darkening) and introducing defects in the crystal lattices. Cd^{2+} ions substitute Cu^+ ions. The Cd^{2+} occupies an octahedral position in the CuBr unit cell, while Cu^+ occupies a tetrahedral position. The difference in charge between Cu^+ and Cd^{2+} causes also a vacancy defect where a Cu^+ ion moves from its original location. Thus, the increase in lattice disorder increases the Cu^+ mobility.

The use of co-activators such as Cd^{2+} benefits the darkening mechanism (deep darkening and fast fading) providing small but highly disordered crystallites.

Sols with different contents of $\text{Cd}(\text{CH}_3\text{COO})_2 \cdot 2\text{H}_2\text{O}$ were studied. Samples containing 0; 0.5; 1; 1.5; and 2 mol% $\text{Cd}(\text{CH}_3\text{COO})_2 \cdot 2\text{H}_2\text{O}$ were studied in the AFM.

The results showed that samples without $\text{Cd}(\text{CH}_3\text{COO})_2 \cdot 2\text{H}_2\text{O}$ tend to produce very large crystals compared to those samples containing co-activators. Even supplying lower temperatures such as 130°C , resulted in crystals as large as 200 nm. On the other hand the samples containing Cd^{2+} as co-activators and heat-treated at the same temperature produced 10 times smaller crystals.

Table 8-2: Relation of co-activator content and crystallite size obtained by AFM measurements

Cd(CH ₃ COO) ₂ ·2H ₂ O content (mol %)	Crystallite size (nm)	Heat-treatment	
		Temperature (°C)	Time (h)
No co-activator	200	130	3
No co-activator	320	200	1
1	30	200	0.6
2	200	200	0.6

The presence of Cd²⁺ results in inhibition of the crystal growth and at the same time provides the photochromic behaviour which was not observed in samples without Cd²⁺.

The use of co-activators such as Cd²⁺; Sn²⁺; S²⁺; introduced to the CuBr unit cell has already been studied in our group in the past [33,48]. The results show that when increasing the co-activator content (Cd²⁺), the crystallite size decreases if compared with the sample containing no co-activator, and increased if compared to samples containing lower contents of co-activator (see Tables 8-2 and 8-3).

Table 8-3: Relation between co-activator content and crystallite size in accordance with to X-ray diffraction powder measurements

Sample	Cd(CH ₃ COO) ₂ ·2H ₂ O content (mol %)	Crystallite size (nm)
Ku 25	0.1	80
Ku26	1	70
Ku28	1.5	75
Ku27	2	75

Data from reference [48]

First, the Cu^+ and Br^- ions start attracting to each other and form the nuclei, which will subsequently grow. This first step ends when all insoluble CuBr has formed CuBr crystals. At this stage the light absorption increases drastically.

After the first step the Ostwald ripening takes place. Small CuBr crystals and large CuBr crystals exist simultaneously. According to the Ostwald ripening, the smaller crystals will dissolve and the dissolved material will increase the size of the larger ones. That makes the number of crystals decrease while they become larger. The larger the crystal becomes, the more pronounced the light scattering caused by those particles. The increased scattering results in increasing absorption, that is more pronounced at smaller wavelengths. The intensity of excitonic bands will be higher mainly due to the scattering increase.

Other authors have investigated glass systems containing Cd^{2+} and attributed the photochromic properties to these ions [69]. Miura [70] measured the photoconduction and photo induced absorption and concluded that glasses with remarkable photoconduction have poor photochromic properties. They propose an electronic conduction mechanism for CdO containing glasses. The CdO glasses show the band-type conduction in which the band gap is approximately 3.5 eV and the Fermi level is located near the centre of the band gap. ESR measurements reveal 3 different peaks: g_1 , g_2 and g_3 , respectively: at 2.019, 2.003 and 1.998. The peaks g_1 and g_2 are attributed to oxygen-associated trapped-hole centres according to Griscom [71]. The peak g_3 is intrinsic for CdO containing glass, its value is very near to that of Cd^{2+} signals ($g = 2.00 - 1.98$ for various oxide glasses doped with CdO) [72]. Furthermore, it is described that doping with Pb^{2+} results in a notable improvement in photochromic property due to intimate interaction between Pb^{3+} and Cd^{2+} ions pairs.

Deri et al. [73] compared the AgBr system doped with Pb^{2+} and Cd^{2+} with AgCl system. First, the increases in saturation photo response and photoelectron lifetime are due to the formation of an impurity band by dopant ions at the grain surfaces. The decay kinetics involve two first order process: a fast decay involving conduction electrons limited by shallow trapping and a slower mechanism involving electrons in the impurity band. At higher temperatures the slow-decay involves the migration of Ag^+ interstitials to capture impurity-

band electrons, whereas at lower temperatures these electrons decay by trapping. The formation of an impurity band in the silver halides by dopant segregation may not be unique to Pb^{2+} and Cd^{2+} . Other divalent closed d-shell dopants may also segregate at grain surfaces [74,75] and could have similar effects on the photoconductivity of the silver halides.

8.3.2 Zinc acetate dihydrate

Cadmium is an element to be banned according to legislations such as the Restriction of Hazardous Substances [42]. It was necessary to find another element that could play the same role as cadmium in the photochromic mechanism. The Cd^{2+} was substituted by Zn^{2+} using zinc acetate dihydrate in the sol composition. Zinc and cadmium are in the same group 12 of the transition metals of the periodic table. Both have a distorted hexagonal close packed crystal structure. Their ionic radius are 0,74 for Zn and 0,97 for Cd and they have relatively similar density at 293K, 7.133 g/cm³ for zinc and 8.65 g/cm³ for cadmium.

As an alternative to the Cd^{2+} as co-activation, a part of the Cd^{2+} was substituted by Zn^{2+} . The precursor used for the sol-gel preparation was $\text{Zn}(\text{CH}_3\text{COO})_2 \cdot 2\text{H}_2\text{O}$.

The Zn^{2+} was chosen because of its similar characteristics in comparison to Cd^{2+} . See the Table 8-4.

Table 8-4: Similar characteristics between Cd and Zn

Characteristics	Zn	Cd
Chemical series	Transition metals	Transition metals
Group	12	12
Period	4	5
Block	d	d
Oxidation State	2+	2+
Crystal structure	Hexagonal	Hexagonal
Atomic Radius	135 Å	155 Å

Data from reference [76, 77]

The presence of Zn^{2+} inhibited the precipitation of $CdBr_2$ crystals before the heat-treatment.

After heat-treatment, $CuBr$ crystals, $CdBr_2$ crystals and $ZnBr$ crystals were found in the X-ray patterns.

The Table 8-5 shows the reduction in size of the $CdBr_2$ crystallites according to the X-ray diffraction measurements.

Table 8-5: $CdBr_2$ crystallites size reduction with increasing Zn^{2+} content

Zn^{2+} content (mol%)	$CdBr_2$ crystal size (nm) 100° C	$CdBr_2$ crystal size (nm) 250° C	$CdBr_2$ crystal size (nm) 350° C
0	29	70	105
0.3	40	61	45
0.6	x	27	29
0.9	x	16	32
1.2	x	x	x

X = No $CdBr_2$ precipitation

On the other hand, the increasing Zn^{2+} content caused the increase in size of CuBr crystallites as follows in the Table 8-6.

Table 8-6: CuBr crystallites size increase with increasing Zn^{2+} content

Zn^{2+} content (mol%)	CuBr crystal size (nm)	CuBr crystal size (nm)	CuBr crystal size (nm)
	100° C	250° C	350° C
0	x	x	93
0.3	x	94	
0.6	x	67	
0.9	x		
1.2	75		
1.5		97	

X = No $CdBr_2$ precipitation

The presence of Zn^{2+} as co-activator together with Cd^{2+} did not drastically interfere with the photochromic behaviour.

This opens the possibility of working with non-toxic materials.

The photochromic behaviour measurements showed that samples containing only Cd^{2+} as co-activators achieved initial transmissions of 80%. After irradiation for the duration of 5 min with UV light, the sample darkens by 34%, the half darkening time is 70 s and during the fading it recovers 50% of the initial transmission in the first 15 min.

Samples containing Zn^{2+} as co-activator in addition to Cd^{2+} achieve initial transmissions of 70%. The transmission changes 22% after 5 min under UV light irradiation. The half darkening time is approximately 70s. After the UV irradiation stops, 50% of the initial transmission is achieved after 11 min.

Table 8-7: Photochromic behaviour of samples containing Cd²⁺ and Cd²⁺/Zn²⁺

Photochromic Characteristics	Samples with Cd²⁺	Samples with Cd²⁺/Zn²⁺
Initial transmission	80 %	70 %
Transmission change	34 %	22 %
Half darkening time	70 s	70 s
Half fading time	15 min	11 min

The addition of Zn²⁺ did not affect the velocity of darkening and fading during the darkening measurements. On the other hand, it caused a decrease in light transmission and in transmission change. In other words, the sample containing Cd²⁺/Zn²⁺ is less transparent and darkens less than the sample without Zn²⁺.

8.3.3 CuBr excitons absorption and the influence of Zn²⁺

The results obtained at Section 7.7 showed that CuBr could be formed at various different temperatures.

The absorption peaks around 400 nm are characteristic for CuBr crystals. They can be observed when the sample is under heat-treatment after holding the temperature for 40 min at 130° C.

The same absorption peaks also appears at 175° C during the heating from 100 to 200° C at a heating rate of 10 K/min.

The crystallization is spontaneous if a temperature above 175° C is reached, but could also be initiated at lower temperatures just by keeping the sample at temperatures of at least 110°C for 10 to 90 min.

Table 8-8 shows the temperatures and holding-time relationships before the formation of CuBr crystals starts.

Table 8-8: Temperature and holding times that enable CuBr crystallization

Temperature (°C)	Holding time (min)
110	90
120	75
130	35
150	20
175	1

Comparing Figs. 7-19 and 7-20 with the other figures (Fig. 7-21, for example) there is a markedly difference on the form of the CuBr absorption band. These samples are special because they do not contain $\text{Cd}(\text{CH}_3\text{COO})_2 \cdot 2\text{H}_2\text{O}$.

In the first two cases, the two exciton absorption bands are placed at 390 and 400 nm approximately, and the band at 390 nm has a smaller intensity than the band at 400 nm.

All other measurements carried out with compositions containing $\text{Cd}(\text{CH}_3\text{COO})_2 \cdot 2\text{H}_2\text{O}$ show the exciton absorption bands located at around 390 nm and 400 nm. The later peak has the larger intensity.

New measurements of samples containing $\text{Zn}(\text{CH}_3\text{COO})_2 \cdot 2\text{H}_2\text{O}$ as a partial substitute for $\text{Cd}(\text{CH}_3\text{COO})_2 \cdot 2\text{H}_2\text{O}$ showed two Cu^+ absorption peaks at 450 and 490 nm.

Table 8-9 lists all the CuBr exciton absorption bands and the respective compositions and heat-treatments.

Table 8-9: Relation of Cu^+ exciton absorption bands: composition and heat-treatment

Composition	CuBr Exciton Absorption bands (nm)		Heat-treatment (° C)
K1	390	400	130
K2	390	400	150
K26	390	400	130
Z4	450	490	250

All analysed samples showed a wide absorption band at approximately 350 nm before and after heat-treatment. This absorption band can be relative to bromocuprate ions.

Another spectra variation can be observed due to the measurements at different temperatures during the heating treatment. The Cu^+ excitons absorption band moves slightly to the side of larger wavelengths while the CuBr crystals grow with the temperature increase.

Fig. 8-14 and 8-15 show this growth and the influence of increasing Zn^{2+} content.

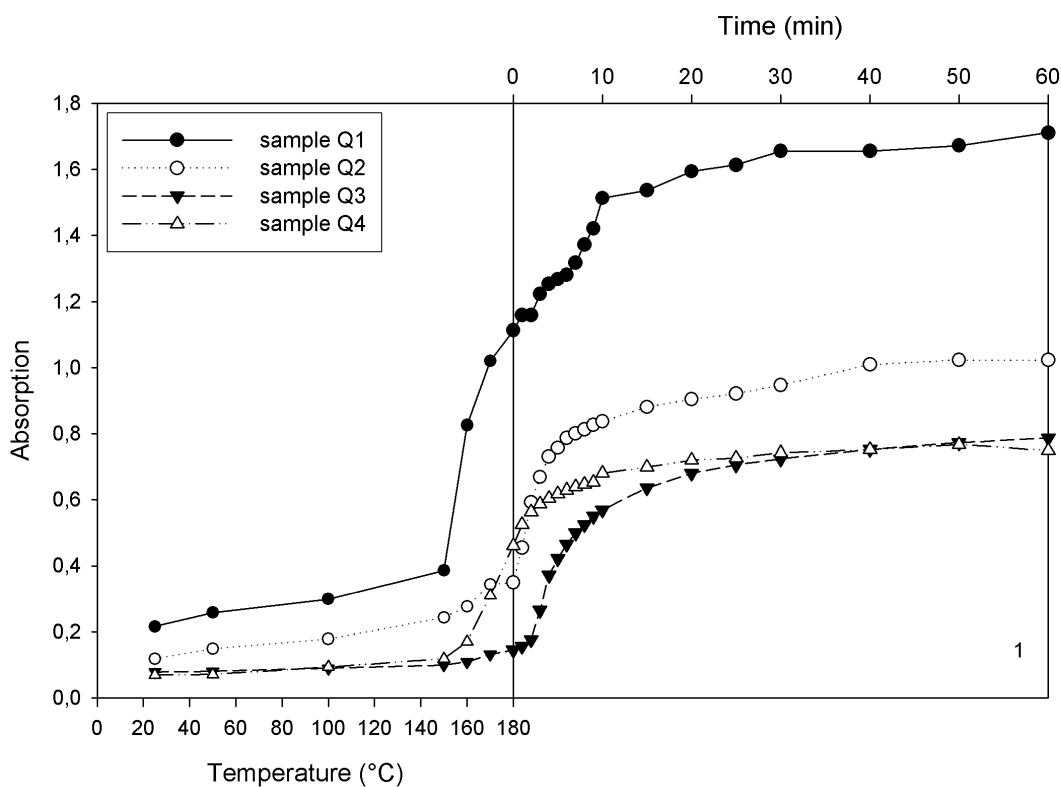


Figure 8-14: Change in CuBr excitons absorption band at 450 nm with crystal growth.

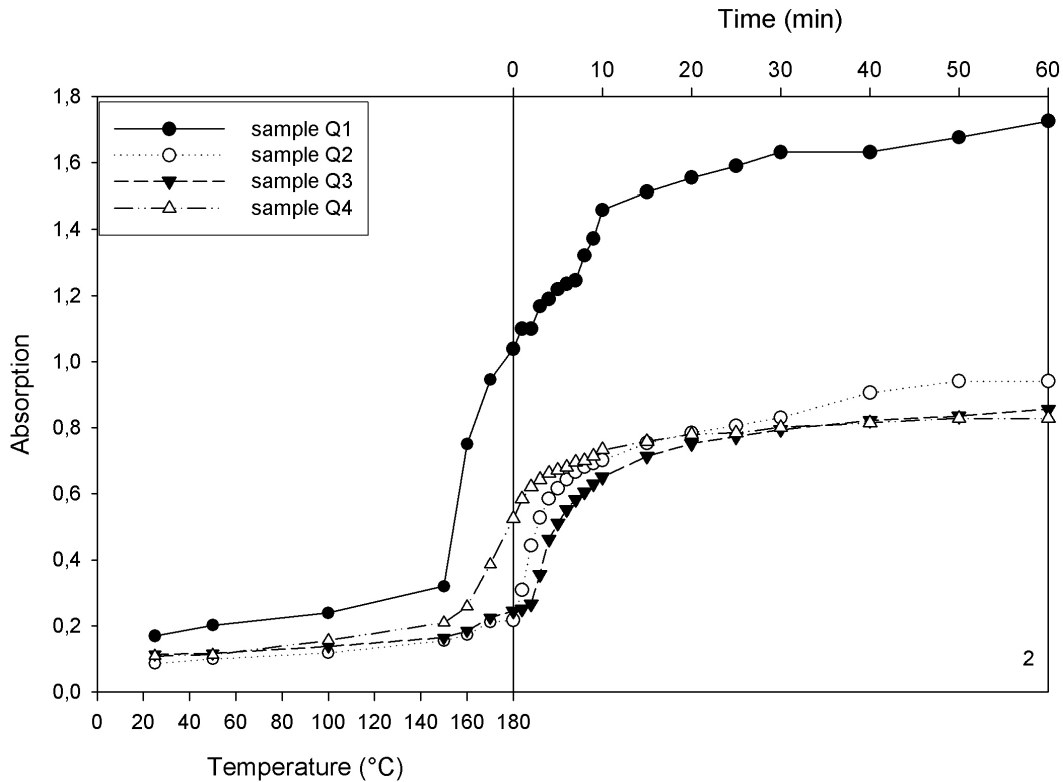


Figure 8-15: Change in CuBr excitons absorption band at 490 nm with crystal growth.

Note that the increase in absorption is caused by the nucleation and growth of CuBr crystals. In the samples containing no Zn^{2+} at all (sample Q1), the nucleation begins at $150^{\circ}C$ during the heating curve up to the heat-treatment temperature of $180^{\circ}C$. On the other hand, increasing the Zn^{2+} content up to 0.6 mol% inhibits the nucleation at temperatures lower than $180^{\circ}C$.

The absorption increase starts after the heat-treatment reaches the plateau temperature and the nucleation takes place during the first 10 minutes. This effect recedes, as soon the Zn^{2+} concentration is higher than 0.6 mol%. For the sample containing 0.9 mol% of Zn^{2+} (sample Q4), the nucleation occurs during the heating curve at $160^{\circ}C$. After 15 min at $200^{\circ}C$ the absorption increase stabilizes.

The Zn^{2+} content does not influence the initial transmission (before irradiation). Notice that all samples containing Zn^{2+} have approximately the same absorption after 10 min up to 60 min at $200^{\circ}C$.

The presence of Zn^{2+} causes an increase in transparency, which is not influenced by the increasing content (compare Figs. 8-12 and 8-13). At the end

(after 60 min) at 200° C, the presence of Zn²⁺ causes an absorption of approximately half of that of the sample without Zn²⁺. This means that the samples containing Zn²⁺ after heat-treatment are the most transparent ones.

8.4 The darkening mechanism

To explain the physical model of the darkening and fading process, it is taken as an analogical explanation the physical model proposed by Araujo [78] for photochromic silver based glasses. In our case, instead of precipitated silver halide microcrystals there are copper halide microcrystals. The photochromic glass coating is composed by an inert glass matrix and microcrystals of CuBr with Cd²⁺ as induced defects or solid solution crystals of CuBr and CdBr₂. Excitation by UV light creates electron-hole pairs. The electrons are trapped and lead to the formation of copper specks. Positive-holes must be trapped as well, otherwise the darkening will not occur since the positive-hole will quickly recombine with the trapped electron. When the positive-hole is trapped by a Cu⁺ ion, a lattice relaxation occurs due to an increase in positive charge. This lattice relaxation causes an energy level increase, which prevents the positive-hole tunnelling from one copper site to another, avoiding the darkening process. However, lattice relaxation is a slow process and would not happen before the electron-hole re-combination occurred. What helps this time is the copper location near a copper speck which, due to an induced dipole effect, raises its energy above the Fermi level. Then the mobility of positive-holes becomes low enough to permit lattice relaxation. If the Fermi level is depressed for any reason, the image potential at large distances from copper, increases the hole- trapping and consequently the darkening rate. On the other hand, raising the Fermi level is an effective way to increase the fading rate.

The darkening netto reaction is:



Equation 8-2

The darkening mechanism in the photochromic crystals is caused by generation of colour centres that absorb a portion of the spectral energy within

the visible light range [40]. Calculations of the optical absorption spectrum of colloidal copper in copper-cadmium halide photochromic glasses reproduced and supported the assumption that the darkening mechanism is according a colloidal model [79].

The chapter 7 describes at section 7.6.2 a reaction that could be considered as colloidal growth while the samples are irradiated (UV light). This prediction is based on the absorption peaks (590 nm 730 nm) shown at Fig. 7-25, which are according to Tick [79] due to copper metallic colloidal particles that were formed under activating radiation.

The existing model of photochromism proposed by Kriltz [33] is based on the photochromic reaction model applied to silver halide glasses. Both glasses (silver halide and silver-free) contain heavy metal halide nanocrystals with defects precipitated in a glass matrix.

Some instances are different in the silver-free halide glasses in comparison to the silver halide glass. They darken in a very thin surface (0.1 mm) referring to bulk glass samples. This means the copper halide nanocrystals have a higher absorption coefficient.

This property allows utilizing very thin layers of copper halide containing glasses as a glass coating generated through sol-gel dip-coating.

Kriltz attribute the darkening mechanism to the generation of excitons through light irradiation with thermal decomposition/decay. The excitation does not take place in a co-activator as for silver halides, but in the activator itself (Cu).

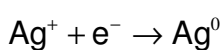
The fading reaction is thermally or optically activated. The electrons in the colloid are excited by a photon and they lead to a plasma oscillation state, which will cause the collapse of the colloid. The electrons in the plasma decay to one electron state and recombine with existing positive-holes centres. The thermal fading reaction is more complicated. The thermal energy is not sufficient to excite electrons from colloids. The positive-holes trapped by Cu^+ ions (i.e. $\text{Cu}^+ \dots \text{h}^+ = \text{Cu}^{2+}$) are thermally excited to vacate the positive-hole back to recombine in the copper colloid. This requires a diffusion of the Cu^{2+} ion through the copper halide microcrystal, which is very slow and determines the velocity of the fading process.

The measurements of absorption bands on darkened samples reveal absorption bands characteristic for copper colloids. These colloids are flattened particles with cap form and seated on spherical copper halide microcrystals [80]. This is allowed by absorption bands attributed to spherical copper colloids (435 nm) that split into two absorption bands, 625 and 303 nm which are relative to ellipsoidal colloids [65]. During the fading process both bands move in the direction of the central band (435 nm) due to the beginning of colloid deformation. The Cu^{2+} absorption bands were also studied during the fading process. The band at 800 nm is affected with respect to its intensity and its spectral position by the colloid band at 625 nm.

The microcrystals that were studied in one of our group's work [33] had in average 0.5 to 2 μm crystal sizes and were formed by spiral growth and smaller crystals sized 30 to 90 nm each. The achieved initial transmission was only 60% and the change in transmission during 15 min of light irradiation (darkening) was 50%. The sample recovered 10% of the transmission in the first 5 min after switching off the irradiation source.

The photochromic reaction in the respective glasses is a complex and complicated mechanism. It is explained most clearly in the case of silver halide based photochromic glasses, i.e. glasses that contain spherical nanoscaled silver halide (AgX , $\text{X}=\text{Cl}_{1-x}\text{Br}_x$) crystals embedded in a glassy matrix. These glasses are relative to the sol-gel based glasses containing copper(I)-halide (CuX) crystals. The mechanism is similar to that which works in photographic films, taking into account the peculiarities of photochromic glasses.

The first step is the light induced excitation of an electron from the valence band to the conduction band which results in a remaining positively charged positive hole in the valence band. The electron and the positive hole will recombine immediately except one of the two charge carriers is trapped. The electrons are necessary to form silver atoms according to:



Equation 8-3

The silver atoms will later cause the darkening of the photochromic glass by forming silver colloids.

In order to have the positive holes trapped, the introduction of Cu^+ ions into the structure of the AgX crystals is required. AgX crystals have an NaCl structure with Ag^+ ions octahedrally coordinated by X^- ions and, vice versa, X^- ions octahedrally coordinated by Ag^+ ions. The replacement of up to 10% of the Ag^+ by Cu^+ creates the desirable chemical disorder since Cu^+ ions prefer the tetrahedral coordinated positions in the anion sub lattice. Therefore, Cu^+ ions become interstitial ions (with respect to the AgX structure) and one Ag^+ vacancy is formed per Cu^+ , which is introduced.

Cu^+ ions can trap the positive holes, which lead to the formation of (in principle) Cu^{2+} :



In this instance, the positive holes are trapped and cannot recombine with the electrons, which were excited towards the conduction band before. Electrons can migrate through the conduction band.

Cu^{2+} ions prefer a distorted octahedral coordination (tetragonally distorted). Thus, Cu^{2+} ions occupy the octahedrally coordinated positions again. But, due to their surplus charge (Cu^{2+} in an Ag^+ position!), a neighbouring Ag^+ is moved to an interstitial position and leaves a vacancy. It is well known that Ag^+ ions in interstitial positions are very mobile. They can migrate to the so-called 'sensitivity centres' (special energetic positions at the surface) where they react with the electrons and form Ag^0 . Normally, there is more than one 'sensitivity centre' per crystal, but as soon as one of them becomes larger than the critical size then only this will continue to grow and form an Ag_n^0 colloid at the boundary between the crystal and the glassy matrix, the others are decomposed. These colloids cause the darkening of the photochromic glass during irradiation. The glass becomes brown coloured.

The shape of these colloids is like a cap on the spherical nanocrystals. Normally, silver colloids show one absorption band at around 450 nm. But in

this case, the resulting absorption spectrum consists of two broader bands which were formed by splitting the single band into two, one of them is shifted to shorter, the other one to longer wavelength. The more the shape of the colloids deviates from spherical the more the two bands are shifted compared with the original position. As long as the glass is irradiated, Ag⁰ is formed and the silver colloids grow.

The trapped positive holes (Cu²⁺ = Cu⁺...h⁺) migrate thermally activated through the crystal (Brownian motion). If the positive holes (Cu²⁺ = Cu⁺...h⁺) approach the colloids within a certain distance, then the trapped electron (Ag⁰ = Ag⁺...e⁻) and the trapped positive holes can recombine. If the number of formed Ag⁰ and the number of recombined charge carriers becomes equal then the equilibrium is reached. The glass will not darken further. After the irradiation is finished, this re-combination leads to a destruction of the colloids formed during irradiation and, hence, the absorption will decrease, the glass becomes colourless again. Due to the thermal activation of this process, the fading of photochromic glasses becomes faster with increasing temperature.

Based on this mechanism, there is a strong connection between the size of the nanocrystals and the photochromic properties: the larger the crystals, the stronger the darkening but the slower the fade and, vice versa, the smaller the crystals the weaker the darkening and the faster the fade. Thus, it is not possible to adjust independently the darkening and fading behaviour of photochromic glasses based on photoactive nanocrystals in a glassy matrix.

Photochromic glasses activated with CuX instead of AgX work in a similar way:



Equation 8-5

First, electrons and positive holes are formed during irradiation. Then, positive holes are trapped and electrons combine with Cu⁺ forming Cu⁰, which will create colloids at the boundary between the nanocrystals and the glass matrix. In principle, a co-activator is not necessary for these glasses with CuX nanocrystals. But to increase the photochromic effect and to make it controllable, it is advantageous to add a co-activator, which creates a suitable

chemical disorder comparable to that, described above, for the AgX crystals by Cu^+ . Often Cd^{2+} ions are used for that purpose, the respective photochromic glasses show darkening and fading behaviour similar to that of the glasses containing AgX: Cu^+ crystals.

The role of Cd^{2+} ions is not so easily seen like in the case of AgX: Cu^+ . Cd^{2+} ions will create Cu^+ vacancies in the cation sub-lattice. Probably, this is connected with the formation of interstitial Cu^+ ions which can migrate/diffuse to the 'sensitivity centres' at the surface of the crystals and form the copper colloids.

It was found that it is possible to prepare photochromic glasses with small CuX: Cd^{2+} crystals by controlled nucleation (number of crystals was increased), which gives fast fading (due to small crystals). At the same time, the darkening of these small crystals was increased (without decreasing the fading too much) by increasing the chemical disorder in the small crystals by Cd^{2+} ions.

9 SUMMARY

The present dissertation investigates photochromic glass coatings made through a sol-gel process and a dip-coating method.

The photochromic properties depend on growing of photochromic nanocrystals dispersed in the glass matrix. These nanocrystals are formed during the heat-treatment procedure.

The sol-gel process is a chemical low temperature method to produce glass. The precursors are organometals such as silicon alkoxide that after hydrolysis and condensation processes molecules are rearranged in silica (Si-O-Si) network. The heat-treatment is responsible for the evaporation of solvents and the densification of the Si-O network.

It was achieved an optimization of the coating quality with the use of C_3H_7COOH in the sol preparation.

The addition of Cd acetate masked the Cd^{2+} , avoiding the precipitation of $CdBr_2$ before the heat-treatment.

The same function was performed by Zn acetate, that when added to the precursor sol inhibited the formation of $CdBr_2$ crystals prior to heat-treatment.

The substitution of a part of Cd^{2+} content by Zn^{2+} was successful in creating photochromic crystals with less Cd^{2+} regarding to severe European laws that plan to ban the use of cadmium in electronic devices.

Samples containing only Cd^{2+} as co-activators achieve initial transmissions of 80%. Samples containing Zn^{2+} as co-activator in addition to Cd^{2+} achieve initial transmissions of 70%. After irradiated for the duration of 5 min with UV light, the first darkens 34%, the samples containing Zn^{2+} changes 22% in transmission. The half darkening time is 70 s for both samples and during the fading it recovers 50% of the initial transmission in the first 15 min and 11 min respectively.

The crystal sizes were between 100 nm to 450 nm. Some single crystals were 40 nm large but they were part of spirally grown crystals with total size of 450 nm.

Although we achieved the enhancement of 20% in initial transmission of samples doped with Cd^{2+} , it is still not possible to get light clear photochromic coatings, with 100% of initial transmission before exposed to activating radiation. Cd^{2+} gives a yellowish coloration to the sample after heat-treatment.

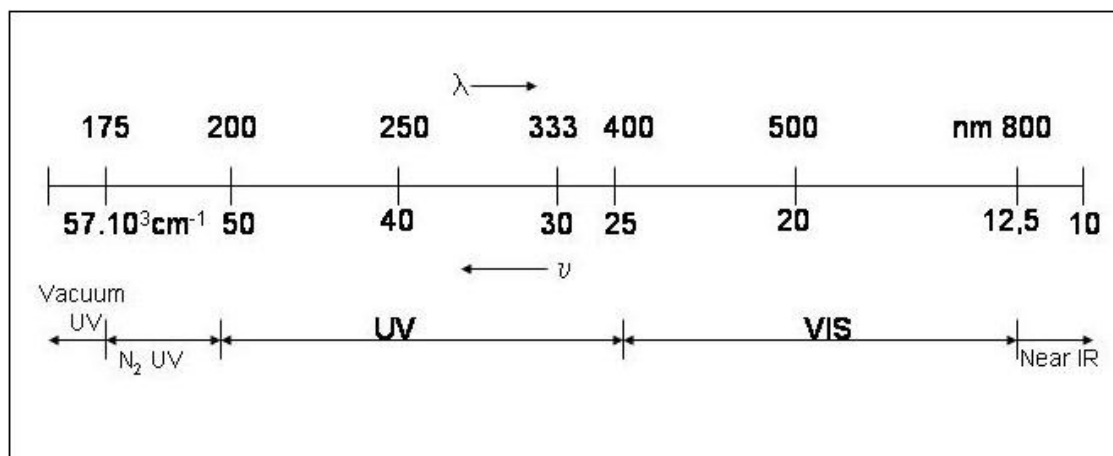
There is space for investigation on alternative heat-treatments which, will be effective in evaporating the organic rest and at the same time inhibitive to excessive crystal growth. It was not achieved the production of crystals smaller than 50 nm and photochromism simultaneously. Alternative heat-treatments might be one of the keys to get coatings that exhibit 100% initial transmission.

There are some left questions as the influence of sodium oxide diffusion from the microscope slide to the photochromic coating during heat-treatment. It would be useful to see how this diffusion influences the crystal growth of photochromic crystals. The use of different coating substrates such as SiO_2 glass, silicon plates besides the usual soda-lime-silica glass microscope slide could give important information. A new sol formulation might be needed to improve the coating adhesion to other substrates than microscope slides.

The content of organic residuals left after heat-treatment was not investigated. It was not the scope of this work, but this might also bring value to further researches. It is known that to generate the SiO_2 network from gels, temperatures higher than 300 °C are needed to provide the carbonization and oxidation of organic rests and poly – condensation. However, these temperatures applied to thin coatings lead to evaporation of the photochromic components. The temperatures used in this work were the ones that corresponded to generation of photochromic crystals not considering temperatures were all organic rests were eliminated.

10 APPENDIX

10.1 Illustration of the ultra violet and visible range of electromagnetic radiation.



10.2 List of all studied compositions

Composition	R _w	R _l	R _{s1}	R _{s2}	R _{Cu}	R _{Cd}	Comments
K26	4	4	0.5		0.1	0.1	Not photosensitive
K27	4	4	0.5		0.1	0.2	Opaque
K28	4	4	0.5		0.1	0.15	Transparent and photochromic
K1	4	4	0.5		0.2		Not photosensitive
K2 (TMOS)	4	4	0.5		0.1	0.05	Opaque
K2 (TEOS)	4	4	0.5		0.1	0.05	Opaque
K3B (CuBr)	4	4		0.6	0.1	0.2	Not soluble, CuBr precipitate in the sol
A1M	5	4	0.5	1.2	0.1	0.2	
K2am	4	5	0.5	1.2	0.1	0.05	
K3am	4	4	0.5	1.2	0.05	0.03	
K4am	4	4	0.5	1.2	0.08	0.04	
K5am	4	4	0.5	1.2	0.1	0.15	
K6am	4	4	0.5	1.2	0.1	0.1	
K7am	4	4	0.5	1.2	0.1	0.2	Transparent and photosensitive
K7am+	4	4	0.5	2.4	0.1	0.2	
K7am-	4	4	0.5	0.6	0.1	0.2	
K8am	4	4	0.5	1	0.1	0.3	
A	6	4	0.5	1	0.1	0.2	
E	4	6	0.5	1	0.1	0.2	
K9a	2	4	0.5	1	0.1	0.2	
L	4	4	0.5	1	0.1	0.2	heat-treatment above 400°C

Composition	R _w	R _l	R _{s1}	R _{s2}	R _{Cu}	R _{Cd}	Comments
M	4	4	0.5	1	0.1	0.2	heat-treatment above 400°C
MP (2-phenoxyethyl acrilate)	4	4	0.5	1	0.1	0.2	R _{acrilate} 0.01
NP100 (silver nitrate)	4	4	0.5	1	0.1	0.15	R _{Ag} 0.001 AgBr precipitate in the sol
Z2	4	4	0.5	1	0.1	0.12	R _{Zn} =0.03
Z4	4	4	0.5	1	0.1	0.09	R_{Zn} =0.06
Z6	4	4	0.5	1	0.1	0.06	R _{Zn} =0.09
Z8	4	4	0.5	1	0.1	0.03	R _{Zn} =0.12
Z10	4	4	0.5	1	0.1		R _{Zn} =0.15
CDT2	4	4	0.5	1	0.1	0.12	R _{Cd Acetate} 0.03
CDT4	4	4	0.5	1	0.1	0.09	R _{Cd Acetate} 0.06
CDT6	4	4	0.5	1	0.1	0.06	R _{Cd Acetate} 0.09
CDT8	4	4	0.5	1	0.1	0.03	R _{Cd Acetate} 0.12
CDT10	4	4	0.5	1	0.1		R _{Cd Acetate} 0.15
O1	4	4	0.5	1	0.05	0.045	R _{Zn} =0.03
O2	4	4	0.25	1	0.05	0.045	R _{Zn} =0.03
O3	4	4	0.5	1	0.05	0.045	R _{Cd Acetate} 0.03
O4	4	4	0.25	1	0.05	0.045	R _{Cd Acetate} 0.03
Q1	4	4	0.5	1	0.1	0.15	No Zn Acetate
Q2	4	4	0.5	1	0.1	0.12	R _{Zn} =0.03
Q3	4	4	0.5	1	0.1	0.09	R _{Zn} =0.06
Q4	4	4	0.5	1	0.1	0.06	R _{Zn} =0.09

10.3 Index of figures

Figure 3-1: Schematic representation of the photochromic glass coating inside a double glazed window in the bleached state and darkened state.	16
Figure 3-2: Dip-coating scheme: dipping the sample; withdraw at a constant velocity; evaporation of solvents.	18
Figure 3-3: Spin-coating schematic representation: deposition of the sol; spin up; spin of and evaporation of solvents.	19
Figure 3-4: Schematic representation of capillary coating.	20
Figure 3-5: Flow-coating technique schema.	20
Figure 5-1: Schematic representation of the sol-gel process.	38
Figure 5-2: Dip-coating instrument.	42
Figure 5-3: Schematic representation of the development from sol-gel to coating containing photochromic microcrystals.	47
Figure 6-1: Illustration of a diode array spectrometer integrated with mini-furnace.	51
Figure 6-2: Schematic representation of a SEM.	53
Figure 6-3: <i>Illustration of the principle of operation of an AFM: tip following the surface contour.</i>	55
Figure 6-4: Laser detection system.	56
Figure 6-5: Ellipsometer consisting of light source L; polarizing unit P; compensation unit C; sample S; analysing unit A; light detector D.	57
Figure 7-1: X-ray diffraction patterns of sample containing 0.9 mol% $\text{Cu}(\text{NO}_3)_2 \cdot 3\text{H}_2\text{O}$ and 1.4 mol% $\text{Cd}(\text{CH}_3\text{COO})_2 \cdot 2\text{H}_2\text{O}$ before heat-treatment.	59

Figure 7-2: X-ray diffraction patterns of sample containing 1 mol% $\text{Cu}(\text{NO}_3)_2 \cdot 3\text{H}_2\text{O}$ and 0.5 mol% $\text{Cd}(\text{CH}_3\text{COO})_2 \cdot 2\text{H}_2\text{O}$ after drying at 100 °C for 12h.....	60
Figure 7-3: X-ray diffraction patterns of samples containing 1 mol% $\text{Cu}(\text{NO}_3)_2 \cdot 3\text{H}_2\text{O}$ and 0.5 mol% $\text{Cd}(\text{CH}_3\text{COO})_2 \cdot 2\text{H}_2\text{O}$. Heat treatment at different temperatures. Presence of crystal phases: CuBr and CdBr_2	62
Figure 7-4: X-ray diffraction patterns of samples dried at 100 °C and holding time of 12 h and variable Cd^{2+} substituted against Zn^{2+}	64
Figure 7-5: X-ray diffraction patterns of samples containing $\text{Zn}(\text{CH}_3\text{COO})_2 \cdot 2\text{H}_2\text{O}$ after heat treatment at 250 °C and holding time of 20 min.	65
Figure 7-6: X-ray diffraction patterns of samples with increasing $\text{Zn}(\text{CH}_3\text{COO})_2 \cdot 2\text{H}_2\text{O}$ content, after heat-treatment at 250 °C and holding time of 1h.	68
Figure 7-7: Polarizing microscope, sample containing 1 mol% of $\text{Cu}(\text{NO}_3)_2 \cdot 3\text{H}_2\text{O}$ and 2 mol% of $\text{Cd}(\text{CH}_3\text{COO})_2 \cdot 2\text{H}_2\text{O}$	69
Figure 7-8: AFM of a coating surface of sample containing 1 mol% of $\text{Cu}(\text{NO}_3)_2 \cdot 3\text{H}_2\text{O}$ and without co-activator (Cd^{2+}) heat-treated at 130 °C and holding time of 3h.....	70
Figure 7-9: AFM of a coating surface of sample containing 1 mol% of $\text{Cu}(\text{NO}_3)_2 \cdot 3\text{H}_2\text{O}$ without co-activator (Cd^{2+}) heat treated at 200 °C and holding time of 1h.....	71
Figure 7-10: AFM of a coating surface of sample containing 1 mol% $\text{Cu}(\text{NO}_3)_2 \cdot 3\text{H}_2\text{O}$ and 1 mol% $\text{Cd}(\text{CH}_3\text{COO})_2 \cdot 2\text{H}_2\text{O}$ heat treated at 200 °C and holding time of 40 min.	72
Figure 7-11: AFM of sample surface containing 1 mol% $\text{Cu}(\text{NO}_3)_2 \cdot 3\text{H}_2\text{O}$ and 2mol% $\text{Cd}(\text{CH}_3\text{COO})_2 \cdot 2\text{H}_2\text{O}$ heat treated at 200 °C and holding time of 40 min.	73

Figure 7-12: AFM of sample surface containing 1 mol% $\text{Cu}(\text{NO}_3)_2 \cdot 3\text{H}_2\text{O}$ and 1.5 mol% $\text{Cd}(\text{CH}_3\text{COO})_2 \cdot 2\text{H}_2\text{O}$ heat treated at 200 °C and holding time of 40 min. 74

Figure 7-13: Surface structure of a sample containing Cd^{2+} and its spirally grown crystals. Sample containing 1 mol% $\text{Cu}(\text{NO}_3)_2 \cdot 3\text{H}_2\text{O}$ and 1.5 mol% $\text{Cd}(\text{CH}_3\text{COO})_2 \cdot 2\text{H}_2\text{O}$ heat treated at 200 °C and holding time of 40 min.. 75

Figure 7-14: SE micrograph of a sample containing 0.9 mol% $\text{Cu}(\text{NO}_3)_2 \cdot 3\text{H}_2\text{O}$; 0.8 mol% $\text{Cd}(\text{CH}_3\text{COO})_2 \cdot 2\text{H}_2\text{O}$ and 0.6 mol% $\text{Zn}(\text{CH}_3\text{COO})_2 \cdot 2\text{H}_2\text{O}$ 77

Figure 7-15: SE micrograph of a sample containing 0.9 mol% $\text{Cu}(\text{NO}_3)_2 \cdot 3\text{H}_2\text{O}$; 0.8 mol% $\text{Cd}(\text{CH}_3\text{COO})_2 \cdot 2\text{H}_2\text{O}$ and 0.6 mol% $\text{Zn}(\text{CH}_3\text{COO})_2 \cdot 2\text{H}_2\text{O}$ 78

Figure 7-16: SE micrograph of a sample containing 0.9 mol% $\text{Cu}(\text{NO}_3)_2 \cdot 3\text{H}_2\text{O}$; 0.8 mol% $\text{Cd}(\text{CH}_3\text{COO})_2 \cdot 2\text{H}_2\text{O}$ and 0.6 mol% $\text{Zn}(\text{CH}_3\text{COO})_2 \cdot 2\text{H}_2\text{O}$ 79

Figure 7-17: BSE micrograph of a sample containing 0.9 mol% $\text{Cu}(\text{NO}_3)_2 \cdot 3\text{H}_2\text{O}$; 0.8 mol% $\text{Cd}(\text{CH}_3\text{COO})_2 \cdot 2\text{H}_2\text{O}$ and 0.6 mol% $\text{Zn}(\text{CH}_3\text{COO})_2 \cdot 2\text{H}_2\text{O}$. X-ray emission signals for Br, Cu, Cd and Zn along a line scan. 80

Figure 7-18: Samples coated at 2 (double), 2, 5, 20 and 30 (double) cm/min. 81

Figure 7-19: Sample containing 2 mol% $\text{Cu}(\text{NO}_3)_2 \cdot 3\text{H}_2\text{O}$, without $\text{Cd}(\text{CH}_3\text{COO})_2 \cdot 2\text{H}_2\text{O}$, heated up to 130 °C and holding time by 130 °C was 75 min. 83

Figure 7-20: Absorption behaviour at 400 nm (CuBr exciton absorption band) during heat-treatment: heating and holding time at 130 °C of sample containing 2 mol% $\text{Cu}(\text{NO}_3)_2 \cdot 3\text{H}_2\text{O}$, without $\text{Cd}(\text{CH}_3\text{COO})_2 \cdot 2\text{H}_2\text{O}$ 84

Figure 7-21: Sample containing 2 mol% $\text{Cu}(\text{NO}_3)_2 \cdot 3\text{H}_2\text{O}$, without $\text{Cd}(\text{CH}_3\text{COO})_2 \cdot 2\text{H}_2\text{O}$, heated up to 200 °C with 50 min of holding time. . 85

Figure 7-22: Absorption behaviour at 397 nm (CuBr exciton absorption band) for sample containing 2 mol% $\text{Cu}(\text{NO}_3)_2 \cdot 3\text{H}_2\text{O}$, without $\text{Cd}(\text{CH}_3\text{COO})_2 \cdot 2\text{H}_2\text{O}$, heated up to 200 °C with 50 min of holding time. ... 86

Figure 7-23: Absorption behaviour of samples containing 1 mol% Cu(NO ₃) ₂ .3H ₂ O and 0.5 mol% Cd(CH ₃ COO) ₂ .2H ₂ O dried and heat treated at variable temperatures.....	88
Figure 7-24: Absorption behaviour of samples containing 1 mol% Cu(NO ₃) ₂ .3H ₂ O and 1 mol% Cd(CH ₃ COO) ₂ .2H ₂ O.....	90
Figure 7-25: Absorption behaviour of samples containing 1 mol% Cu(NO ₃) ₂ .3H ₂ O and 1.5 mol% Cd(CH ₃ COO) ₂ .2H ₂ O.....	92
Figure 7-26: Absorption behaviour of samples containing 0.9 mol% Cu(NO ₃) ₂ .3H ₂ O; 0.8 mol% Cd(CH ₃ COO) ₂ .2H ₂ O and 0.6 mol% Zn(CH ₃ COO) ₂ .2H ₂ O.....	93
Figure 7-27: Darkening behaviour of sample containing Zn ²⁺ irradiated for the duration of 5 min.	95
Figure 7-28: Absorption behaviour of sample containing Zn ²⁺ irradiated for the duration of 5 min. Subtracted spectra for different exposure times.	96
Figure 7-29: Darkening and fading behaviour of sample containing 0.9 mol% Cu(NO ₃) ₂ .3H ₂ O; 1.1 mol% Cd(CH ₃ COO) ₂ .2H ₂ O and 0.3 mol% C ₁₀ H ₁₄ CdO ₄	97
Figure 7-30: Darkening and fading behaviour of samples containing (line) 0.5 mol% Cu(NO ₃) ₂ .3H ₂ O; 0.4 mol% Cd(CH ₃ COO) ₂ .2H ₂ O and 0.3 mol% Zn(CH ₃ COO) ₂ .2H ₂ O and (dots) 0.5 mol% Cu(NO ₃) ₂ .3H ₂ O; 0.4 mol% Cd(CH ₃ COO) ₂ .2H ₂ O and 0.3 mol% C ₁₀ H ₁₄ CdO ₄	98
Figure 7-31: Darkening and fading behaviour of sample containing 0.5 mol% Cu(NO ₃) ₂ .3H ₂ O; 0.4 mol% Cd(CH ₃ COO) ₂ .2H ₂ O and 0.3 mol% Zn(CH ₃ COO) ₂ .2H ₂ O dried at 50 °C and holding time of 24h and heat treated at 200 °C for 20 min.	100
Figure 7-32: Darkening and fading behaviour of sample with memory effect.	101
Figure 8-1: Illustration of a CdBr ₂ crystal.....	105

Figure 8-2: Scheme of a ZnBr ₂ crystal.....	105
Figure 8-3: Schematic representation of γ -CuBr cubic.	106
Figure 8-4: Hydrolysis reaction in acid sols.	107
Figure 8-5: Darkening and fading behaviour of samples showing the influence of HBr content.	108
Figure 8-6: Condensation reaction in basic sols.....	109
Figure 8-7: Transmission behaviour of sample showing the effect of acetic acid addition.....	109
Figure 8-8: CuBr precipitation reactions during sol-gel preparation.....	110
Figure 8-9: Reaction of Cd complexation during sol-gel preparation.....	110
Figure 8-10: Darkening behaviour of samples containing C ₁₀ H ₁₄ CdO ₄ with different drying temperatures.	111
Figure 8-11: Precipitation of silver during the sol-gel preparation.....	112
Figure 8-12: Transmission behaviour of samples heat treated at 130 °C for 60min. Comparison between a TEOS and a TMOS containing sample.	113
Figure 8-13: Reaction of CdBr ₂ formation.....	113
Figure 8-14: Change in CuBr excitons absorption band at 450 nm with crystal growth.	122
Figure 8-15: Change in CuBr excitons absorption band at 490 nm with crystal growth.	123

10.4 Index of tables

Table 3-1: Description of the measurable photochromic characteristics	25
Table 5-1: List of all chemicals used for the preparation of the sol.....	35
Table 5-2: List of the most studied compositions (in Mol%)	40
Table 5-3: List of all studied withdraw velocities and the corresponding visual aspect after drying and heat-treatment for the composition K28	43
Table 5-4: Description of used temperatures during drying stage and its consequence to visual aspect	44
Table 5-5: Description of the variation in heat-treatment and resulting effect on photochromic crystal growth.....	46
Table 7-1: X-ray diffraction angle for sample containing (a) 0.9 mol% $\text{Cu}(\text{NO}_3)_2 \cdot 3\text{H}_2\text{O}$ and 1.4 mol% $\text{Cd}(\text{CH}_3\text{COO})_2 \cdot 2\text{H}_2\text{O}$ before heat-treatment	60
Table 7-2: Sample after drying for 12h at 100 °C; Ratio Cu:Cd = 1:0.5.....	61
Table 7-3: Identified crystals in experimental data and literature in samples heated from 110 °C up to 170 °C.	63
Table 7-4: Crystallite size variation with increasing $\text{Zn}(\text{CH}_3\text{COO})_2 \cdot 2\text{H}_2\text{O}$ content	66
Table 7-5: Crystal structure present for samples containing $\text{Zn}(\text{CH}_3\text{COO})_2 \cdot 2\text{H}_2\text{O}$; experimental and literature data comparison.	67
Table 7-6: Average crystallite size compared to the literature	76
Table 7-7: Enumeration of occurring absorption bands during heat-treatment at various temperatures and comparison with literature	87
Table 7-8: Samples with different drying temperatures and heat-treatments and their influence on transmission behaviour at the visible light range (wavelength at which the human eye is most sensitive).....	89

Table 7-9: Influence of heat-treatment on the CuBr crystal precipitation in transmission.....	91
Table 7-10: Copper halide absorption bands containing both Zn ²⁺ and Cd ²⁺ as co-activator.....	94
Table 7-11: Absorption peaks formed during irradiation compared to the literature.	96
Table 7-12: Darkening and fading characteristics for sample containing 0.9 mol% Cu(NO ₃) ₂ .3H ₂ O; 1.1 mol% Cd(CH ₃ COO) ₂ .2H ₂ O and 0.3 mol% C ₁₀ H ₁₄ CdO ₄	98
Table 7-13: Darkening and fading characteristics Darkening and fading of samples containing (line) 0.5 mol% Cu(NO ₃) ₂ .3H ₂ O; 0.4 mol% Cd(CH ₃ COO) ₂ .2H ₂ O and 0.3 mol% Zn(CH ₃ COO) ₂ .2H ₂ O and (dots) 0.5 mol% Cu(NO ₃) ₂ .3H ₂ O; 0.4 mol% Cd(CH ₃ COO) ₂ .2H ₂ O and 0.3 mol% C ₁₀ H ₁₄ CdO ₄	99
Table 7-14: Darkening and fading characteristics for sample containing 0.5 mol% Cu(NO ₃) ₂ .3H ₂ O; 0.4mol% Cd(CH ₃ COO) ₂ .2H ₂ O and 0.3mol% Zn(CH ₃ COO) ₂ .2H ₂ O dried at 50 °C and holding time of 24h and heat treated at 200 °C for 20 min.	101
Table 8-1: Crystallites present on the coatings identified by X-ray powder diffraction.....	103
Table 8-2: Relation of co-activator content and crystallite size obtained by AFM measurements	115
Table 8-3: Relation between co-activator content and crystallite size in accordance with to X-ray diffraction powder measurements.....	115
Table 8-4: Similar characteristics between Cd and Zn	118
Table 8-5: CdBr ₂ crystallites size reduction with increasing Zn ²⁺ content.....	118
Table 8-6: CuBr crystallites size increase with increasing Zn ²⁺ content	119

Table 8-7: Photochromic behaviour of samples containing Cd^{2+} and $\text{Cd}^{2+}/\text{Zn}^{2+}$
..... 120

Table 8-8: Temperature and holding times that enable CuBr crystallization . 121

Table 8-9: Relation of Cu^+ exciton absorption bands: composition and heat-
treatment..... 121

11 BIBLIOGRAPHY

- [1] Pilkington and the flat glass industry. Section104.PDF. Available at: www.pilkington.com. Access on 8.12.2004.
- [2] CO₂ emissions from new passenger cars: monitoring
Available at: <http://www.europa.eu.int/scadplus/leg/en/lvb/l28055.htm>
Access on: 04.11.2005.
- [3] McInnes, Gordon.: " A Comparison of GHG Inventories and Reduction Goals for Different Countries in Europe"; Goals and Economic Instruments for the Achievement of Global Warming Mitigation in Europe, Kluwer Academic Publishers, Netherlands (1999) 99-112.
- [4] "CO₂ Bilanz der Bundesrepublik Deutschland", Umwelt und Prognose Institut e.V.
Available at: <http://www.upi-institut.de/upi33.htm>
Access on 04.11.2005.
- [5] Nakićenović, N.; Swart R., "Emissions Scenarios", Intergovernmental Panel on Climate Change, Cambridge University Press (2000) 103-166.
- [6] Bell, M.: "Energy efficiency in existing buildings: the role of building regulations"; RICS Foundation Publications, COBRA (2004).
- [7] Technology development in support of next generation fenestration.
Available at:
<http://www.eere.energy.gov/buildings/tech/windows/technology.html>
Access on 23.08.2005.
- [8] "Sustainable building resource book: Materials: Doors and Windows", Austin Energy Green Building Program,

Available at: http://www.ci.austin.tx.us/greenbuilder/srcbk_6-7.htm

Access on 24.08.2005.

- [9] Klein, Lisa C., Sol Gel Optics: Processing and Applications, Kluwer Academic Publishers (1994).

- [10] Smith, H.; Mennig, M., "Wet coating technologies for glass", The sol-gel gateway, Institut für Neue Materialien, Saarbrücken, Germany
Available at: <http://www.solgel.com/articles/Nov00/coating.htm>
Access on 12.10.2005.

- [11] Brown, G.H., Photochromics, Wiley-Interscience, New York (1971) 643-685.

- [12] Vogel, W., Glass Chemistry, Springer, Berlin, Heidelberg, New York, (1992) Chapter 12.

- [13] Veit, M., Dissertation, Friedrich-Schiller-Univ, Jena (1982).

- [14] Moser, F., Nail, N.R., Urbach,F., Phys. Chem. Solids, **3** (1957) 153.

- [15] Callister, W.D., Material Science and Engineering an Introduction, John Wiley and Sons, In. (1997)

- [16] Wainfan, N., Phys. Rev. **105** (1957) 100.

- [17] Müller, M.; Voigt, J.; Krlitz, A., Silikattechnik **7** (1988) 221-223.

- [18] Veit, M: Fotochrome Gläser. Mitteilung bl.Chem. Ges. DDR **29** (1982) 3, 49-54.

- [19] Marquardt, C.L., Gliemeroth, G., J. Appl. Phys. **50** (1979) 4589-4590.

- [20] Araujo, R.J., Borrelli, N.F., J. Appl. Phys. **47** (1976) 1370.
- [21] Moser, F., Nail, N.R., Urbach, F., Phys. Chem. Solids, **9** (1959) 217.
- [22] West, W., Saunders, V.I., J. Phys. Chem. **63** (1959) 45.
- [23] Müller, M., Personal Advisory Information, Otto Schott Institut, Jena, February 2006.
- [24] Armistead, W.H. and Stookey, S.D., Science **144** (1964) 150.
- [25] Garfinkel, H.M., Applied Optics, **7** (5), (1968) 789-794.
- [26] Gliemeroth, G. Patent DE 20 60 748 (1970).
- [27] Sakka, S. US-Patent 3607320.
- [28] Araujo, R.J., U.S.Patent No. 3 325 299 (1967).
- [29] Araujo, R.J. and Tick, P.A., U.S.Patent No. 4 166 745 (1979).
- [30] Kadono, K. and Tanaka, H. Science and Technology of New Glasses, Proceedings of the international conference of science and technology of new glasses, Zenkyoren Building, Tokyo, October 16-17 (1991) 223.
- [31] Koch, E. and Wagner, C.Z., Physik. Chem. **38B** (1937) 295.
- [32] Mees, C.E.K. and James, T.H., "The theory of the photographic process", 3th Edition, New York Macmillan Company and London Collier-Macmillan Limited, (1966) 1-30.
- [33] Kritz, A., "*Untersuchungen zur Koaktivierung silberfreier fotochromer Gläser*", PhD thesis, Friedrich Schiller Universität , Jena (1989)

- [34] Paul, A., "Chemistry of Glasses, Second Edition", Chapman & Hall, p.116.
- [35] Zayat, M., Einot, D., Reisfeld, R., J. Sol Gel Sci. Technol. **10** (1997) 203-211.
- [36] Nogami, M., Zhu, Y., Nagasaka, K., J. Non-Cryst. Solids **134** (1991) 71-76.
- [37] Kriltz, A., Fachel, R., Müller, M., Bürger, H., J. Sol Gel Sci. Technol. **11**(2) (1998) 197-200
- [38] Kriltz, A.; Fachel, R.; Müller, M.; Bürger, H. et al., Glastechn. Ber. Glass Sci. Technol. **73** (2000) 239.
- [39] Suyal, G. "Synthesis of nanocomposite glass-like films containing semiconductor nanocrystals and noble bimetallic colloids by sol-gel route and their characterization", PhD thesis, Saarbrücken (2002).
- [40] Marquez, H., Rincon, J. Ma., Celaya, L.E., Applied Optics, **29** (25) (1990) 3699-3703.
- [41] Natsume, Y., Sakata, H., "Zinc oxide films prepared by sol-gel spin coating", Thin Solid Films **372** (2000) 30-36.
- [42] "Restriction of the use of certain hazardous substances in electrical and electronic equipments ", Directive 2002/95/EC of the European Parliament and of the Council of 27 January 2003
Available at:
http://europa.eu.int/eurlex/pri/en/oj/dat/2003/l_037/l_03720030213en00190023.pdf
Access on 05.09.2005

- [43] “31991L0338 Council Directive 91/338/EEC of 18 June 1991 amending for the 10th time directive 76/769/EEC on the approximation of the laws, regulations and administrative provisions of the Member States relating to restriction on the marketing and use of certain dangerous substances and preparations”
Available at:
<http://europa.eu.int/eurlex/lex/lexUriServ.do?uri=CELEX:31991:0338:EN:HTML>
Access on 04.11.2005
- [44] Adriano, D.C., “Trace Elements in Terrestrial Environments – Biochemistry, Bioavailability and risks of metals”, second edition, Springer verlag New York (2001) 264-306
- [45] Schmidt, H., J. Non-Cryst. Solids **100** (1985) 51
- [46] Léaustic, A., Riman, R.E., J. Non-Cryst. Solids **135** (1991) 259-264.
- [47] Sakka, S., J. Non-Cryst. Solids, **73** (1985) 651-660.
- [48] Facht, R., “Anorganisches fotochrome Schichten und Pulver nach dem Sol-Gel-Verfahren”, Abschlußbericht, MU 966/3-1,2 Deutsches Forschungsgemeinschaft, Jena (1999).
- [49] Birch, W.R., „Coatings: an introduction to the cleaning procedures“, The Sol-Gel Gateway,
Available at: <http://www.solgel.com/articles/June00/Birch/cleaning2.htm>
Access on 15.09.2005.
- [50] Klug, H. P.; Alexander, L.E., “X-ray Diffraction Procedures for Polycrystalline and Amorphous Materials”, Second Edition, John Wiley & Sons, New York (1974) 1-57.

- [51] Glusker, J. P.; Trueblood, K. N., "Crystal Structure Analysis", Second Edition, Oxford University Press, New York (1985) 3-42.
- [52] Perkampus, H. H., "UV-VIS Spectroscopy and Its Applications", Springer Laboratory, Berlin - Heidelberg (1992).
- [53] Müller, M., Personal Advisory Information, Otto Schott Institut, Jena, October (2005).
- [54] Hayat, M.A., "Principles and Techniques of Scanning Electron Microscopy", Vol. 1, Van Nostrand Reinhold Company, New York (1974).
- [55] Lüth H.: "Solid Surfaces, Interfaces and Thin Films", Springer Berlin, Heidelberg, New York (2001) 121-127.
- [56] Goldstein, J. I., Newbury, D. E., Echlin, P., Joy, D. C., Roming Jr., A. D., Lyman, C. E., Fiori, C., Lifshin, E., "Scanning Electron Microscopy and X-ray Microanalysis", 2nd Edition, Plenum Press, New York, (1992).
- [57] Binnig, G., Quate, C. F., Physical Review Letters **56** (1986) 930-933.
- [58] Roberts, C. J.; Davies, M.C.; Tendre S. J. B.; Williams, P.M., Encyclopaedia of Spectroscopy and Spectrometry, Vol.3, Academic Press, London (2000) 2051-2059.
- [59] Fischer, A. J., Encyclopaedia of Spectroscopy and Spectrometry, Vol.3, Academic Press, London (2000) 2060-2066.
- [60] Azzam, R.M.A.; Bashara, N.M., "Ellipsometry and Polarized Light", North Holland, Amsterdam (1977).
- [61] Azzam, R.M.A., Surface Science **56** (1976) 6-18.
- [62] Physikalische Chemie Forschungspraktikum, Jena University (2006).

- [63] Jellison Jr., G.E., Encyclopaedia of Spectroscopy and Spectrometry, Vol.1, Academic Press, London (2000) 402-411.
- [64] Efros, Al. L., Efros, A.L., Soc. Phys. Semicond. **16** (7) (1982) 772.
- [65] Hoover, L.H., Appl. Optics **26** (1987) 689.
- [66] Rüssel, C., personal advisory information. Otto Schott Institut, Jena, April (2005).
- [67] Seward III, T.P.; American Ceramic Society Meeting, 76th Chicago, (1974) 78 available at:
<http://jcrystal.com/steffenweber/gallery/StructureTypes/st3.html>
access on: 31.01.2006.
- [68] Volmer, M.: Kinetik der Phasenbildung; Steinkopf, Dresden, (1939).
- [69] Meiling, G.S., Phys. Chem. Glasses **14** (1973) 118-121.
- [70] Miura, Y.; Osaka, A.; „Takahashi, K.: Optical Properties in Cadmium Borosilicate Glasses“, Collected papers, XIV International Congress on Glass (1986).
- [71] Griscom, D.L., J. Non-Cryst. Solids **13** (1973/74) 251-285.
- [72] Imagawa, H., Phys. Chem. Glasses **10** (1969) 187-191.
- [73] Deri, R.J., Haynam, Ch., Spoonhower, J.P., Phys. Stat. Sol. (b) **109** (1982) 645.
- [74] Baetzold, R., Appl. Phys. Letters **26** (1975) 709.
- [75] Tan, Y.T., Surface Sci. **61** (1976) 1.

- [76] "Cadmium" Wikipedia The Free Encyclopaedia,
Available at: <http://en.wikipedia.org/wiki/Cadmium>
Access on 05.02.2006.
- [77] "Zink" Wikipedia The Free Encyclopaedia,
Available at: <http://en.wikipedia.org/wiki/Zinc>
Access on 05.02.2006.
- [78] Araujo, R.J., J. Non-Cryst. Solids **47** (1982) 69-86.
- [79] Trotter, D.M., Jr., J.R. Schreurs, Tick, P.A., J. Appl. Phys. **53** (1982) 4657-4672.
- [80] Marquardt, C.L., Giuliani, I.F., Willians, R.T., J. Appl. Phys. **47** (1976) 4915.
- [81] Grundlagen Rastersondermikroskopie Betriebsanleitung ULTRAOjective S.I.S, Otto Schott Institut, Jena (2006)
- [82] Stephan window,
Available at: <http://www.polar.de/polar.htm?produkte2.htm>
Access on 07.04.2005

12 SELBSTSTÄNDIGKEITSERKLÄRUNG

Ich erkläre, dass ich die vorliegende Arbeit selbstständig und unter Verwendung der angegebenen Hilfsmittel, persönlichen Mitteilungen und Quellen angefertigt habe.

London, den 30.03.2006

13 LEBENS LAUF

Persönliche Daten

Name *Juliana Meirelles*
Geburtsdatum *24.02.1977*
Geburtsort *Goiânia – Brasilien*
Familien Stand *Ledig*

Ausbildungsdaten

Fev. 1988 – Dec. 1991 (Schule) Colégio Marista Goiania/Go - Brasilien
Fev. 1992 - Dec. 1993 (Gymnasium) Disciplina in Goiânia/GO - Brasilien
Jan. 1994 – Jan. 1995 Rotary International Austauschprogram in Denmark
Fev. 1995 - Dec. 1995 (Gymnasium) Visao in Goiânia/GO - Brasilien
Fev. 1996 – Juli 2001 Studium der Material Ingeniörowissenschaft an der
Universidade Federal de São Carlos/SP – Brasilien
Aug. 1999 – Juli 2000 Praktikum am Otto Schott Institut für Glaschemie
der Friedrich Schiller Universität Jena
Juli 2001 Diplom in Material Ingeniörowissenschaft
Mai 2001 – Jan. 2002 Junior Ingeniörin am Saint Gobain Advanced
Ceramics. Rio Claro/SP - Brasilien
Seit Mai 2002 Wissenschaftliche Mitarbeiterin am Otto Schott
Institut für Glaschemie der Friedrich Schiller
Universität Jena

